1998

ARAC modeling of SARMAP tracer releases

Philip Vogt
San Jose State University

INFORMATION TO USERS

This manuscript has been reproduced from the microfilm master. UMI films the text directly from the original or copy submitted. Thus, some thesis and dissertation copies are in typewriter face, while others may be from any type of computer printer.

The quality of this reproduction is dependent upon the quality of the copy submitted. Broken or indistinct print, colored or poor quality illustrations and photographs, print bleedthrough, substandard margins, and improper alignment can adversely affect reproduction.

In the unlikely event that the author did not send UMI a complete manuscript and there are missing pages, these will be noted. Also, if unauthorized copyright material had to be removed, a note will indicate the deletion.

Oversize materials (e.g., maps, drawings, charts) are reproduced by sectioning the original, beginning at the upper left-hand corner and continuing from left to right in equal sections with small overlaps. Each original is also photographed in one exposure and is included in reduced form at the back of the book.

Photographs included in the original manuscript have been reproduced xerographically in this copy. Higher quality 6" x 9" black and white photographic prints are available for any photographs or illustrations appearing in this copy for an additional charge. Contact UMI directly to order.

UMI

A Bell & Howell Information Company
300 North Zeeb Road, Ann Arbor MI 48106-1346 USA
313/761-4700 800/521-0600

ARAC Modeling of SARMAP Tracer Releases

A Thesis Presented to

The Faculty of the Department of Meteorology

San Jose State University

In Partial Fulfillment

of the Requirements for the Degree

Master of Science

By

Philip Vogt

May 1998

APPROVED FOR THE DEPARTMENT OF METEOROLOGY

R. Bornstein

Prof. Robert Bornstein, Chair

Scot G.R. Rafk

Prof. Scot Rafkin

Ronald Baskett

Mr. Ronald Baskett

APPROVED FOR THE UNIVERSITY

William Fisher

ABSTRACT

ARAC MODELING OF SARMAP TRACER RELEASES

by Philip J. Vogt

The Lawrence Livermore National Laboratory Atmospheric Release Advisory Capability (ARAC-2) second generation operational diagnostic emergency response models were used to simulate multiple tracers released during the 1990 San Joaquin Valley Air Quality Study/Atmospheric Utility Signatures, Predictions and Experiments - - Regional Model Adaptation Project field program. A total of 16 tracer releases were modeled, four simultaneous tracers released from different locations during four intensive data-collection periods.

Model accuracy, calculated using ratios of measured to calculated two-hour average air concentrations at sample locations, was found comparable to previous ARAC-2 model evaluation studies out to 50 km. In addition, new baseline model performance value at distances to 500 km was established. Based on six tracer experiments that produced over 50 concentration measurements pairs each, the ARAC-2 models were found accurate to within a factor two for 10%, and within a factor of ten for 30%, of the time on the 500 km scale.

ACKNOWLEDGMENTS

The author wishes to thank Prof. Robert Bornstein for his help in the preparation of this document. Sincere appreciation is addressed to Ronald Baskett who guided the modeling effort, and to Kevin Foster for help in processing raw data into the Model Evaluation Tools database. Additionally, my deepest thanks to my fellow workers at ARAC for putting up with the time and effort I required for this project.

TABLE OF CONTENTS

LIST OF TABLES

Table

LIST OF FIGURES

1. INTRODUCTION

A. San Joaquin Valley Air Quality Study

The San Joaquin Valley Air Quality Study (SJVAQS) was formulated in 1986 to study how to mitigate persistent air quality problems in the San Joaquin Valley (SJV). In 1988, the SJVAQS was linked to the Atmosphere Utility Signatures, Predictions, and Experiments (AUSPEX), a consortium sponsored by PG&E, Electric Power Research Institute, and Bay Area Air Quality Management District. The collaboration, referred to as the SJVAQS/AUSPEX Regional Model Adaptation Project (SARMAP), was designed to investigate the roles of emission, meteorology, and chemistry on SJV ozone production and transport. Its 1990 Summer field experiments were designed to determine the contributions of local versus transported emissions to high ozone concentrations in the SJV. Tracers were released at four sites, either around the San Francisco Bay Area (SFBA) or in the SJV.

Previous SARMAP modeling efforts included prognostic wind field modeling, as well as tracer trajectory and transport modeling. Tanrikulu and Soong (1991) used the NCAR/PSU meso-model MM5 and 4-D data assimilation (4DDA) nudging to compare model data to an early compilation of observed near-surface wind and temperature fields for the 3-5 August 1990 case; results indicated that 4DDA improved model accuracy. Stauffer (1995) examined the effectiveness of MM5 at predicting atmospheric wind speeds and directions on the morning of 4 August, particularly in data-void areas. 4DDA

nudging of observations produced improvements in the simulation of the Fresno Eddy, a circulation that forms about 400 m above the surface in the southeastern SJV.

Seaman (1995a) also used MM5 to examine formation and dissipation mechanisms of the Sacramento and Fresno eddies and of the low-level jet (LLJ) during 2-4 August. Suggested mechanisms included down-slope flows, daytime growth of the mixed layer, and temporal regional wind direction changes. Seaman et al. (1995b) used MM5 for the 2-7 August and 25-30 July 1990 cases. Results for surface wind speeds, directions, temperatures, and mixed layer depth indicate improved model performance with 4DDA, even when half the observed data were removed.

Mulberg et al. (1993) used the following three wind models to produce input for the photochemical Urban Airshed Model (UAM) to compare analyzed and computed ozone concentrations for the 11-13 July 1990 period: the diagnostic CALTECH (CIT), Diagnostic Wind Model (DWM), and prognostic SAI Mesoscale Model (SAIMM). Both diagnostic models matched the wind observations better than the prognostic model, although they both under-predicted speed values, while the prognostic model over-predicted them.

Lolk (1993) used SAIMM and UAM to calculate parcel trajectories from the SFBA and northern SJV to the city of Sacramento during the 11-13 July and 7-9 August 1990 periods. Results indicate that both surface and elevated plume transport into the Sacramento region was possible during these periods. Smith and Lehrman (1993) compared measured concentration maxima

and calculated center of near-surface mass trajectories to examine tracer releases from Pittsburg and Hayward on 27 July, as well as releases from Pittsburg, Hayward and San Jose on 3 August. Results indicate that both the Pittsburg and Hayward releases moved down the east side of the SJV, while the San Jose release of 3 August traveled down the west side of the valley.

Umeda (1993) used MM5 wind fields and a Lagrangian particle model to calculate tracer transport for the Pittsburg and San Jose releases of 3 August. Results indicate wind fields produced by MM5 did not transport material as fast and as far as observed. Qualitative results show a much larger model area plume than actual observations indicate. Umeda (1996) used the Colorado State University Regional Atmospheric Modeling System (RAMS) with a Lagrangian Particle Model to simulate the same two releases. Results were improved for the Pittsburg release for both plume location and magnitude, but those for the San Jose release had the calculated plume too far west and had concentration values too low.

Tanrikulu and Stauffer (1995) used MM5 with 4DDA to simulate the Pittsburg and San Jose Tracer releases of 3-4 August. Model results had the Pittsburg tracer traveling east and then south, while the San Jose release split: one branch passed through Altamont Pass and the second moved south and east through Pacheco Pass.

B. Atmospheric Release Advisory Capability (ARAC)

Operational models used by the Lawrence Livermore National Laboratory (LLNL) ARAC emergency response program have been typically used on domains of 1-90 km or 2000-4000 km. ARAC provides computerized consequence analyses to federal emergency managers for radiological and other hazardous material releases to the atmosphere to minimize exposure to the population at risk. Second generation ARAC-2 models have supported emergency responses for the U.S. Departments of Energy and Defense since the early 1980s (Sullivan et al. 1993).

The models have been evaluated primarily against gaseous tracer releases which were either surface or elevated, and either neutrally-buoyant, or buoyant (Table 1). Results indicate that ARAC-2 models can estimate tracer concentrations for scales from 1 to 50 km within a factor of two up to 50% of the time, and within a factor of five up to 85% (ARAC 1996).

ARAC-2 model accuracy has been generally determined by how many measured and calculated concentration pairs matched in space and time fall within a specified factor (Foster and Dickerson, 1990 and Sullivan et al. 1993). The majority of the studies in Table 1 completed to date are over advective distances of 1 to 90 km (i.e., the meso-γ to meso-β scales; Orlanski 1975, Thunis and Bornstein 1996). Topography, atmospheric complexity, and release characteristics, however, varied significantly. Model accuracy thus varied, e.g., predictions were good for both the 1971 Idaho National Environmental Lab (INEL) and 1974 Savannah River Plant (SRP) studies due to their

smooth topography and simple meteorological conditions, but those for the Atmospheric Studies in Complex Terrain (ASCOT) were not as good due to its highly complex terrain and stable atmospheric conditions.

Studies on continental scales of 2000-4000 km include the: U.S.-Canadian 1983 Cross-Appalachian Travel Experiment (CAPTEX), 1987 Across North America Tracer Experiment (ANATEX), and 1994 European Tracer Experiments (ETEX). CAPTEX results showed a miss-aligned plume centerline, but comparison of centerline concentrations at all distances paired well with no systematic bias (Rodriguez 1987). Results were better (plume centerline better located) for ANATEX, which used both the National Weather Service Nested Grid Model (NGM) for wind input and a spatially varying mixing height (Rodriguez and Cederwall 1990). Real-time ETEX results showed some match to measured data (Pace and Nasstrom 1997), while subsequent calculations with better meteorological data and dispersion parameters produced better results. The Chernobyl nuclear accident, and its subsequent ATMES Chernobyl reconstruction study, occurred on a continental scale, and required a hemispheric domain.

Whereas previous ARAC-2 applications have been either carried out on the meso or synoptic scales, the current study is the first evaluation of these models with domains ranging from 100-500 km on the macro-γ scale (Orlanski 1975, Thunis and Bornstein 1996). The 1990 SARMAP tracer data set will be used in this study. While previous tracer simulations with this

data have only simulated the 3 August Pittsburg and San Jose, releases this study models all 16 SARMAP releases.

2. ARAC-2 MODELING SYSTEM

Five codes form the operational ARAC-2 modeling system (Fig. 1): TOPOG creates a topographic grid over the modeling domain, MEDIC interpolates and extrapolates observational and large scale gridded wind data to the 3-D modeling grid, CG-MATHEW adjusts MEDIC wind fields to be mass consistent after inclusion of terrain channeling and deflection effects, ADPIC simulates 3-D particle transport and diffusion using a Random Displacement Method (RDM), PLOT_CONTOUR isopleths ADPIC concentration values. A sixth code TIMEHIS compares measured to calculated concentrations in time and space. Following is a basic description of each code, with additional detail available in the ARAC Model User Guide (ARAC 1996).

TOPOG creates the underlying block-cell terrain surface for the CG-MATHEW and ADPIC models by averaging terrain height data from on-line worldwide databases to the problem-specific location and resolution. It also defines the horizontal and vertical grid resolutions (Δx, Δy, Δz) of the modeling domain.

One limitation with block-cell terrain, is that when a single cell is surrounded by higher cells, no wind can exist in it because five of it's sides (except its top) are closed off. Consequently, particles that diffuse downward into the cell become trapped, except for upward diffusion. TOPOG thus compares

each cell with its surrounding cells, and if it is at least one Δz less than each of the surrounding eight cells, it's terrain height is smoothed by filling in the hole one Δz at a time until one or more cell faces opens up.

MEDIC produces horizontal wind vectors at each grid cell corner by extrapolation of data obtained from (surface and upper-air) observations or from large-scale model output. Extrapolated wind fields are sensitive to small changes in input parameters (such as SBL and PBL depths, horizontal and vertical extrapolation rotation limits, and surface layer power law exponent). Adjustments are made to input parameters until a flow field consistent with observed conditions is achieved.

Three separate atmospheric layers are treated in the extrapolation procedure. In the lowest (or surface) layer, surface effects dominate and no directional shear with height is allowed. In the highest (or geostrophic) layer, surface effects have dissipated and winds reflect larger-scale synoptic flow. In the central (or boundary) layer conditions are mixed between the surface and geostrophic layers, and both speed and directional shear occur.

The basic extrapolation scheme used in MEDIC is r^{-2} weighting of surface station data in the horizontal, and a fit to either observed profiles or to a power-law in the vertical. The boundary layer extrapolation exponent input parameter can be adjusted (based on observations) to determine how closely vertical extrapolation should reproduce upper-air data. MEDIC extrapolation is carried out without terrain. The terrain is then pushed up through the bot-

tom of the grid, shifting atmospheric layers upward, and finally producing terrain following surface and boundary layers.

Wind fields from MEDIC are then passed to CG-MATHEW, which generates mass-consistent winds by minimal adjustment of fields through a constrained variational minimization using finite-difference methods and through a conjugate gradient (CG) solution. The original MATHEW code (Sherman 1978) obtained mass consistency by use of successive over-relaxation techniques. A disadvantage of this method is an artificial reduction in wind speeds. CG methodology uses generalized symmetric boundary conditions, allowing for control of normal and tangential adjustments at the horizontal or vertical terrain boundaries, respectively (Sugiyama et al. 1994).

The optimized CG method is significantly faster than over-relaxation, and use of two boundary conditions permits the same level of accuracy as with old MATHEW. Additionally, two boundary conditions provide greater flexibility in matching potential flow solutions in two- and three-dimensions. The new boundary conditions also prevent artificial speed reductions and eliminate flow artifacts in complex terrain.

Minimal adjustment maintains consistency with available meteorological (surface and upper air) measurements, with atmospheric stability conditions governing the relative change in vertical and horizontal wind components (i.e., flow over or around terrain features). The adjustment is irrotational, and neither momentum nor energy conservation is imposed.

ADPIC is a numerical, three-dimensional Lagrangian particle-diffusion code capable of the calculation of time-dependent pollutant distributions under various conditions, including strongly distorted wind fields, calm conditions, wet and dry deposition, radioactive decay, and time-variable turbulence. It solves the 3-D advection-diffusion equation using the Random Displacement Method (RDM), i.e., the Lagrangian, grid-independent, random walk, Monte-Carlo method described by Ermak and Nasstrom (1994). Thousands of marker particles are used to represent the mass or radioactivity of multiple time-varying atmosphere releases, and ensemble-mean concentrations are calculated from particle locations. In addition, RDM treats deposition processes through particle-surface interactions.

RDM is thus based upon the "conservation of species" principal first expressed as the 3-D Eulerian advection-diffusion equation:

$$\frac{\partial \overline{C}}{\partial t} = -\overline{u}\frac{\partial \overline{C}}{\partial x} - \overline{v}\frac{\partial \overline{C}}{\partial y} - \overline{w}\frac{\partial \overline{C}}{\partial z} + \frac{\partial}{\partial x}\left(K_x \frac{\partial \overline{C}}{\partial x}\right) + \frac{\partial}{\partial y}\left(K_y \frac{\partial \overline{C}}{\partial y}\right) + \frac{\partial}{\partial z}\left(K_z \frac{\partial \overline{C}}{\partial z}\right), \qquad (1)$$

where $\overline{C}$ is mean species air concentration; $\overline{u}$, $\overline{v}$, and $\overline{w}$ mean wind components from CG-MATHEW in the x, y, and z directions, respectively; t time; and K_x, K_y, and K_z parameterized eddy diffusivities for three coordinate directions, respectively. K_x and K_y are assumed equal and uniform to K_H, based on the Draxler (1976) semi-empirical relationship as a function of time and of the standard deviation of horizontal velocity. He used the following equation for σ:

$$K_H = \frac{\sigma \cdot t}{1 + d\left(t/\tau_H\right)^{1/2}}, \qquad (2)$$

where t is time. A value for constant d=0.36 best fits his close-in diffusion data. Based on this number, τ_H=50 s for surface releases and 160 s for elevated releases are recommended by Hanna et al. (1982). Note that this formulation results in the currently used $K_H \propto t$ for $t<\tau_H$, and $K_H \propto t^{1/2}$ for $t>\tau_H$.

The PBL vertical turbulence parameterization for this study is based on surface boundary layer scaling parameters (Lange 1989) as follows:

$$K_{hl}(z) = \frac{k u_* z}{\phi} e^{-cz/h}, \qquad (3)$$

where k is the Von Karman constant (0.4), u_* friction velocity, ϕ a function of near-surface stability, h mixed layer height, and c a constant. For the free troposphere ($z>h$), K_Z is constant.

RDM uses stochastic differential equations that describe the processes in (1), but in a Lagrangian framework (Boughton et al. 1987; Ermak, 1992; Rodean et al. 1992). The stochastic equations are integrated in time to calculate independent trajectories representing the movement of individual fluid elements. The time step used in this numerical technique is restricted to prevent a particle from moving more than a single grid cell in any time step due to the effects of mean wind advection plus turbulent diffusion (the standard CFL condition). For the accurate determination of concentration in each nested sampling grid (discussed below), the time step is further restricted to

prevent a particle from moving through more than a single sampling grid cell.

A fundamental assumption in the Lagrangian formulation is that the turbulence time and space scales are small relative to those of advection. The time scale ("eddy lifetime") of turbulence is assumed smaller than the time over which concentrations are calculated. RDM-ADPIC code solutions to the advection-diffusion equation have been validated to within 5% for known analytical solutions with both homogenous and in-homogenous turbulence (Ermak and Nasstrom 1994).

ADPIC handles up to nine pollutant sources, each with its own: source type, location, rate, geometry, log-normal particle size distribution, deposition velocity, and decay rate (for radionuclides). Release rates and center heights of each source are independent and variable with time, and the initial 3-D position of each marker particle comprising any source has a tri-dimensional Gaussian distribution.

ADPIC can remove particles through dry gravitational settling (based on particle size) and by the flux of material from the surface layer to the ground (based on a specified deposition velocity). Inputs to ADPIC for the dispersion parameterization include the following time-varying atmospheric parameters: stability class, mixing layer height, and Monin-Obukhov length. ADPIC can also calculate time-dependent plume rise, and has an explosive cloud-rise algorithm with final heights of buoyant sources dependent on

wind speed, atmospheric stability, and both effluent and environmental temperatures.

PLOT_CONTOUR input includes concentrations values produced by ADPIC at user-selected heights. To improve near-source analysis, up to four nested grids of diminishing size are used. Each interior grid has half the horizontal grid spacing of the next outer grid. Source rate values are converted to concentration values, which are then converted to dose values using a "dose conversion factor". Up to five contours of interest can be displayed on a single plot (e.g., environmental standards).

ADPIC concentrations are bilinearly interpolated to specific sampler-point locations by TIMEHIS, which then compares calculated and measured data to determine a ratio of measured to calculated values in space and time. Ratios are averaged to determine a scaling factor when source strength was unknown and a generic release amount was used.

3. SARMAP SIMULATIONS

Summer ozone levels in the SJV often exceed the federal standard due to a combination of local emission and regional meteorological conditions. The extent to which local versus transported emissions contribute to such high ozone concentrations was not known, and thus the SARMAP project was initiated. SARMAP was designed to examine multi-day episodes that exhibit build-up, peaking, and clean-out phases. During the Summer of 1990, five episodes occurred during which intensive meteorological, emission, and

concentration data were collected. Additionally, during four of these episodes, inert perflourocarbon tracers were released, and downwind surface concentrations measured with stationary surface samplers (Thuiller et al. 1994).

A. Data Sources

The SARMAP study area covers over 150 000 km^2, including coastal regions, mountains, and valleys (Fig. 2). Figure 3 shows geographical features within the study area. Key considerations in the design of the meteorological data network were the collection of 3-D data in important locations and the resolution of key meteorological phenomena. Such locations include coastal range gaps that allow air from the Bay Area to access the SJV, while key phenomena include the Fresno Eddy, and the development of the nocturnal LLJ; data and sites were audited for accuracy (Thuiller et al. 1994).

Surface data collected at over 160 mast locations (Fig. 4), including 2 m surface temperature, humidity, solar radiation values, and wind directions and speeds at 2 to 15 m above the ground. Velocity data used in this study were the 1-hr vector averages collected each hour from 1 July to 31 August 1990.

Upper-air meteorological data were collected at almost 50 sites (Fig. 5) by radar profilers, Doppler acoustic sounders (sodars), or rawinsonde balloons. Balloon sites were located to obtain temperature and humidity data throughout the study area, at regular spatial intervals (as much as possible), while

profilers and sodars were primarily located at coastal sites or areas affected by marine air. Additional sodars and the profilers were located to resolve important phenomena, such as the LLJ, eddies, or slope flows. With the exception of the Oakland and Vandenberg NWS sites, balloons were only launched during intensive study episodes (at approximately three to six hour intervals), while profilers and sodars ran continuously through most of the experiment.

Four perflourocarbon tracers were used during four intensive study periods (Table 2), as they can be detected at low concentration levels and have no environmental impact. Tracer experiments were designed to determine the transport of pollutants, both from the SFBA and within the SJV.

Tracer release sites were not co-located with meteorological measuring sites, and the tracers were released in a fine mist from generator tanks involving an attached compressed air, flow meter, and spray nozzle. Tracer samples were collected at 72 sites (Fig. 6), beginning shortly after release initiation. These 72 sites were generally distributed evenly over much of the study domain, and produced a low-density sampling network. Near ground sampling was done by air-samplers that included an air pump and 24 individual sample bags. The pump ran continuously for 48 hours, while a sample bag was collected every two hours on each odd UTC hour (Rappolt and Quan 1992).

B: Data Incorporation

Four simultaneous tracer releases were simulated in each individual approximate 36 hour run, which used all available surface, upper-air, and tracer data. The model domain was selected to encompass the SJV field study area (Figs. 2 and 3) i.e., 440 by 440 km horizontally and 3000 m vertically, with a grid spacing of 80 x 80 cells horizontally and 30 layers vertically; consequently, cells are 5.5 by 5.5 km wide and 100 m high. The 3000 m vertical range was selected to both provide maximum resolution of low-level features and to resolve the Sierra Nevada mountain range. Additionally, most experiment upper-air meteorological data ranged from the surface up to between 2-3 km. The 5.5 km horizontal grid spacing provides adequate resolution of most domain terrain features, including key coastal gaps and valleys.

Meteorological data sets for input to MEDIC were prepared at hourly intervals using ARAC Model Evaluation Tools software (Foster 1994). Each meteorological data set includes all surface and upper-air observations for that hour. If a particular upper-air or surface station did not have an observation during that hour, the observation nearest in time was substituted. Substitute surface data were limited to the nearest one hour, while upper air data were limited to 6 hours. Additionally, winds required at time steps between observations were linearly interpolated in time.

Surface wind data at different heights were vertically interpolated to a reference height selected as 10 m (using a power law) in MEDIC; which was subsequently extrapolated to horizontal grid points. SBL height was fixed at

25 m, while the PBL height was assumed to vary diurnally (where local time is seven hours behind UTC) from 250 to 1000 m (Fig. 7). Given the significant number of upper-air stations and their excellent spatial and temporal resolution, the profile extrapolation method was selected to meld surface and upper air measurements (instead of parameterized extrapolation). Additionally, a small vertical extrapolation exponent was selected for a more rapid approach to upper air data from surface values.

Stability criteria for wind adjustments to terrain in CG-MATHEW were selected hourly, consistent with the best estimates of SJV stability; the same values were also used in ADPIC. Mixed layer height values, selected hourly using the best estimated SJV height, ranged from 250 to 1500 m; a roughness height of 20 cm was used to represent the SJV. These three parameters were used over the entire model domain; consequently, they may not best represent domain regions away from the SJV. ADPIC inverse Monin-Obukhov L^{-1} values were determined graphically for each hour using surface roughness and stability, following Golder (1972).

A 2 m diameter sphere centered 2 m off the ground represented the fine mist projected by each tracer release system. As the release height for the elevated Pittsburg site release case was unknown, the center of the sphere was placed at the height of the bottom of the second grid cell (110 m). A constant release rate was assumed for each release, with total tracer release amount divided by duration used to determine release rate. Tracers were modeled as

neutrally-buoyant gases with no deposition velocity. The four simultaneous releases were each modeled using 50 000 marker particles (Figs. 8a and b).

The quantitative methodology recently adopted by ARAC (Foster 1994) for model evaluation is similar to previous evaluation accuracy factors, which are ratios of matched (in space and time) measured and calculated air concentration pairs (Sullivan et al. 1993). The previous method, however, used only matched pairs when both values were greater than zero, while the current method compares calculated values (zero or non-zero) to measurements. Model accuracy is expressed by the percentage of ratios from matched pairs (both measured and calculated values greater than zero) relative to all measured concentrations (measured values greater than zero, but calculated values greater than or equal to zero). Accuracy factor ratios are calculated to be unity or greater, i.e. larger of either measured or calculated value appears in numerator.

This method was also used in the current study for continuity with previous ARAC studies, and because the Mathew/ADPIC models are designed to produce these statistics. Due to the low-density of sampling locations, however, rigorous point to point comparisons can produce low accuracy factors due to the inability of the observational network to fully characterize tracer plumes.

4. RESULTS

Results are presented in order of model accuracy, which was highest when the local flow was primarily driven by regional forcing. The 27-29 July releases were associated with a typical strong summer thermally-driven on-shore flow. An unseasonably strong upper-level synoptic trough, however, dominated flow patterns for the 23-24 August case, also producing well defined southwesterly flow over the entire domain. A typical thermal on-shore flow through the Carquinez Gap also prevailed during the Pittsburg releases during both the 13-14 July and 3-4 August cases, but flow patterns were lighter and locally driven at the other three release locations during both of these cases.

A. Case 1: 27-29 July

Four simultaneous four-hour releases of perflourocarbon tracers began at 2300 UTC on 27 July from sites (Table 3) in Hayward, Modesto, and Pittsburg (ground level and elevated). The experiment was designed to examine pollutant transport into the southern SJV from the SFBA and northern SJV.

At 0000 UTC on 28 July, a thermal low at 850 hPa is located over New Mexico (Fig. 9) with troughing extending westward to the California coast. By 1200 UTC on 28 July gradients above the surface continued to relax resulting in light wind conditions. At 500 hPa a high pressure ridge built into the western U.S. (Fig. 10a), following a trough that moved eastward over the moun-

tain states. Figure 10b shows a thermal low at 850 hPa centered over northwestern Arizona.

The weak upper winds and the thermal trough east of California produced a diurnal variation in the on-shore flow near the surface. Moderate on-shore flows developed during daytime on both the 27th and 28th in association with moderate pressure and temperature gradients, while weak on-shore flows prevailed each night.

At 2200 UTC on 27 July, modeled surface winds (Fig. 11a) show a pattern typical for the entire case, i.e. flows were westerly over much of the domain, except in the SJV where light northwesterly conditions prevail, a pattern normal for late afternoon summer days. Figure 11b shows concurrent modeled winds at 400 m AGL slightly stronger than those at the surface, except over the western SJV and central Coastal Range where flow became unexpectedly weak. Winds above this level (not shown) became westerly over most of the domain, with northwesterly winds persisting over SJV. These conditions produced an on-shore flow pattern into the SJV through the Carquinez and Altamont gaps that persisted throughout the entire case; however, wind-flow patterns remained weak and locally driven over the eastern and southern SJV.

Two-hour average air concentration contour plots at 1 m above ground, prepared to coincide with tracer measurement times and height of obtained measurements, display five contours ranging from 10 to 1000 *fl/l*. This range is based upon the range of tracer measurements, with the mini-

mum contour value of 10 fl/l matched to the smallest tracer measurement, and with the largest contour value of 1000 fl/l matched to the highest order-of-magnitude measured tracer value.

Figures 12a and 13a show that both the Pittsburg elevated and surface releases initially moved rapidly westward, then curved southeastward down the SJV. After 12 hours (Figs. 12b and 13b) both plumes are stretched along the eastern SJV as a result of their southern edges moving down the SJV and their northern parts moving slowly northeastward. After 18 hours (Figs. 12c and 13c) the northern sections of both the elevated and surface releases have separated and moved over the central Sierra Nevada. Finally, Figs. 12d and 13d show the model plume after 24 hours over the southern SJV, but still north of Bakersfield, while its northern section has advected out of the domain.

The plume location initially matches measured tracer values, but after six hours measurements indicate a more latitudinal plume-width (to the west) in the central and southern SJV than was modeled. The ADPIC model produces well mixed concentrations within the boundary layer. As a result, little vertical structure to the plume in the lowest layers is possible, and consequently, this plume narrowness is most likely due to inadequate plume diffusion. In addition as tracers from both releases were detected all the way down to Bakersfield, the model under-advected the plume throughout the simulation. Note that no tracer data were measured at sites in the area of the northern section of the plumes.

Figure 14 shows time-series comparisons of measured and computed values for the duration of the run at six sites. Note concentration scales vary, and the time period at Oildale is extended for clarity. Sites were selected as near as possible to the modeled plume centerline, and are geographically located as follows: Lodi (Fig. 14a) and Woodward Reservoir (Fig. 14b) are near the source location at the north end of the SJV, Madera (Fig. 14c) and Fresno (Fig. 14d) are mid-way down the valley, and Corcoran (Fig. 14e) and Oildale (Fig. 14f) are far downwind at its south end.

Results indicate that for the northern SJV sites, the calculated maximum concentration and total plume exposure (dosage) agree well with observed values. In the mid-valley region, the two selected sites are on the edge of the model plume, which passed between them. Results show peak values in good agreement. A delay from the under-advection discussed above is, however, evident, while overall exposure is under-predicted due to the inadequate latitudinal plume extent (also discussed above). In the south end of the SJV, the near plume-centerline Corcoran site results show over-prediction, due to the too narrow predicted plume. The time-lag has increased further downwind due to slow model transport, although the maximum predicted value is close to the measured value at Oildale.

The same six sites were selected for the surface release time-series comparisons. The model significantly over-predicts concentrations at the northern sites (Figs. 15a and b), but matches their time of maximum. The modeled plume centerline passed over these sites, but the real plume did not; how-

ever, measurements are insufficient to accurately determine the real plume centerline and edges. As the plume is narrow at sites close to the source, slight errors in wind direction produce large changes in measured concentrations.

Similar results were obtained for mid-valley (Figs. 15c and d) and the southern SJV sites (Figs. 15e and f). Even greater under-estimations of plume-edge calculated concentrations at these sites occurred due to an even narrower (relative to the elevated plume) surface-release real-world plume; additionally, peak concentrations are thus even more over-predicted than with the elevated release.

Scatter plot comparisons of 116 elevated (Fig. 16) and 51 surface release (Fig. 17) matched pairs, respectively, (including only those with both measured and calculated values greater than zero) both indicate an overall bias towards under-prediction. Note that the solid diagonal line is the "factor of 1" line (or 1:1 ratio), while the dashed lines on both sides represent (in order) factors of: 2, 5, 10, 100, and 1000. The inadequate latitudinal model spread has caused low calculated concentration values at the majority of sites (i.e., those away from the plume centerline) and high calculated concentrations at the fewer sites near the centerline. The fewer data points for the surface release could be due to a real surface plume more narrow than the elevated plume. Model plumes were too narrow for both cases, and could have been outside the real surface plume but inside the real elevated plume; and as a result, more elevated matched pairs were obtained.

Model accuracy factors were obtained from 307 elevated, and 135 surface release matched pairs (as above, but also including measured greater than zero and calculated equal to zero). Elevated Pittsburg release model accuracy (Fig. 18) was within a factor of two 20%, and within a factor of ten 32%, of the time at distances up to 50 km (Table 4). These values are comparable to similar ARAC-2 results for that scale (Sullivan et al. 1993). Accuracy was reduced to 7%, and 20%, for these two factors, respectively, at distances up to 500 km (all distances within model domain). Overall model accuracy at distances less than 50 km for this elevated release

Accuracy for the 13 July Pittsburg surface release, however, are only within a factor of two 4%, and within a factor of ten 16%, of the time at distances less than 500 km, due to the difficulty of modeling the narrow measured plume. As only two sampler sites were available within 50 km (inadequate to fully characterize the tracer plume), no accuracy factors were calculated.

Figure 19a shows that the modeled plume for the Hayward release initially traveled eastward through the Altamont Gap, before curving to the southeast down the western SJV. The plume subsequently elongated over the SJV, with its leading edge west of Fresno and its back edge lingering in the Altamont Gap (Fig. 19b). The modeled plume is completely within the SJV, bounded by I-5 and Hwy-99 after 18 hours (Fig. 19c). Measurements over the southern SJV show the model advecting the plume too slowly, as in the previous Pittsburg releases. Modeled plume locations qualitatively match

measured tracer data through most of the model run, until measurement data for this tracer became sparse after 1900 UTC on 28 July (Fig. 19d). The modeled plume best matches the latitudinal extent of the measured tracer plume, although its width (generally comparable to the Pittsburg releases) is still somewhat too narrow.

Time series comparisons of measurement and computed values were made for six sites selected using similar criteria for the Pittsburg releases. Altamont (Fig. 20a) and Modesto (Fig. 20b) are near the release location in the northern SJV. Altamont was located on the north edge of the calculated plume, while measured data shows it having near-centerline values. Results for both of these sites, however, indicate extended periods of plume exposure. Modesto was located on the eastern edge of the calculated plume and results show an initial secondary maximum concentration at 0700 UTC, with the primary maximum at 1700 UTC, measured data also shows two peaks, but in reverse order. The two peaks (both measured and calculated) were due to the eastern edge of the plume advancing east and retreating west twice over the site.

Crows Landing (Fig. 20c) and El Nido (Fig. 20d) are mid-way down the SJV. Crows Landing was located near the south edge of the calculated plume, while measured data again (as at Altamont) indicates near-centerline values, results at both sites show extended plume exposures similar to Altamont and Modesto results. Predicted values at El Nido, near the calculated plume centerline, match measurement data for time of exposure, maximum concentra-

tion, and total dosage. Maximum values are, however, slightly over-predicted, similar to the Pittsburg releases, but to a lesser extent.

Mendota (Fig. 20e) and Calfax/Turk (Fig. 20f) are located towards the southern end of the valley. Results for Mendota, at the western edge of the calculated plume, shows under-predicted concentration values (similar to Altamont and Crows Landing), again due to inadequate latitudinal plume-spreading (although less than for the Pittsburg releases); however, plume timing was correctly modeled. Calfax/Turk (near calculated plume centerline) value results matches measurement data, but with a slight over-prediction (similar to El Nido). While the Hayward release shows the best latitudinal plume spread, comparisons at sites near the plume centerline and edge still indicate some inadequate latitudinal spread.

Figure 21 compares 56 matched pairs (selected as in Fig. 16). It shows data grouped near the factor 1 line due to the better simulated plume latitudinal spread of this case, but still with a slight under-prediction bias. The model was accurate within a factor of two 15%, and within a factor of ten 45% of the time for distances less than 500 km (best statistical results of study).

The modeled plume for the Modesto release initially moved southeastward down the SJV (Fig. 22a) with the surface wind flow. Tracer data again indicates an under advected plume with an under predicted lateral extent (Figs. 22b and c). Additionally, the modeled plume became elevated (not shown), and thus near surface concentrations were low. After 18 hours, however, the elevated section of the plume moved southward and mixed down-

wards over the southern SJV, producing too high surface concentrations at Buttonwillow (but not at Oildale) by 2300 UTC on 28 July (Fig. 22d). Concurrently, the section of the plume south of Fresno began to move northeastward up the Sierra foothills, associated with afternoon up-slope flow.

Due to limited measurements, only four sites were selected for time-series comparisons (same criteria for Pittsburg and Hayward releases). Results for Turlock-Monte Vista (near release location and close to calculated plume centerline) show good plume timing, but the same over prediction as in the Pittsburg releases (Fig. 23a). The Hanford site results (Fig. 23b) mid-way down the valley shows a time-lag and under-prediction, again similar to the Pittsburg releases. Over the southern SJV, results for Oildale (Fig. 23c) shows two separate measured plume maxima, i.e., at 1900 and 2300 UTC. While ARAC calculations match the second maximum (associated with the downward mixing of the elevated plume) with only a small time lag, they do not capture the first one. Results at the single available data point for Buttonwillow (Fig. 23d) does, however, match the time of arrival at the surface of the maximum of the downward mixed elevated plume.

Figure 24 (only 16 matched pairs) again shows a general under-prediction of measurements, except that two high measured values near the source were closely matched. Not enough measurements were made in the plume to evaluate meaningful model accuracy for this release.

B. Case 2: 23-24 August

Four simultaneous surface tracer releases began at 1300 UTC on 23 August from sites in Bakersfield, Hayward, Pittsburg, and Fresno (Table 5). This experiment was intended to duplicate 13-14 July episode (Case 3), but with the San Jose release moved to Hayward.

At 1200 UTC on 23 August (Fig. 25a), an unseasonably strong 500 hPa trough was located over the western United States and Canada in conjunction with a ridge over the Gulf of Alaska. The trough was centered over western Alberta, with cyclonic flow extending to southern California. By 1200 UTC on 24 August (Fig. 25b), the trough axis retrograded to Victoria Island, and strong cyclonic flow covered the western United States. The 850 hPa thermal trough at 1200 UTC on 23 August (Fig. 26a) was the weakest of all four cases, and cold air advection covered northern California. By 1200 UTC on 24 August (Fig. 26b), a closed-contour 850 hPa low covered much of the western United states, with its axis over Nevada and southern California. These patterns thus resulted in strong southwesterly flow at all levels of the atmosphere during the tracer experiment.

At 1300 UTC on 23 August, modeled surface conditions (Fig. 27a) were mostly lighter and more variable over the domain than in Case 1, except for the southwesterly on-shore flow over the SFBA (associated with the upper level disturbance). This situation extended up to the 400 m AGL level (Fig. 27b). While the surface flow pattern persisted over the next six hours, the strong southwesterly flow expanded northward over the northern half of the

domain (Fig. 28) to dominate the northern and central SJV. Strong northwesterly to northerly winds, however, concurrently developed over southeastern SJV. These conditions produced a strong regionally driven flow pattern over the model domain for the duration of this case.

The modeled plume for the Pittsburg release moved to the east and north (Fig. 29a), was spread by diffusion (Fig. 29b), and then passed over the northern SJV (Fig. 29c) and over the central Sierra Nevada (Fig. 29d). Figure 30 is a time-series comparisons of calculated to measured data at four sites selected using the same criteria as for the 27 July case. All measurement sites are located south and east of the computed plume centerline. Lodi (Fig. 30a) and Collegeville (Fig. 30b) are closest to the release point, and results show a match between observed and predicted plume exposure times. Their underpredicted concentrations are, however, consistent with a predicted plume centerline displaced too far to the north and west.

Furthest downrange, Pardee Reservoir (Fig. 30c) modeled values match the observations for time of exposure, maximum concentration, and total dosage, while Angels Camp (Fig. 30d) results show under-prediction. Figure 31 compares all nine measured and calculated pairs, and shows the underprediction discussed above. As the plume passed rapidly out of the model domain in northern SJV, too few matched pairs were obtained to evaluate model accuracy.

The modeled plume for the Hayward release first moved slowly eastward (Fig. 32a), then after six hours accelerated northeastward to the northern

SJV (Fig. 32b), and then dissipated over the central Sierra Nevada (Figs. 32c and d). Six tracer sites were selected for time-series comparisons using criteria similar to previous cases. Results for Livermore (Fig. 33a) and Altamont (Fig. 33b) sites, nearest to the source, again show good timing with observed data, but under-predicted values, as the calculated plume passed just south of these sites.

Results at two sites mid-way downwind, Modesto (Fig. 33c) and Collegeville (Fig. 33d), however, also show both under-prediction and a time lag. While Modesto is on the southern edge of the calculated plume, Collegeville is nearer its centerline. But two sites at the eastern edge of the sampler network, Woodward Reservoir (Fig. 33e) and Pardee Reservoir (Fig. 33d), show excellent matches to measured data. Results at all of these sites are consistent with a simulated plume that is: 1) elevated above the boundary layer as it flows across the coastal range, 2) neither descends nor diffuses to the surface, and 3) impacts the Sierra on the eastern SJV.

Figure 34 compares 10 matched pairs, with results again indicating an under-prediction bias due to the elevated nature of the plume over most the SJV. The number of matched pairs was again not sufficient to compute statistically meaningful model accuracy.

The modeled plume for the Fresno release was initially relatively stationary (Fig. 35a), but then moved east-southeastward just south of the Kings River (Figs. 35b-d). The few available tracer data, however, indicate that the

actual plume probably moved up the Kings River, i.e., north of the modeled plume.

Due to the limited measurement data, only two (near-release) sites were selected for time-series comparisons, Fresno (Fig. 36a), and Kings River (Fig. 36b). The timing of the first (and largest) observed maximum at both sites is matched, but the secondary measured peak (14 hours after the release) is not modeled well. The secondary measured peaks are probably due to an unmodeled flow reversal. Meaningful model accuracy statistics again can not be evaluated due to the limited number of comparisons.

The modeled plume for the Bakersfield release initially barely moved (Fig. 37a), and then traveled to the east-southeastward through the Tehachapi Pass (Figs. 37b and c). Measurement data indicate that the real plume branched into two separate valleys, i.e., Tehachapi Pass (correctly modeled) and one located east-northeast of Bakersfield (not modeled). The plume then exited the model domain within 24 hours.

Due to the limited measurement data, only three sites were selected for time-series comparison, all downwind of the release point: Edison (Fig. 38a), Caliente (Fig. 38b), and Tehachapi (Fig. 38c). Results at all three sites show a match with plume timing, but over-predicted concentrations, consistent with the model plume erroneously passing through only one of the two valleys.

Figure 39 compares 19 matched pairs with results showing grouping near the factor 1 line, and no significant bias because of the confinement of

the model plume to only one valley. A sufficient number of matched pairs were again not available for meaningful model accuracy statistics.

C. Case 3: 13-14 July

Four simultaneous surface tracers releases began at 1300 UTC on 13 July from sites in Bakersfield, San Jose, Pittsburg, and Fresno (Table 6). Tracer release locations were selected to characterize both the transport of pollutants from the Bay Area to the SJV with normal on-shore pressure gradients, and in-valley transport from Bakersfield and Fresno.

At 1200 UTC on 13 July, a closed-contour high with a central height of 570 dm was centered over southern Nevada (Fig. 40a). By 1200 UTC on 14 July (Fig. 40b), the high opened into a broad ridge covering the southwestern U.S. At 850 hPa (Fig. 41a), a strong thermal trough, marked with temperatures between 25 and 30°C, covered the SJV and southern California, extended into Nevada, Utah, and Arizona; it persisted until 1200 UTC on 14 July (Fig. 41b).

Strong surface temperature and pressure gradients persisted both night and day over the duration of this release, and thus resulted in a strong observed coastal on-shore flow associated with the well-defined surface thermal trough. Wind flow patterns, however, within the SJV were less well defined and thus dominated by local effects. By 0700 UTC on 14 July, the on-shore flow did, however, extended down to the southern SJV. Strong daytime thermal heating produced deep mixing depths over the SJV, with isolated

showers and thundershowers over the Sierra Nevada and southern California midday on both the 13th and 14th.

Model results for time of release at 1300 UTC on 13 July (Fig. 42a) show the mostly on-shore surface flow conditions in the SFBA extending as far south as Pacheco Gap. Surface flow over the delta, however, curves northeastward towards Sacramento, with weak convergent wind-flow near Fresno and near calm conditions around Bakersfield. Concurrently At 400 m AGL (Fig. 42b), winds were stronger and more northwesterly over the coastal regions than at the surface. A core of on-shore flow from the Carquinez Straits extends to the vicinity of Merced, with variable wind flow patterns over the central and southern SJV. Light northerly conditions prevailed at levels above 400 m (not shown). By 0700 UTC on 14 July, the on-shore flow at 400 m AGL extended to the southern SJV (Fig. 43), producing the furthest extent of down valley winds for any case; this strong regional flow pattern prevailed for the remainder of the run.

The modeled plume for the Pittsburg release curved towards the northeast (Fig. 44a) following the surface winds, and after six hours its leading edge approached Sacramento. As elevated portions of the plume were caught in the core of upper-level northwesterly winds, Figure 44b shows that the plume elongated into a north-south orientation with maximum concentrations north of Merced. After 18 hours (Fig. 44c), the modeled plume separated into two sections, one which moved down the SJV and the other which moved eastward over the central Sierra Nevada. Six hours later, the southern sec-

tion of the plume was located over Fresno, while its northern section was over the Sierra Nevada (Fig. 44d). This splitting of the plume is similar to that of the 27 July case, although more of the plume moved north for this release. Measurements are sparse for this tracer, and include suspect data (not removed), since this was the first of four cases, and they appear around the other three release sites from this case, i.e., Fresno, Bakersfield, and San Jose.

Similarly to the 27 July case, no tracers were measured in the area of the northern plume, and six sites were selected for time-series comparisons using the same criteria as for previous cases. Of the two sites near the release point, Altamont was near the plume edge (Fig. 45a) and Brentwood was near its centerline (Fig. 45b). Under-prediction of concentration is seen at the plume-edge (as in previous Pittsburg cases), but a match with timing, plume exposure, and total dosage is evident at the near-centerline site.

At two sites near the model plume centerline mid-way down the SJV, Turlock (Fig. 45c) and El Nido (Fig. 45d), results again (similar to previous cases) show over-prediction due to inadequate model diffusion. Less of a time-lag is, however, evident in this release relative to previous cases. The comparison at Raisin City (Fig. 45e) show measured peak values close to calculated values, with a two-hour time lag (less than in previous cases). The (southern most) Delano site (Fig. 45f) results show two measured peak values, but calculated values are close in time and maximum concentrations for only the second peak. Model results due not indicate that the plume reached the southern SJV in time for the first observed maximum, and this disagreement

is inconsistent with the good results obtained at the other sites. The time lag at all the other sites is smallest for this case, due to the penetration of the strong on-shore flow through the length of the SJV.

Figure 46 compares 39 matched pairs, again indicating an under-prediction bias. The latitudinal extent of the plume is wider than for previous Pittsburg releases, but is still insufficient. A total of 107 matched pairs were used to calculate statistical ratios. Figure 47 indicates that the ratios of all matched pairs at distances up to 50 km, the model was accurate within a factor of two 22%, and within a factor of ten 44%, of the time. Accuracy was reduced to 12%, and 22%, respectively, for distances up to 500 km.

The modeled plume for the San Jose release remained nearly stationary for the first six hours (Fig. 48a), then moved slowly southeastward down the Santa Clara Valley (Fig. 48b), and then entered the SJV through the Pacheco Pass (Fig. 48c). Only the Morgan Hill site reported any measurements of this tracer. Figure 49 shows that the maximum calculated value is within a factor of two of the measured value, but that the duration of plume exposure is significantly longer than observed. It is not possible to calculate model accuracy statistics from the single measurement point.

The model produced a plume for the Bakersfield release that initially traveled slowly to the northwest (Fig. 50a), then back over the site (Fig. 50b) and then finally passed just north of the Tehachapi Pass (Fig. 50c) in association with the weak surface and upper-level flows. Measurement data show that the simulated southeast plume travel was too slow, and similarly to the

23 August case, the real plume appears to have branched into several valleys, including the unnamed valley to the east, Tejon Pass to the south, and additionally, northward towards Fresno.

Due to the limited number of measurements, only two sites (on the southern edge of the modeled plume) were selected for time-series comparisons. Results from the Caliente site (Fig. 51a) shows two peaks in the measurement data, while calculations show only a single peak, extended exposure to the slow-moving simulated plume, and a four-hour time-lag; the Tehachapi site results (Fig. 51b) also indicates a four-hour delay. Unlike the 27 July case, model values were under-predicted at both sites, even though the simulated plume was transported in only one direction.

Figure 52 compares the 12 matched pairs, and again indicates a bias for under-prediction. Statistical results based on 50 matched pairs are poor for this case, and show the model is accurate within a factor of two only 2%, and within a factor of ten only 6%, of the time.

The limited measurements indicate that the real plume for the Fresno release moved northeastward from Fresno towards the southern Sierra Nevada, while the model plume traveled parallel to the mountains towards the southeast and south (Figs. 53a-c). Surface wind-flow is initially weak and locally-driven at the release point, but as the run progressed, they increased and became first northwesterly and then northerly. Winds aloft were also northwest or northerly, and thus the analyzed meteorological data did not resolve

the required up-slope flow. No meaningful model accuracy statistics can be evaluated due to the lack of tracer matches.

D: Case 4: 3-4 August

The high SJV ozone concentrations during this period resulted in the most extensive analysis and modeling studies by other researchers, including the modeling of two of the tracer releases. Four simultaneous surface tracer releases began at 1300 UTC on 3 August from the same Case 3 sites (Table 7).

Similar to the synoptic conditions on 27-29 July (Case 1), a 500 hPa ridge built over the western United States, and at 1200 UTC on 3 August (Fig. 54a) its axis laid along the west coast. By 1200 UTC on 4 August (Fig. 54b), the axis moved inland and heights rose significantly over the Pacific Northwest and western Canada. Figure 55a shows the 850 hPa ridge at 1200 UTC on 3 August built eastward over the Pacific Northwest. As a result of the ridging, low heights extended westward (off the coast) from the desert southwest over southern and central California. By 1200 UTC on 4 August (Fig. 55b), a closed-contour 850 hPa ridge had built into the Pacific Northwest, southwestern Canada, and the northern plains states. The thermal trough continued to cover southern California and Arizona, extending off the coast.

The synoptic pattern produced a moderate, on-shore flow near the surface, and slightly off-shore flow above the PBL, particularly over southern California. Surface heating produced a moderate thermal trough in the SJV on both the 3rd and 4th, and resulting pressure and temperature gradients

produced moderate daytime surface on-shore flow. Weaker gradients produced less surface on-shore flow during the night of the 3rd.

Modeled surface winds at 1300 UTC (time of release) on 3 August (Fig. 56a) show a weak flow over much of the domain, except areas of moderate on-shore flow through the Carquinez, Altamont, and Pacheco gaps. Northwesterly flow predominates over the SJV, except over its eastern and southern sections where light and variable conditions prevail. Concurrently at 400m AGL (Fig. 56b), anticyclonic flow dominates the Pacific and coastal regions south of the SFBA. Moderate on-shore flow at this level over Carquinez Strait diverges north and south against the Sierra foothills. Northwest flow covered the northern and central SJV, with an eddy visible southeast of Fresno. Above 400 m (not shown), winds became light and disorganized, except for continued anticyclonic flow over the Pacific and coastal range, with easterly flow at most levels over Nevada. Similar conditions prevailed throughout the period, including development at 500 m AGL of another Fresno eddy at 1900 UTC on 4 August (Fig. 57).

The modeled plume for the Pittsburg release moved due east until the vicinity of Stockton (Fig. 58a), where it turned towards the southeast (Fig. 58b) and then followed the Sierra foothills down the length of Highway 99 to Bakersfield (Fig. 58c). Qualitative results show a match with measured tracer data until the plume reached the vicinity of Fresno, with the largest latitudinal extent of all cases. The modeled plume, however, became dispersed after 24 hours (Fig. 58d), and did not travel as far south as indicated by the tracer data.

Additionally, south of Fresno, the modeled plume slows on the eastern side of the SJV and then returns northward due to the development of the 4 August Fresno eddy.

Six sites were selected for time-series comparisons using criteria from the previous cases. Results for Brentwood (Fig. 59a) and Turlock Lake (Fig. 59b), both near the release point and the model plume centerline, show over-predicted values as seen in previous cases. Three sites were selected for the mid-valley region of this release, and results for Raisin City (Fig. 59c), near the model plume centerline, shows the over-prediction of the first two sites.

Note Fresno (Fig. 59d) and Kings River (Fig. 59e) are displayed with extended time scales. Fresno was located near the model plume centerline, and results show a match with the first observed peak, but not with the second peak associated with the 4 August Fresno eddy. Kings River was also located near the modeled plume edge, and results also show under-predicted values. Measured and calculated data show extended tracer exposure, with two peaks. All three sites indicate a time-lag, as seen for similar (previous cases) mid-valley site results. Only one near-centerline site, Bakersfield (Fig. 59f), was selected for the southern SJV. Results show a time-lag for the modeled plume, shorter duration of exposure, and over-predicted values (but within a factor of two).

Figure 60 compares 93 matched pairs, and again indicates model under-prediction, even with the largest latitudinal spread. Figure 61 shows model accuracy factors computed using ratios obtained from 210 matched pairs for

ranges of 50 and 500 km. Model accuracy was within a factor of two 18%, and within a factor of ten 40%, of the time at distances up to 50 km. Model accuracy, however, decreased to 6% and 21%, respectively, for distances up to 500 km.

Figure 62a shows the modeled plume for the San Jose release barely moved during its first six hours, but measurement data indicates it moved northeastward through the Altamont Gap and into the SJV. It then moved slowly down the Santa Clara Valley in the next six hours (Fig. 62b), but measurements indicate the real plume was only located south of Modesto. After a total of 18 hours (Fig. 62c), the modeled plume finally entered the SJV through the Pacheco Gap, while measurements indicate that it was already in the vicinity of Fresno. After 24 hours, the modeled plume dissipated over the western SJV, while measurements show the plume still only over the southern SJV (Fig. 62d). As the observed meteorological data did not resolve the required flow out of San Jose through the Altamont Gap, no meaningful model accuracy statistics can be made.

The model plume for the Bakersfield release again barely moved after six hours (Fig. 63a), then moved to the southeast after 12 hours (Fig. 63b). Measurements, however, indicate that the plume moved both there and up the valley east of Bakersfield, as seen in the previous two Bakersfield cases. After 18 hours (Fig. 63c), the modeled plume moved slowly southeast, while measurements indicate the plume both there and still lingering near Bakersfield, consistent with a persistent unmodeled near-calm pattern. The

model plume exited the domain after 18 hours. Figure 64 compares the 14 matched pairs, and with the exception of the near-source sites, poor results are evident, due to the unmodeled branched and lingering plume situation. An insignificant number of matched pairs was obtained for this release for statistical analysis of model accuracy.

Model calculations show that the plume for the Fresno release moved slowly southeastward along the Sierra mountains (Figs. 65a-d), similar to the 13 July Fresno case, but the limited tracer data indicates that the plume moved due east. Meteorological observations did not produce the required degree of up-slope flow, but instead generated a cross-slope flow. Therefore model accuracy can not be evaluated for this case.

5. CONCLUSION

The ARAC-2 operation emergency response diagnostic models were used to simulate the 1990 SARMAP field experiment. This experiment included four tracer releases during each of four intensive-data collection periods. The MATHEW/ADPIC codes were used, with 5.5 km horizontal and 100 m vertical grid spacing, over a 440 by 440 km by 3000 m domain centered over the SJV. Observed meteorological surface and upper-air data from over 160 mast (taken hourly) and almost 50 upper-air sites (taken every 3-6 hours), were interpolated to model grid points every hour. These winds were mass adjusted over block-cell terrain using a Conjugate-Gradient solution to MATHEW. Each tracer release was simulated using 50 000 marker particles.

Horizontal and vertical dispersion, mixing layer height, PBL height and stability, and surface roughness values were selected to best match the SJV, and thus may not represent conditions away from the Valley.

The ARAC-2 models were evaluated against tracer measurement data obtained from a sampler network of only 72 fixed surface-based samplers over the large study area. For most simulations, usually less than five measurement points with non-zero values were available to characterize tracer plumes during any given two-hour time period. The widely scattered site locations, combined with some probably spurious data (not removed from simulations), made it difficult to accurately locate measured plume centerlines and estimate total spatial coverage. Ratios of measured and calculated 2-hour average air concentrations paired in space and time at all available sampler sites were used to quantify model accuracy.

Results depend on wind flow patterns at the time of release. When regional flow patterns were moderate to strong and well defined (27 July elevated release from Pittsburgh, and 13 July and 3 August surface Pittsburg releases), model results were comparable to previous ARAC-2 model evaluation studies at ranges up to 50 km, as expected. When meteorological data density was sufficient to accurately model wind fields, the modeled plume matched measured data up to, and in some cases, beyond 50 km; this was better than expected at such large distances. However, for most Pittsburg, Hayward, and Modesto releases the model lagged the measurements over the course of the run due to vertical smoothing of faster upper-air data and speed

reductions associated with the achievement of mass consistency. Results in these cases were not as good as expected. A decrease in vertical grid spacing would better resolve the low-level jets that are confined within shallow layers.

Model results were poor when light to near calm winds and poorly defined flow patterns prevailed at the time of release. In some cases, the modeled plume traveled in the wrong direction because the release occurred into a diffluent zone, e.g., Bakersfield releases showed evidence that the plume branched into several different valleys, while the predicted plume traveled into only one. In other cases, flow patterns at the time of release were variable, with locally generated heat flows, not accurately resolved by the observations; consequently the modeled plume traveled in the wrong direction, e.g., the Fresno and 3 August San Jose releases. In most of these cases, no quantitative comparisons could be made because of too few measured tracer plume data points.

Time-series analyses of measured and calculated concentrations showed a tendency for the model to over predict concentrations at sites near the modeled plume centerline and, under-prediction at sites near the plume edge. Additionally, scatter-plots of measured and calculated values (when both measured and calculated values are greater than zero) indicate an overall model bias toward under-prediction. Because ADPIC produces homogeneous vertical plumes in the boundary layer, these two results are consistent for dispersion parameters that produce inadequate horizontal spread (and

thus a too-narrow plume) on the macro-γ (100-500 km) scale. Parameters used for this study were the default meso-γ to meso-β (1 to 90 km) scale values, and not the ones used for longer range macro-α to macro-β (2000-10 000 km) scale simulations, that produce greater horizontal spread. Development of a new middle-range diffusion parameter is needed. Based on a given simulation, horizontal diffusion parameters could be automatically determined as a function of grid-scale in ADPIC, as formulated by Pielke (1984). Sensitivity studies should be carried out to evaluate impacts from uncertainties in various input parameters.

This study produced a new baseline performance value for the ARAC-2 models up to 500 km. Table 4 summarizes six cases in which a significant number of matched measured-computed concentration pairs were available. Based upon these cases, the ARAC-2 models were accurate within a factor of two 10% and within a factor of ten 30% of the time on the 500 km scale. Statistical results of this order are not unexpected due to the scale of the simulation, fixed grid-wide model atmospheric stability parameters (mentioned above), density of sampler network, complex meteorology, and complicated terrain. While these values are low, qualitative evaluation of location and timing of the modeled plume and measurement data generally indicate better model performance. Improvements in the results can be expected after development of appropriate horizontal dispersion parameters for this scale.

Future work on 1990 SARMAP database could include modeling individual releases on domains scaled to fit the region of interest. The San Jose,

Bakersfield and Fresno releases that were poorly modeled could be run on smaller domains, with appropriate boundary layer dispersion parameters.

The Department of Energy Office of Emergency Response is supporting a complete upgrade and modernization of the ARAC models. As part of this multi-year effort a new diagnostic model suite ARAC-3 (LODI/ADAPT) is under development. Improvements include continuous terrain, meteorological input (both diagnostic and prognostic winds), and dispersion code formulation. The current study, as well as other previous ARAC-2 model evaluation studies, will be re-run using ARAC-3 models.

In addition to the new diagnostic models, ARAC is implementing a prognostic model program based on the Navy Operational Regional Atmospheric Predictions System (NORAPS) hydrostatic model and the Coupled Ocean-Atmosphere Model Prediction System (COAMPS) non-hydrostatic model. All cases studied could be re-simulated to both evaluate the prognostic codes and to improve model results in regions of poorly defined wind flow, or those dominated by local effects.

REFERENCES

ARAC 1996: User's guide to the CG-MATHEW/ADPIC models. UCRL-MA-103581 Rev 4, Lawrence Livermore National Laboratory, Livermore, CA., 255 pp.

Boughton, B.A., Delaurentis, J.M., and Dunn, W.E., 1987: A stochastic model of particle dispersion in the atmosphere. *Boundary-Layer Meteor.*, **40**, 147-163.

Draxler, R.R., 1976: Determination of atmospheric diffusion parameters. *Atmospheric Environment*, **10**, 99-105.

Ermak, D.L., 1992: Dense-gas dispersion advection-diffusion model. UCRL-JC109697, Lawrence Livermore National Laboratory, Livermore, CA., 100 pp.

_____, and Nasstrom, J.S., 1994: Numerical simulation of the langevin equation for skewed turbulence. UCRL-JC-118404, Lawrence Livermore National Laboratory, Livermore, CA., 7 pp.

Foster, K., 1994: RAS division model evaluation database description. UCRL-ID-118631, Lawrence Livermore National Laboratory, Livermore, CA., 20 pp.

_____, and Dickerson, M., 1990: An updated summary of MATHEW/ADPIC model evaluation studies. UCRL-JC-104134, Lawrence Livermore National Laboratory, Livermore, CA., 28 pp.

Golder, D., 1972: Relationships among stability parameters in the surface layer. *Bound.-Layer Meteor.*, **3**, 47-58.

Hanna, S.R., Briggs, G.A., and Hosker, R.P., Jr. 1982: Handbook on atmospheric diffusion. DOE/TIC-11223, U.S. Dept. of Energy, 102 pp.

Lange, R. (1989): Transferability of a three-dimensional air quality model between two different sites in complex terrain. *J. Appl. Meteor.*, **28**, 665-679.

Lolk, N.K., 1993: An assessment of regional transport in the Sacramento, California area using wind fields generated by a prognostic model. *AWMA Regional Photochemical Measurement and Modeling Studies Conference*, San Diego, CA., Air & Waste Manage. Assoc., 594-606.

Mulberg, E., Jackson, B., King, D., and Wheeler, N., 1993: A comparison of

three wind models for the broader Sacramento area. *AWMA Regional Photochemical Measurement and Modeling Studies Conference*, San Diego, CA., Air & Waste Manage. Assoc., 607-611.

Orlanski, I., 1975: A rational subdivision of scales for atmospheric processes. *Bull. Amer. Meteor. Soc.*, **56**, 529-530.

Pace J.C., and Nasstrom, J.S., 1997: ARAC results from phase II of the European Tracer Experiment. *Proc. Sixth Topical Meeting on Emergency Preparedness and Response*, San Francisco, CA., Am. Nuc. Soc., 521-524.

Pielke, R., 1984: *Mesoscale Meteorological Modeling*. Academic Press, 468 pp.

Rappolt, T.J. and Quan, S.L., 1992: Perflourocarbon tracer experiments performed in the San Joaquin Valley of California during the SJVAQS/AUSPEX program - summer of 1990. *85th Annual Meeting & Exhibition of AWMA*, Kansas City, MO., Air & Waste Manage. Assoc., 19 pp.

Rodean, H.C., et al., 1992: Comparison of two stochastic models of scalar diffusion in turbulent flow. UCRL-JC-110377, Lawrence Livermore National Laboratory, Livermore, CA., 4 pp.

Rodriguez, D.J., 1987: A particle-in-cell technique for simulating the long range transport of pollutants. UCRL-98418, Lawrence Livermore National Laboratory, Livermore, CA., 19 pp.

_____, and Cederwall, R.T., 1990: A preliminary evaluation of ADPIC model performance on selected ANATEX releases using observed, analyzed and dynamically predicted winds. *Air Pollution Modeling and its Applications, VIII.* H. van Dop and D.B. Steyn, Eds., Plenum Press, 439-446.

Seaman, N.L., 1995a: Influence of the boundary layer on two terrain-forced meso-circulations: The Fresno eddy and Schultz eddy. *Proc. 7th conference on Mtn. Meteorology*, Breckenridge, CO., Amer. Meteor. Soc., 358-363.

_____, Stauffer, D.R., and Lario-Gibbs, A.M., 1995b: A multiscale four-dimensional data assimilation system applied in the San Joaquin Valley during SARMAP. Part I: Modeling design and basic performance characteristics. *J. Appl. Meteor.*, **34**, 1739-1760.

Sherman, C.A., 1978: A mass-consistent wind model for wind fields over complex terrain. *J. Appl. Meteor.*, **17**, 312-319.

Smith, T.B., and Lehrman, D.E., 1993: Long-range tracer studies in the San Joaquin Valley. *AWMA Regional Photochemical Measurement and Modeling Studies Conference*, San Diego, CA., Air & Waste Manage. Assoc., 151-157.

Stauffer, D.R., 1995: Multiscale dynamic analysis of meteorology in complex terrain for air-quality applications, *Proc. 7th conference on Mtn. Meteorology*, Breckenridge, CO., Amer. Meteor. Soc., 345-353.

Sugiyama, G., Lee, R.E., and Walker, H., 1994: Conjugate gradient MATHEW. UCRL-ID-118629, Lawrence Livermore National Laboratory, Livermore, CA., 29 pp.

Sullivan, T.J., Ellis, J.S., Foster, C.S., Foster, K.T., Baskett, R.L., Nasstrom, J.S. and Schalk, W.S., 1993: Atmospheric Release Advisory Capability: Real-time modeling of airborne hazardous materials. *Bull. Amer. Meteor. Soc..*, **74**, 2343-2361.

Tanrikulu, S., and Soong, S., 1991: Use of the four-dimensional data assimilation method in mesoscale meteorological models, Preprints, *7th Joint conference of Applications of Air Pollution Meteorology with AWMA*, New Orleans, LA., Amer. Meteor. Soc., J238-J241.

_____, and Stauffer, D. R., 1995: A numerical simulation of the transport of atmospheric tracers in the San Joaquin Valley of California. *Proc. 7th conference on Mtn. Meteorology*, Breckenridge, Co., Amer. Meteor. Soc., 354-357.

Thuiller, R.H., Blumenthal, D.L., Roberts, P.T., Gerlter, W.A., and Watson, J.G., 1994: Meteorological field measurement program for SJVAQS/ AUSPEX. PG&E research and development environmental health and safety report 009.2-93.4, Pacific Gas & Electric Co., San Ramon CA., 207 pp.

Thunis, P., and Bornstein, R.D., 1996: Hierarchy of mesoscale flow assumptions and equations. *J. Atmos. Sci.*, 53, 380-397.

Umeda, T., 1993: Lagrangian particle analysis of SARMAP meteorological fields. *Proc.. Regional Photochemical Measurement and Modeling Studies, Volume 2*, San Diego, CA., Air & Waste Manage. Assoc., 636-643.

_____, Bay Area Air Quality Management, cited 1996: Bay-Area north central coast photochemical modeling investigation of ozone formation and transport, Task 1 - RAMS/UAM modeling results of the 3-5

August 1990 SARMAP ozone episode [Available on line at http://sparc2.baaqmd.gov/MontereyPrj/reports/Task1/].

Table 1. ARAC-2 Model Evaluation Studies

Sponsor	Location	Date	Topography/ meteorology	Release height (m)	Sampler dist. (km)
NOAA	INEL	1971	Rolling plain Slightly unstable daytime flows	surface	5 to 90
SRP	SRP	1974	Rolling coastal plain Slightly unstable daytime flows	62	3 to 30
DOE	Three Mile Island, PA	1980	Flat river valley Daytime flows	60	1 to 8
EPRI	Kincaid, IL	1980-81	Flat Plain Day and Night flows	187	1 to 50
ASCOT	Geysers, CA	1980	Coastal interior valley Stable nocturnal flow	surface and 60	0.5 to 10
ASCOT	Geysers, CA	1981	Coastal interior valley Stable nocturnal flow	surface and 60	0.5 to 10
MATS	SRP	1983	Rolling coastal plain Slightly unstable daytime flows	62	30
ENEL	Montalto, Italy	1984	Coastal plain Unstable sea breeze	10 and 50	1.5 to 6.5
ASCOT	Brush Creek, CO	1984	Mountain valley Stable nocturnal flow	surface and 220	0.5 to 10
Riso	Oresund Strait, Denmark	1984	Neutral flow (cold water to land)	95	22 to 42
PG&E	Diablo Canyon, CA	1986	Coastal hills Neutral sea breeze	1.5 and 71	0.5 to 40
ASCOT	Rocky Flats, CO	1991	Plateau Stable and neutral flow	10	8 and 16

Table 2. Perflourocarbon Tracer Abbreviations

Tracer Chemical Name	Abbreviation	Molecular Wt.
Perflouromethylcyclopentane	PMCP	300
Perflouromethylcyclohexane	PMCH	350
Perflour-1,2-dimethylcyclohexane	PDCH	400
Perfourotrimethylcyclohexane	PTCH	450

Table 3. Case 1 (27-28 July) Tracer Release Information

Site	Time Period (UTC)	Tracer Type	Amount (kg)
Pittsburg - Elevated	2300-0300	PMCH	16.4
Pittsburg - Surface	2300-0300	PMCP	20.0
Hayward	2300-0300	PTCH	18.6
Modesto	2300-0300	PDCH	10.0

Table 4. Model Accuracy Results (cases with ≥50 total matched pairs)

Release Location	Release Height	Release Date	Wind Flow*	Number of Matched Concentration Pairs**			Accuracy within 50 km (%)		Accuracy within 500 km (%)	
				M > 0 & C > 0	M > 0 & C = 0	Total	Factor 2	Factor 10	Factor 2	Factor 10
Pittsburg	Surface	13 July	Strong	39	68	107	22	44	12	27
Bakersfield	Surface	13 July	Weak	12	38	50	0	7	2	6
Pittsburg	Surface	27 July	Moderate	51	84	135	0	0	4	16
Pittsburg	Elevated	27 July	Moderate	116	191	307	20	36	7	20
Hayward	Surface	27 July	Moderate	56	27	83	0	0	15	45
Pittsburg	Surface	3 Aug	Moderate	93	117	210	15	41	6	21

* Mean boundary layer surface flow definitions:

Weak	<5 m/s
Moderate	5-10 m/s
Strong	>10 m/s

** M = Measured concentration; C = Calculated concentration

Note: Accuracy is expressed by the percentage of the total matched pairs that fall within the specified factor. For example for the first 50 km, the 13 July Pittsburg surface release the model was accurate within a factor of 2 ratio for 22% of the 107 measured concentrations above zero.

Table 5. Case 2 (23-24 August) Tracer Release Information

Site	Time (UTC)	Tracer	Amount (kg)
Pittsburg	1300-1700	PMCP	18.9
Hayward	1300-1700	PMCH	19.1
Fresno	1300-1600	PDCH	9.8
Bakersfield	1300-1600	PTCH	10.9

Table 6. Case 3 (13-14 July) Tracer Release Information

Site	Time (UTC)	Tracer	Amount (kg)
Pittsburg	1300-1700	PMCP	20.7
San Jose	1300-1700	PMCH	19.1
Bakersfield	1300-1600	PTCH	9.5
Fresno	1300-1600	PDCH	9.5

Table 7. Case 4 (3-4 August) Tracer Release Information

Site	Time (UTC)	Tracer	Amount (kg)
Pittsburg	1300-1700	PMCP	20.5
San Jose	1300-1700	PMCH	19.1
Bakersfield	1300-1600	PTCH	9.1
Fresno	1300-1600	PDCH	9.5

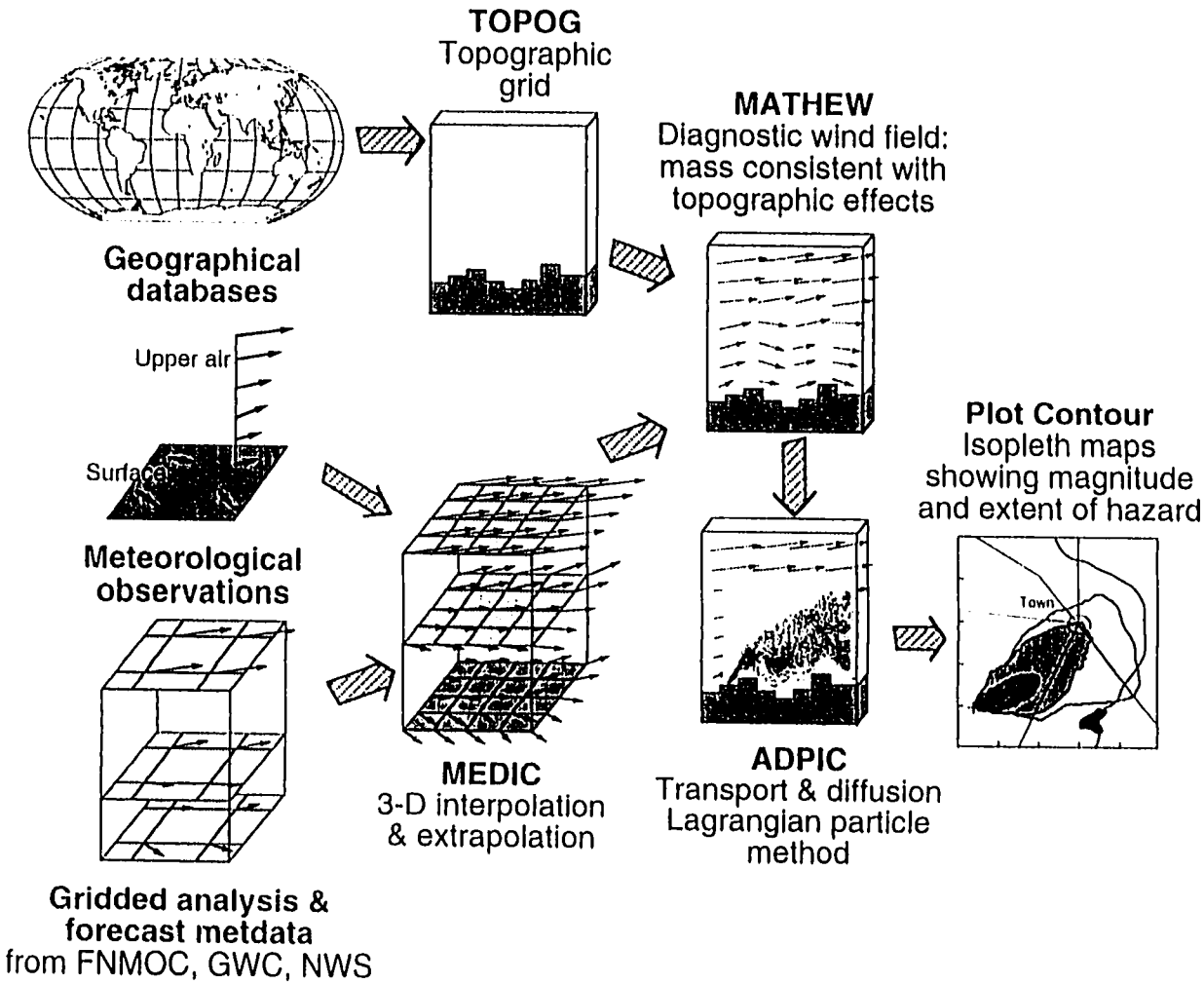
TOPOG
Topographic grid
MATHEW
Diagnostic wind field: mass consistent with topographic effects
Geographical databases
Upper air
Surface
Meteorological observations
Plot Contour
Isopleth maps showing magnitude and extent of hazard
Town
MEDIC
3-D interpolation & extrapolation
ADPIC
Transport & diffusion Lagrangian particle method
Gridded analysis & forecast metdata
from FNMOC, GWC, NWS

Fig. 1

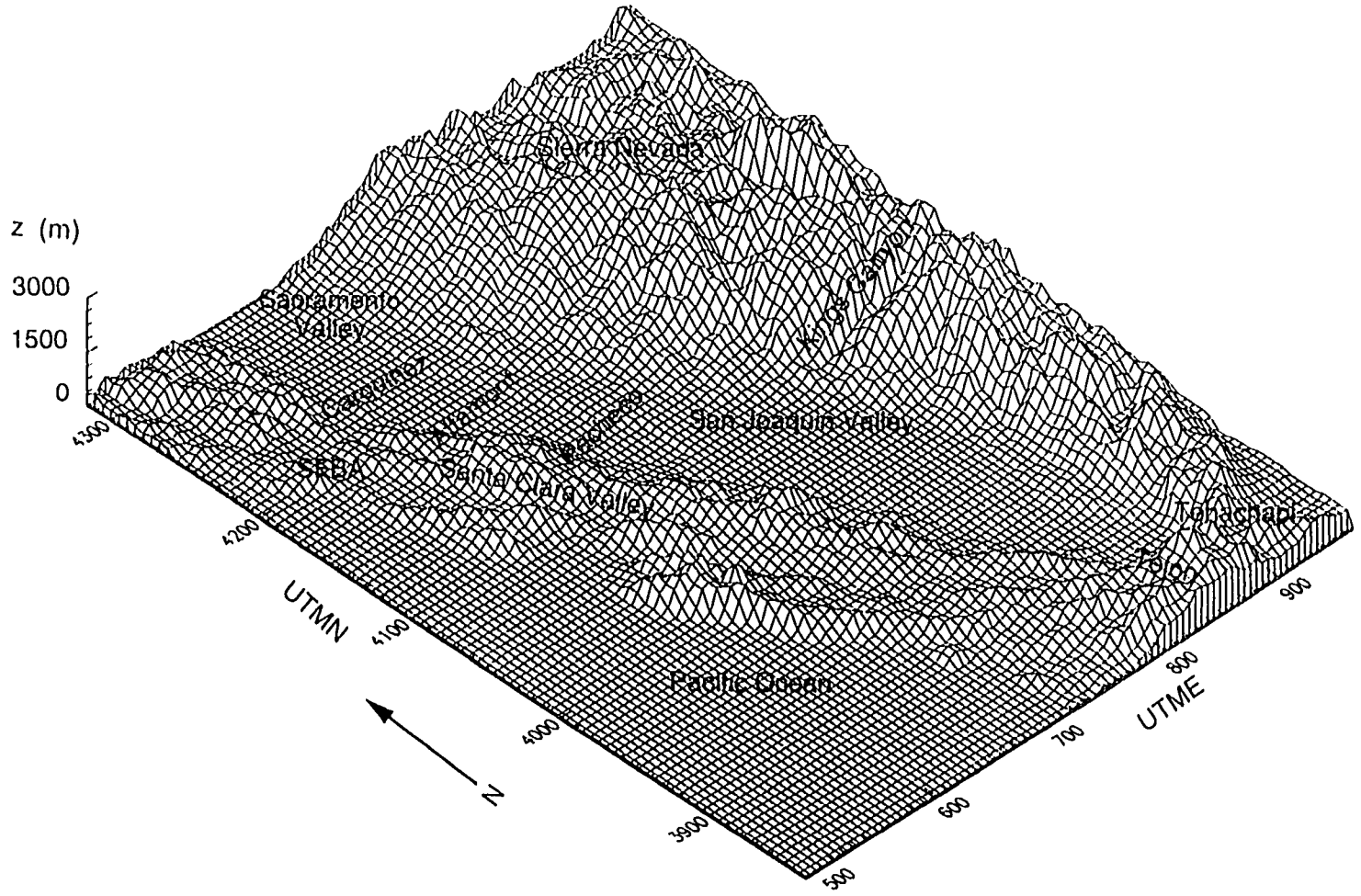
z (m)
3000
1500
0
Sacramento Valley
Sierra Nevada
Carquinez
SFBA
Santa Clara Valley
San Joaquin Valley
Tehachapi
Pacific Ocean
UTMN
4300
4200
4100
4000
3900
UTME
500
600
700
800
900
N

Fig. 2

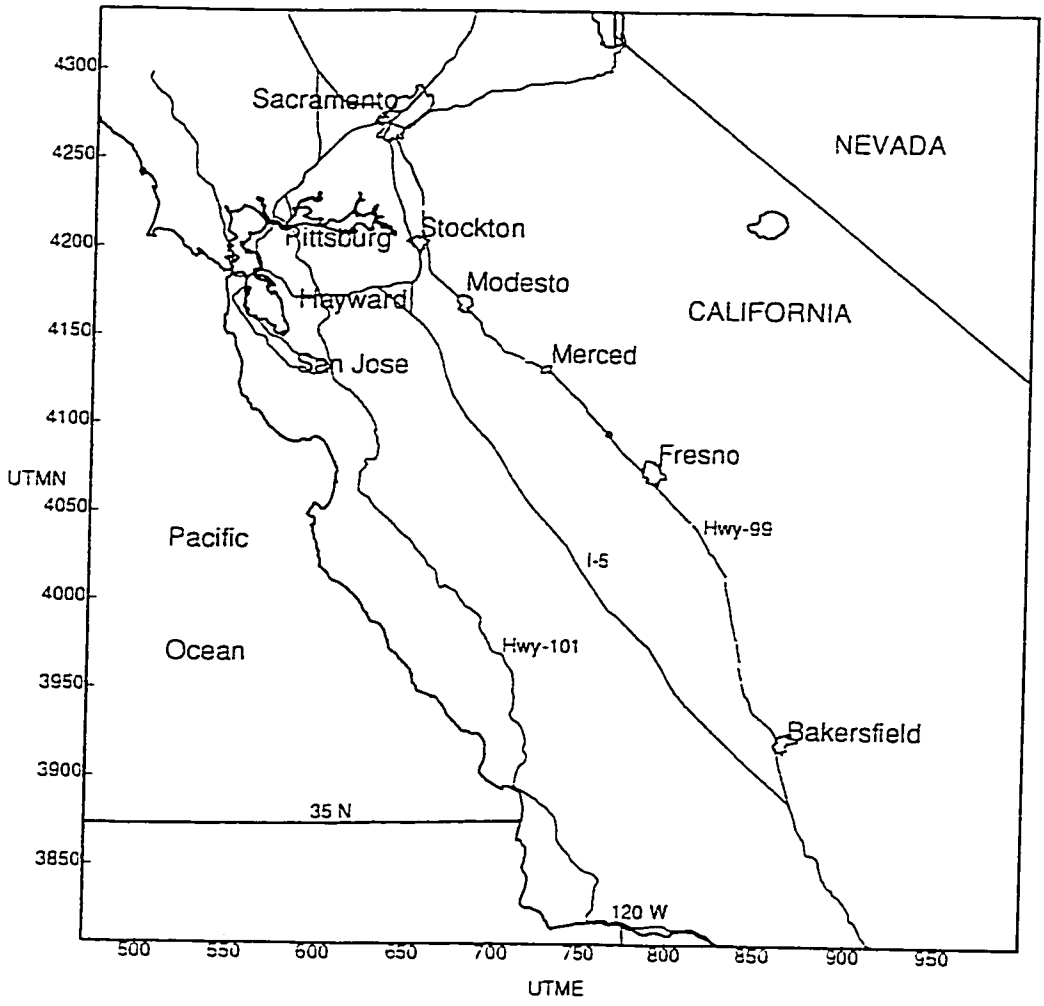
Sacramento
NEVADA
Pittsburg
Stockton
Modesto
Hayward
CALIFORNIA
San Jose
Merced
Fresno
Pacific
Ocean
Hwy-99
I-5
Hwy-101
Bakersfield
35 N
120 W
UTMN
UTME
4300
4250
4200
4150
4100
4050
4000
3950
3900
3850
500
550
600
650
700
750
800
850
900
950

Fig. 3

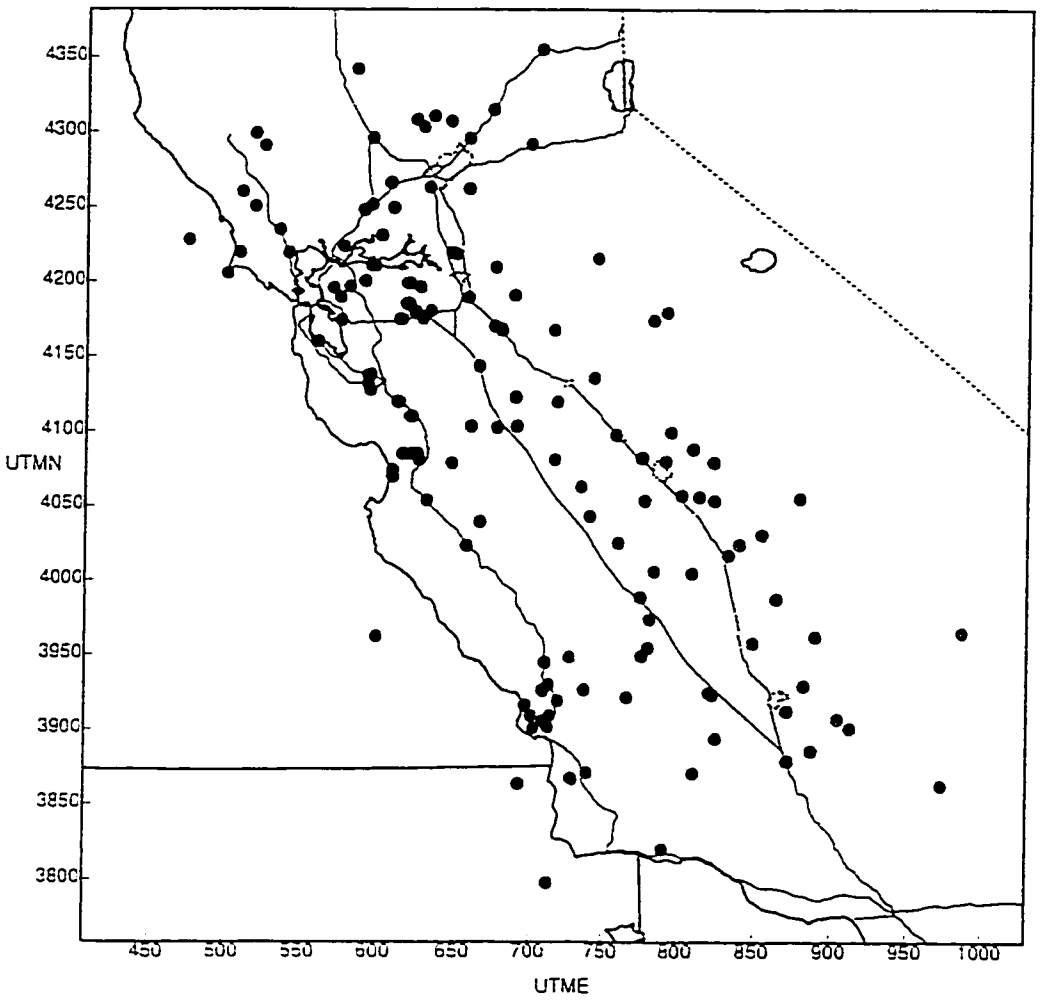
4350
4300
4250
4200
4150
4100
UTMN
4050
4000
3950
3900
3850
3800
450
500
550
600
650
700
750
800
850
900
950
1000
UTME

Fig. 4

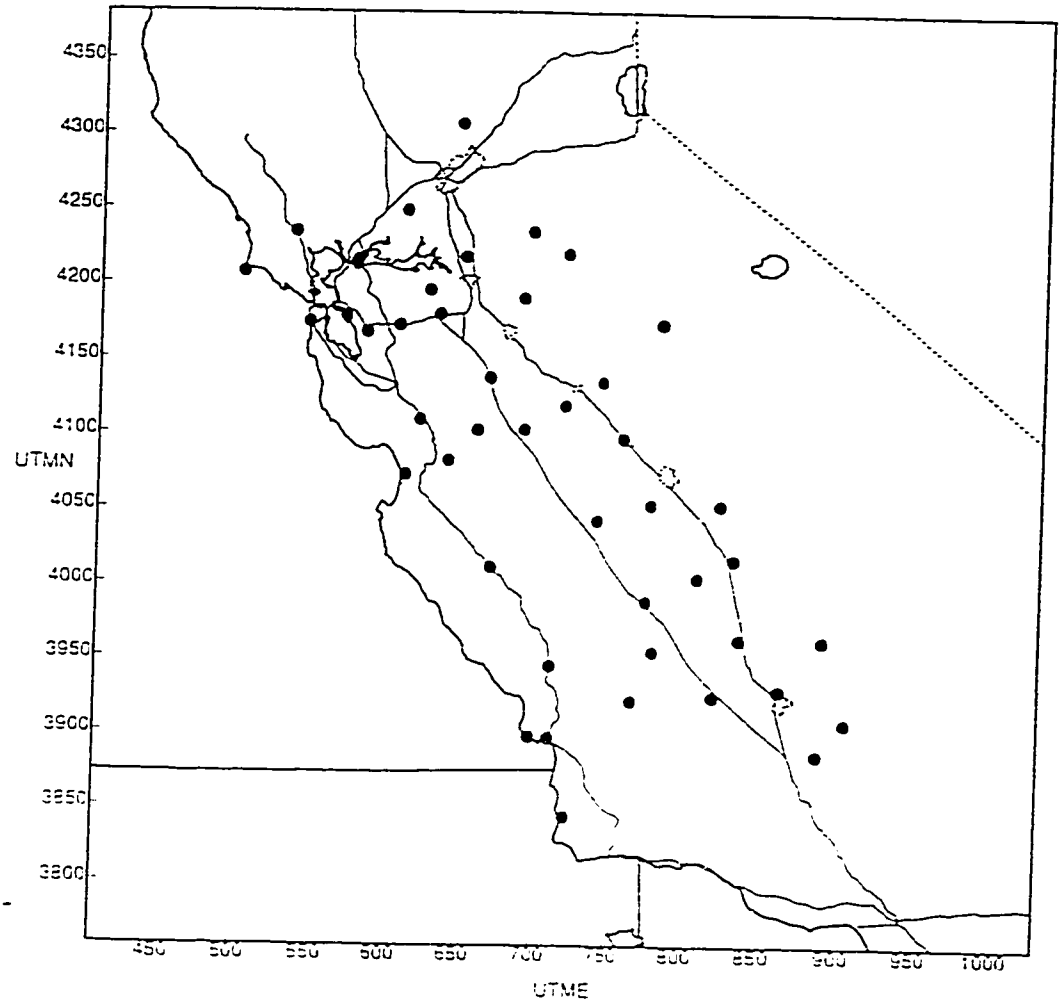
4350
4300
4250
4200
4150
4100
UTMN
4050
4000
3950
3900
3850
3800
450
500
550
600
650
700
750
800
850
900
950
1000
UTME

Fig. 5

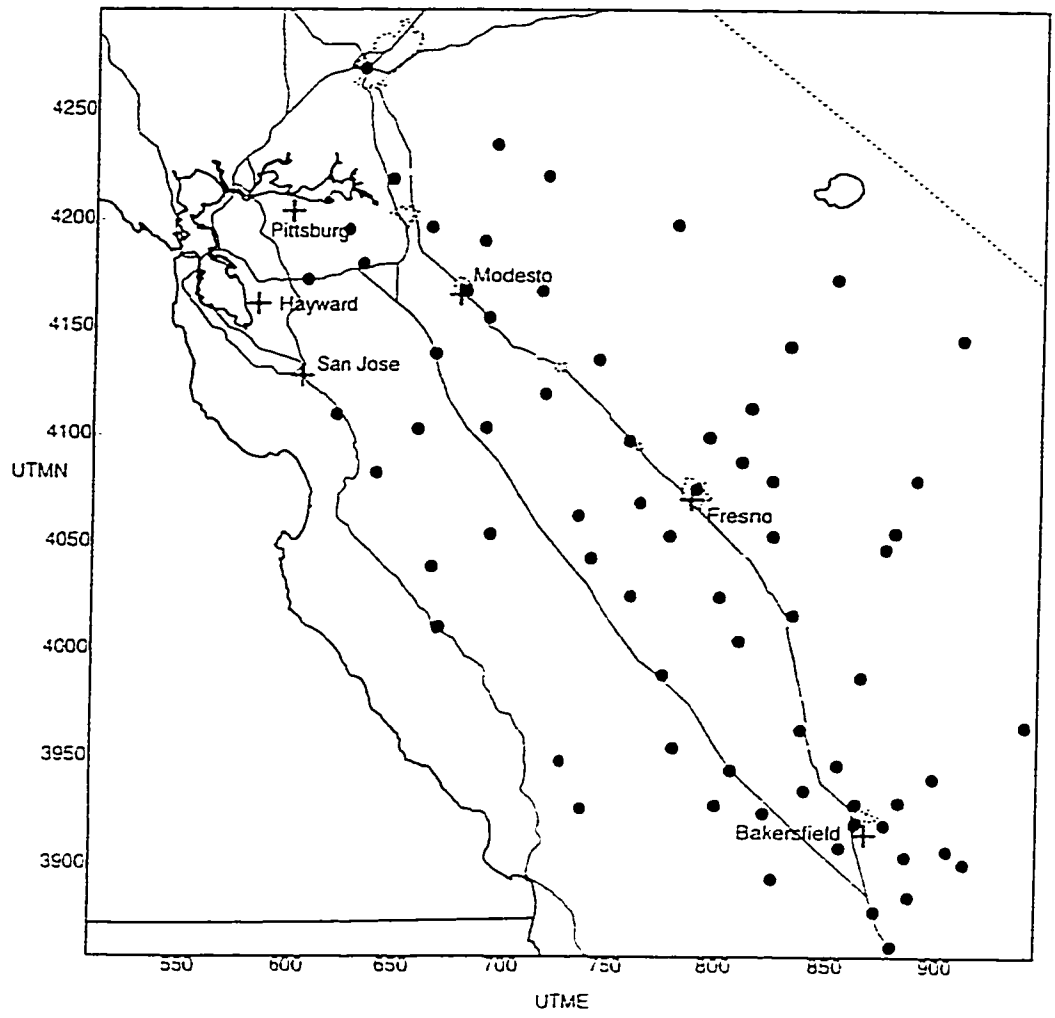
4250
4200
4150
4100
4050
4000
3950
3900
UTMN
Pittsburg
Hayward
Modesto
San Jose
Fresno
Bakersfield
550
600
650
700
750
800
850
900
UTME

Fig. 5

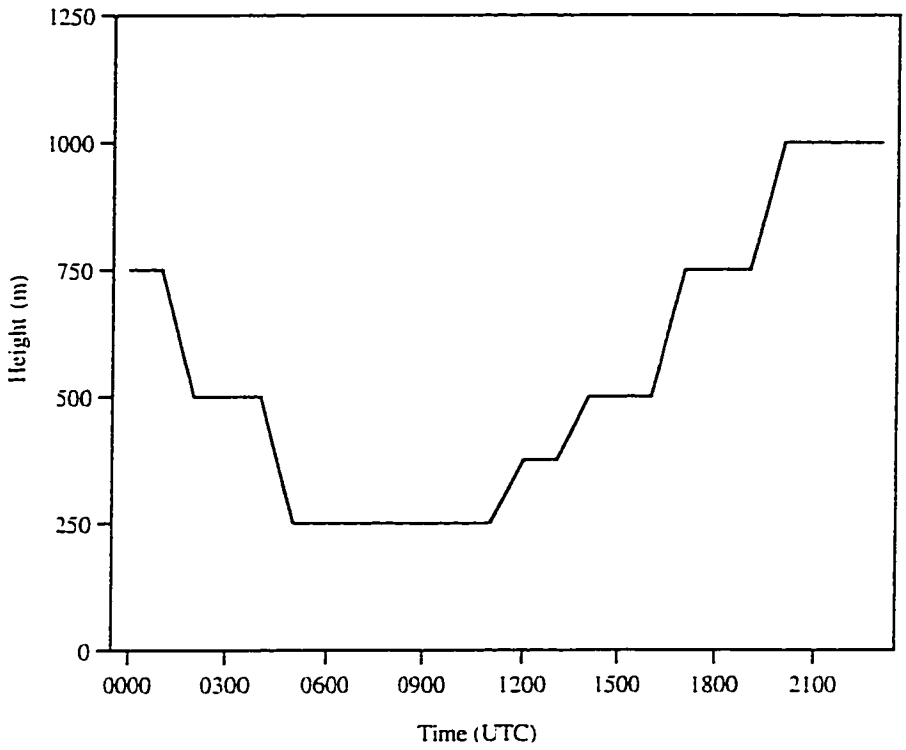
1250
1000
750
500
250
0
Height (m)
0000
0300
0600
0900
1200
1500
1800
2100
Time (UTC)

Fig. 7

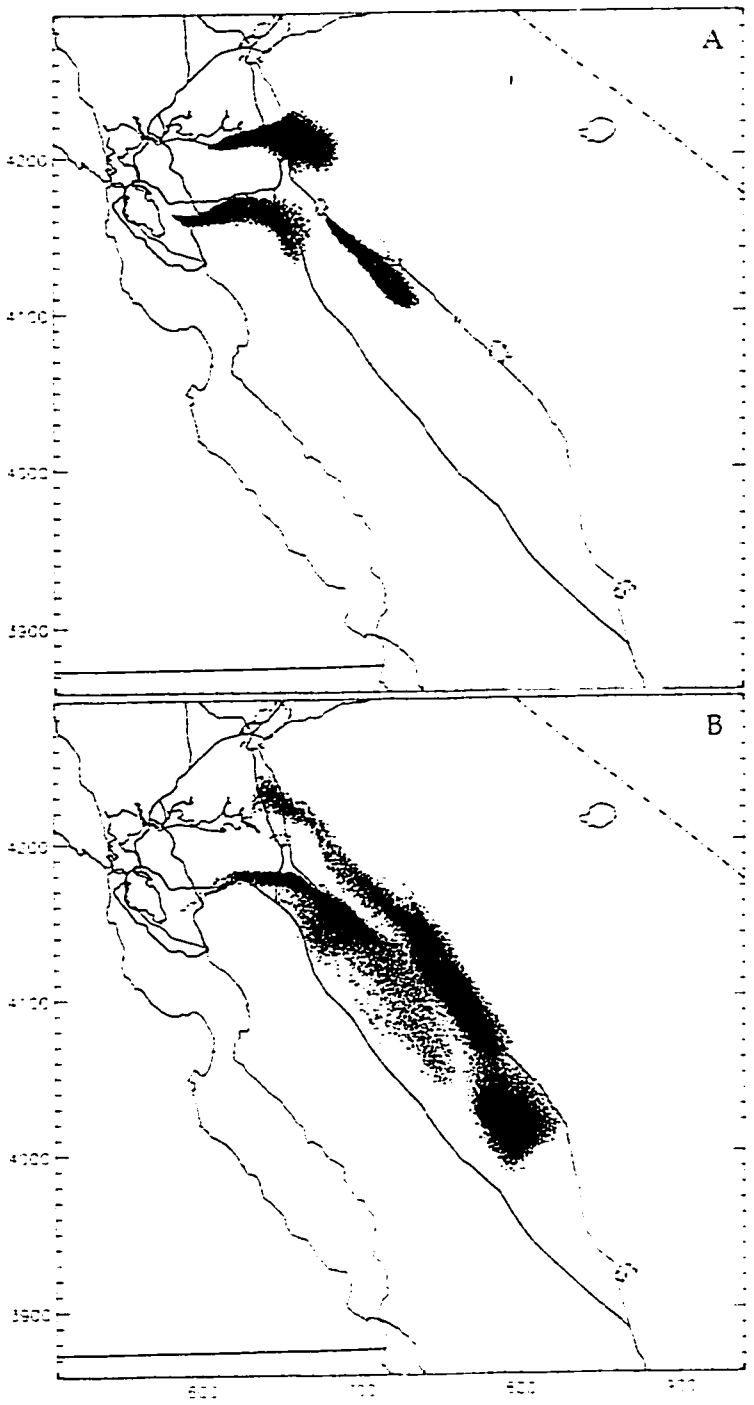

Fig. 8

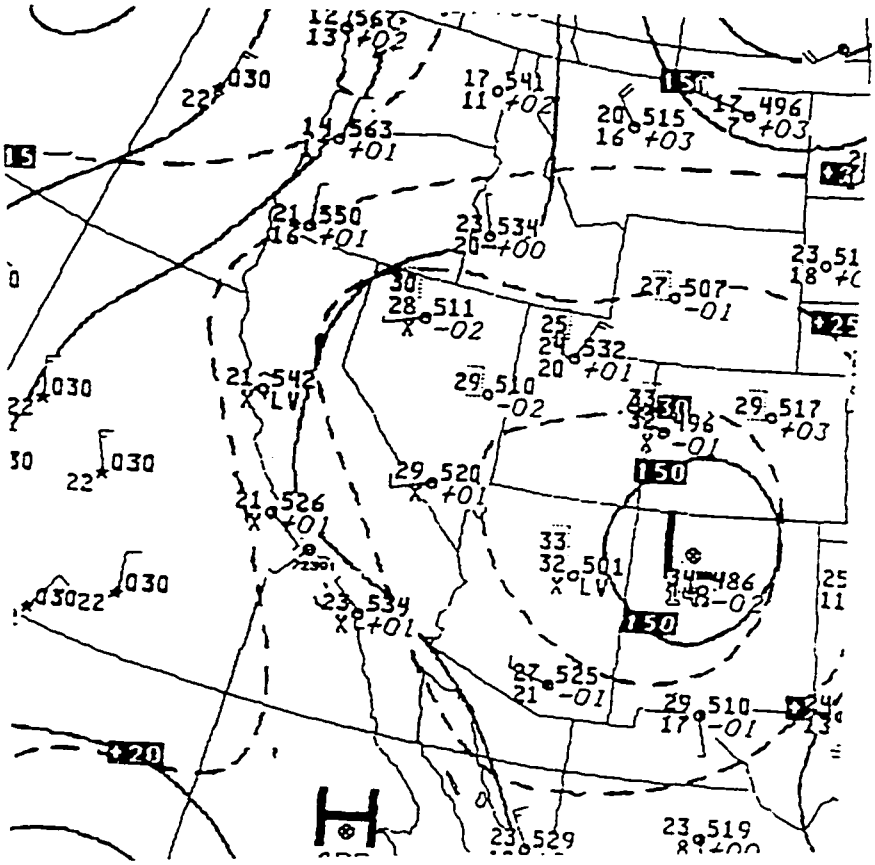

Fig. 9

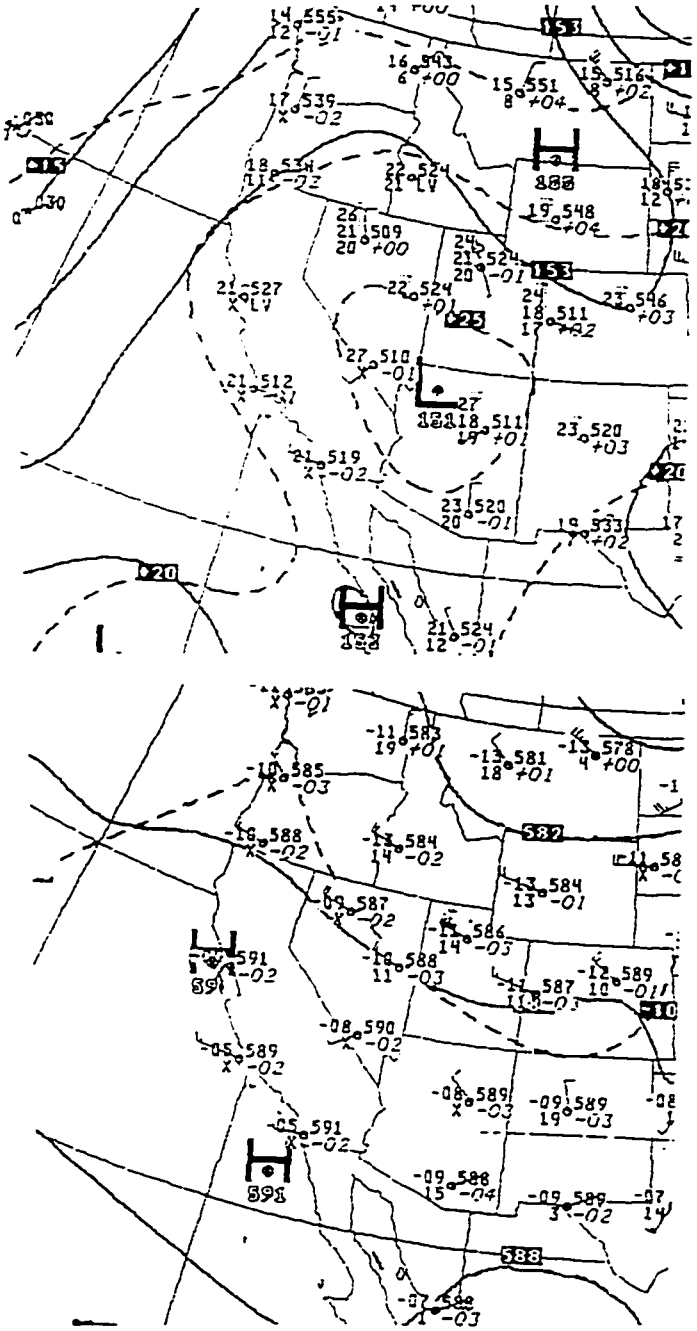

Fig. 10

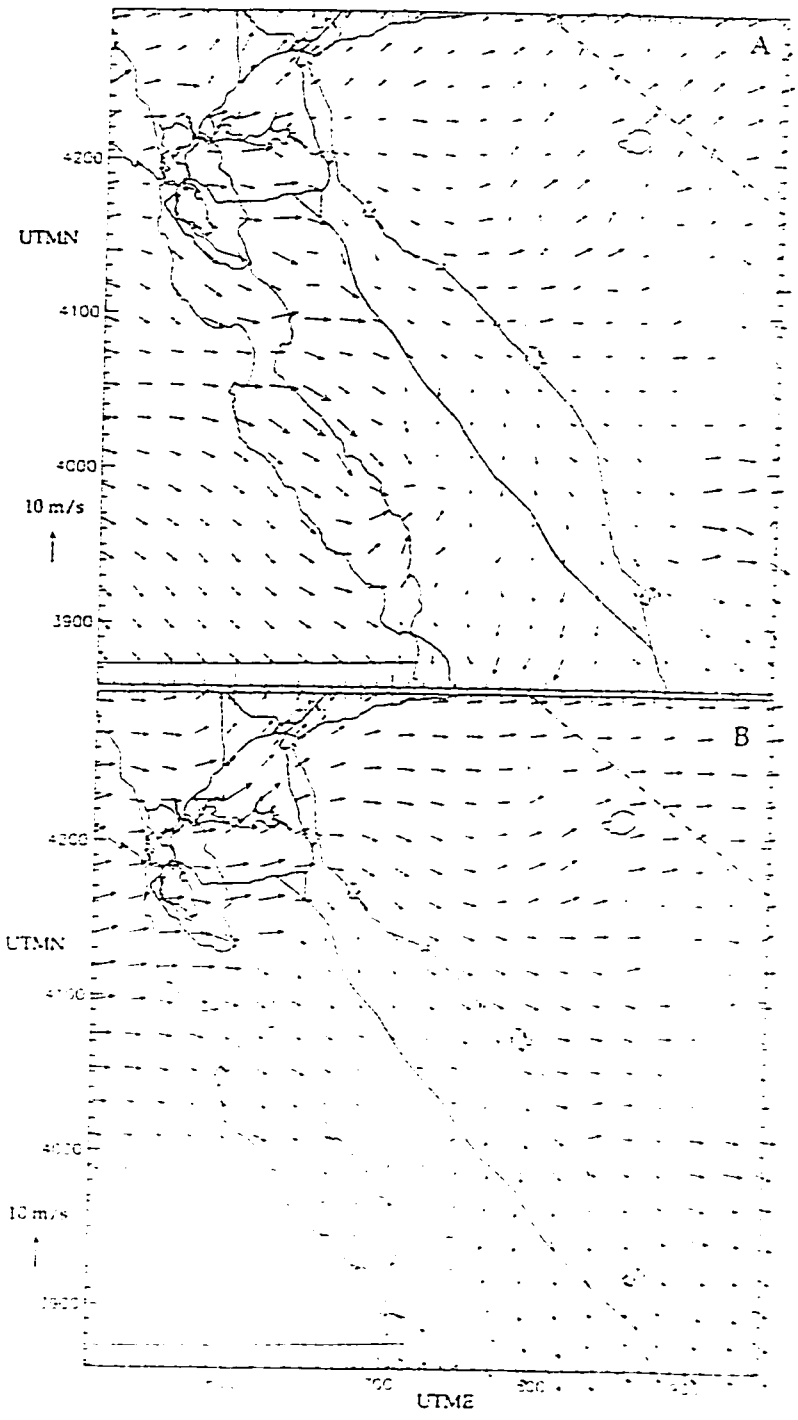

Fig. 11

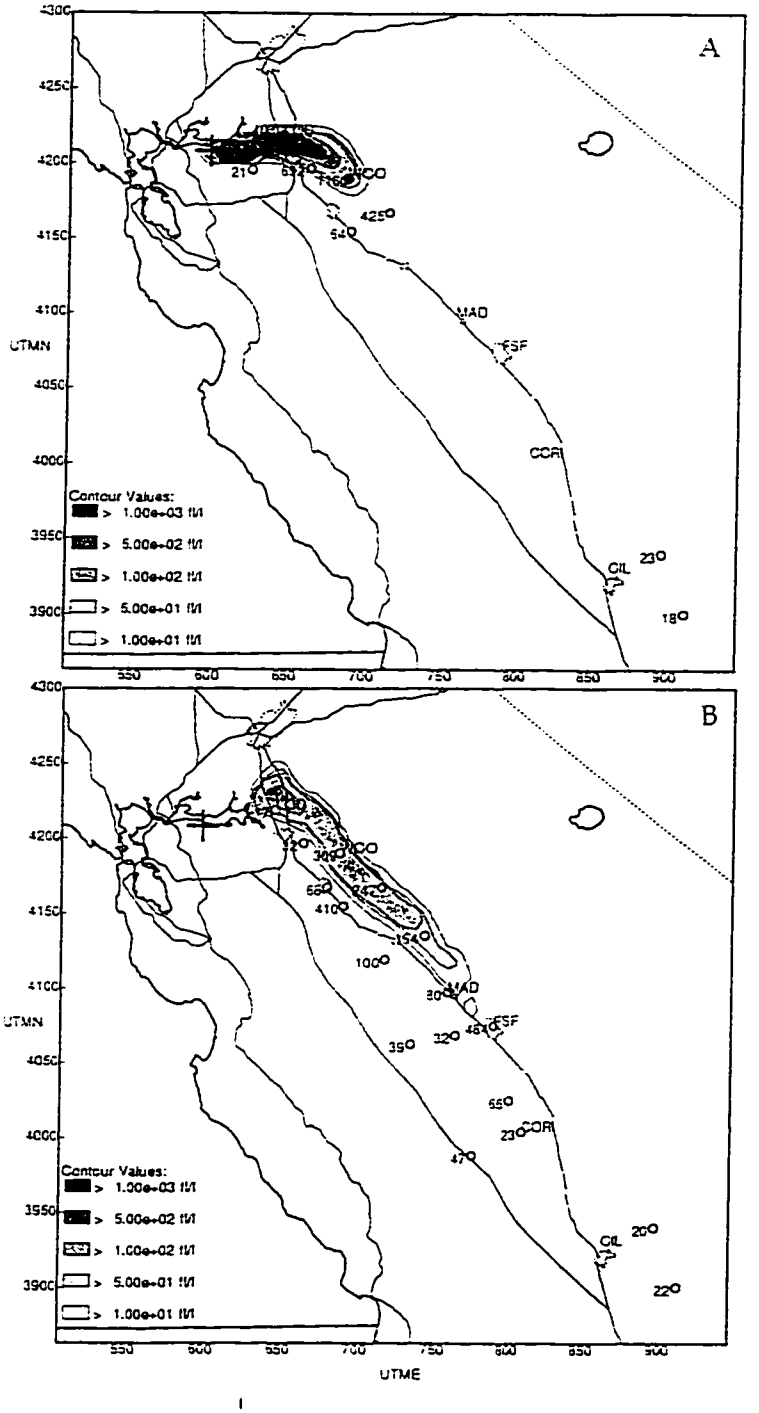
A
B
UTMN
UTME
Contour Values:
> 1.00e+03 ft/t
> 5.00e+02 ft/t
> 1.00e+02 ft/t
> 5.00e+01 ft/t
> 1.00e+01 ft/t
MAD
FSF
CORI
CIL

Fig. 12

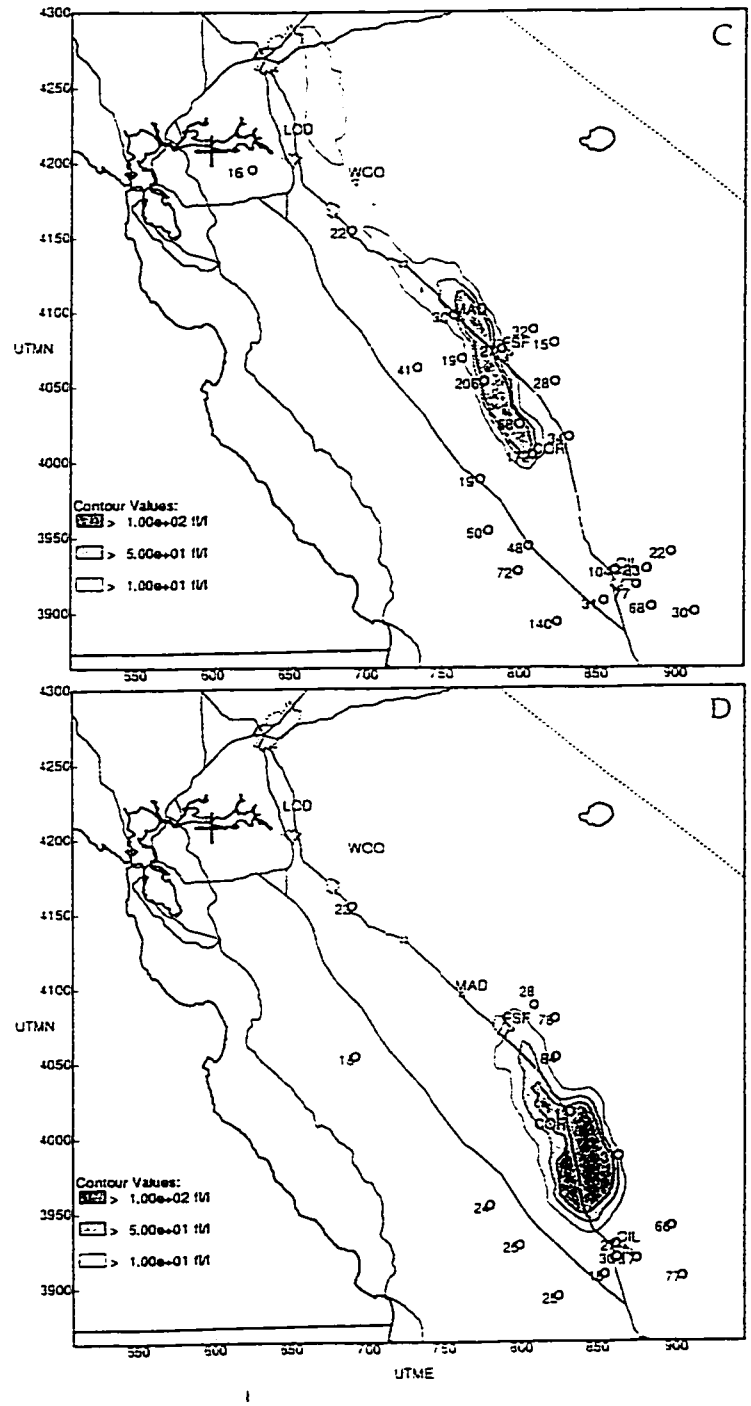

Fig. 12 (continued)

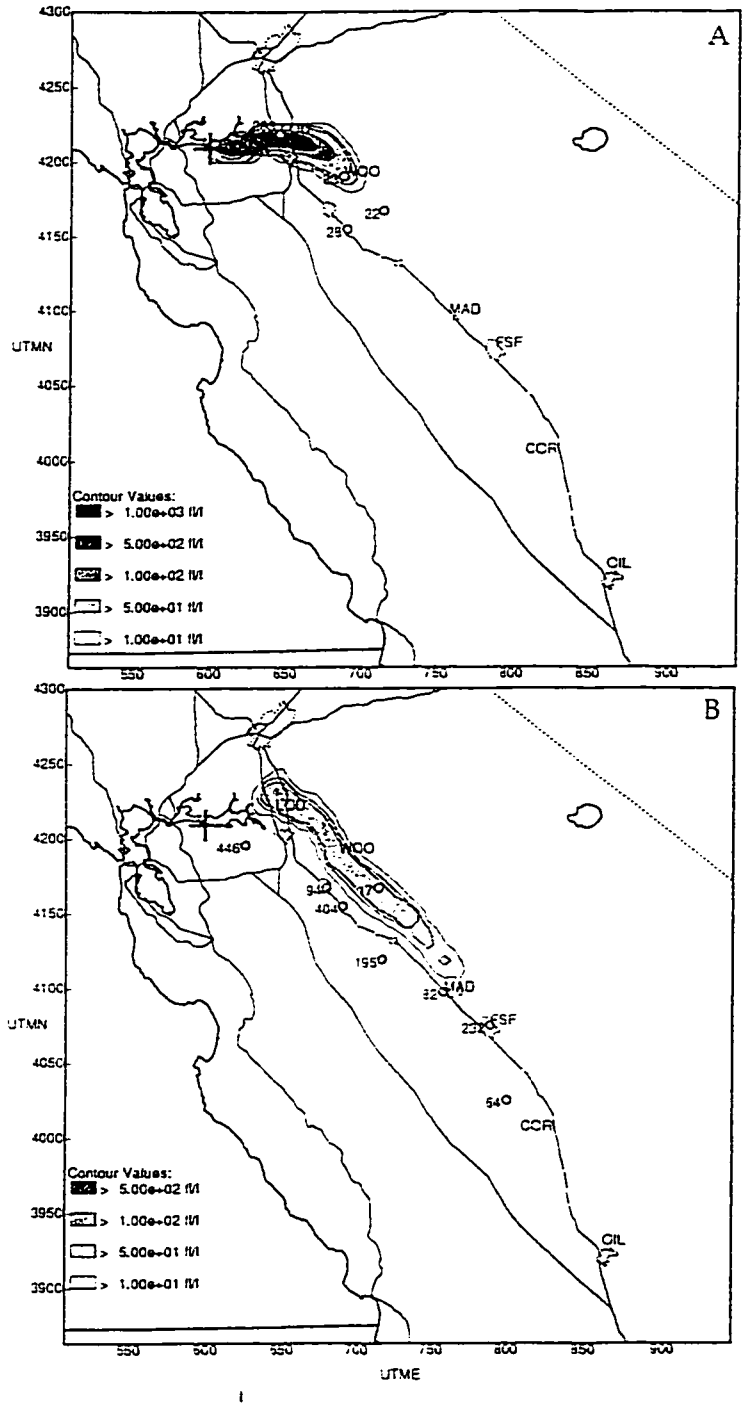
A
B
UTMN
UTME
MAD
ESF
CCR
CIL
Contour Values:
> 1.00e+03 ft/t
> 5.00e+02 ft/t
> 1.00e+02 ft/t
> 5.00e+01 ft/t
> 1.00e+01 ft/t

Fig. 13

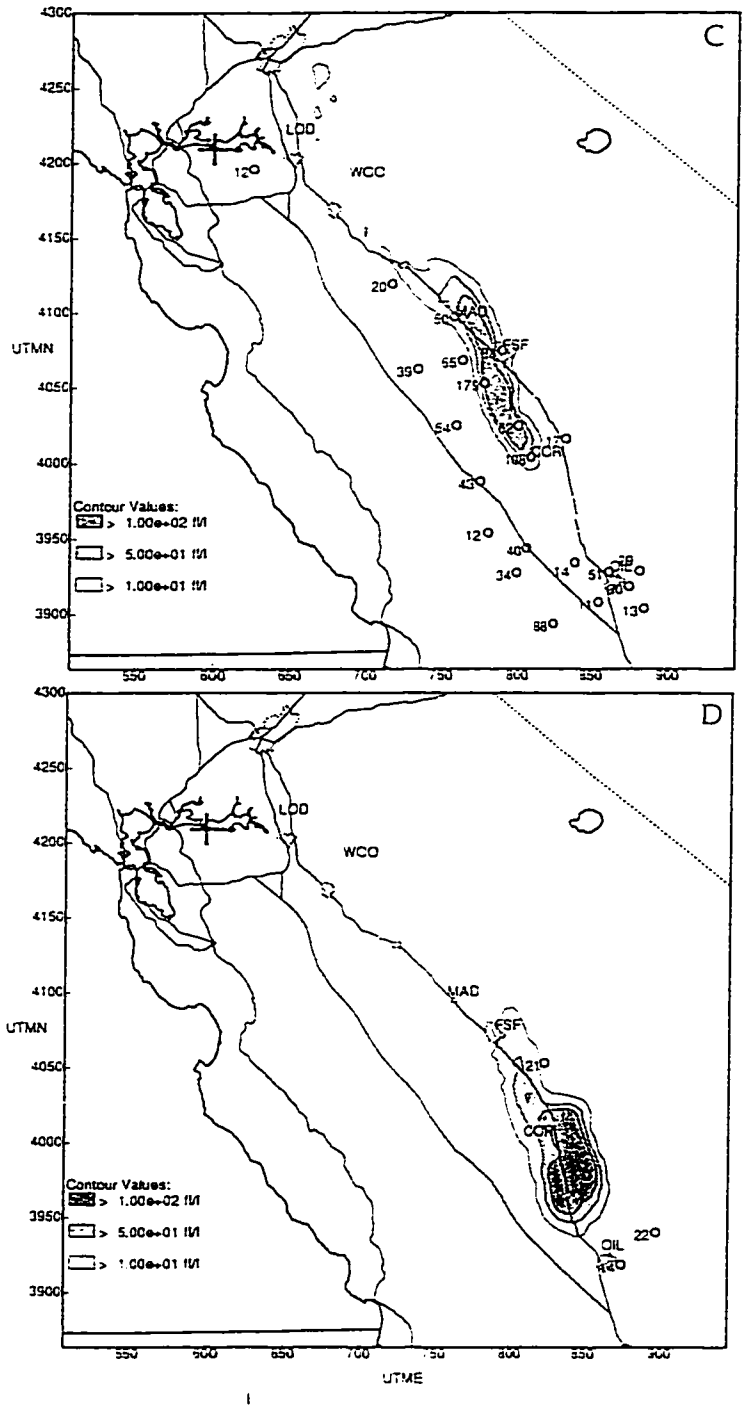

Fig. 13 (continued)

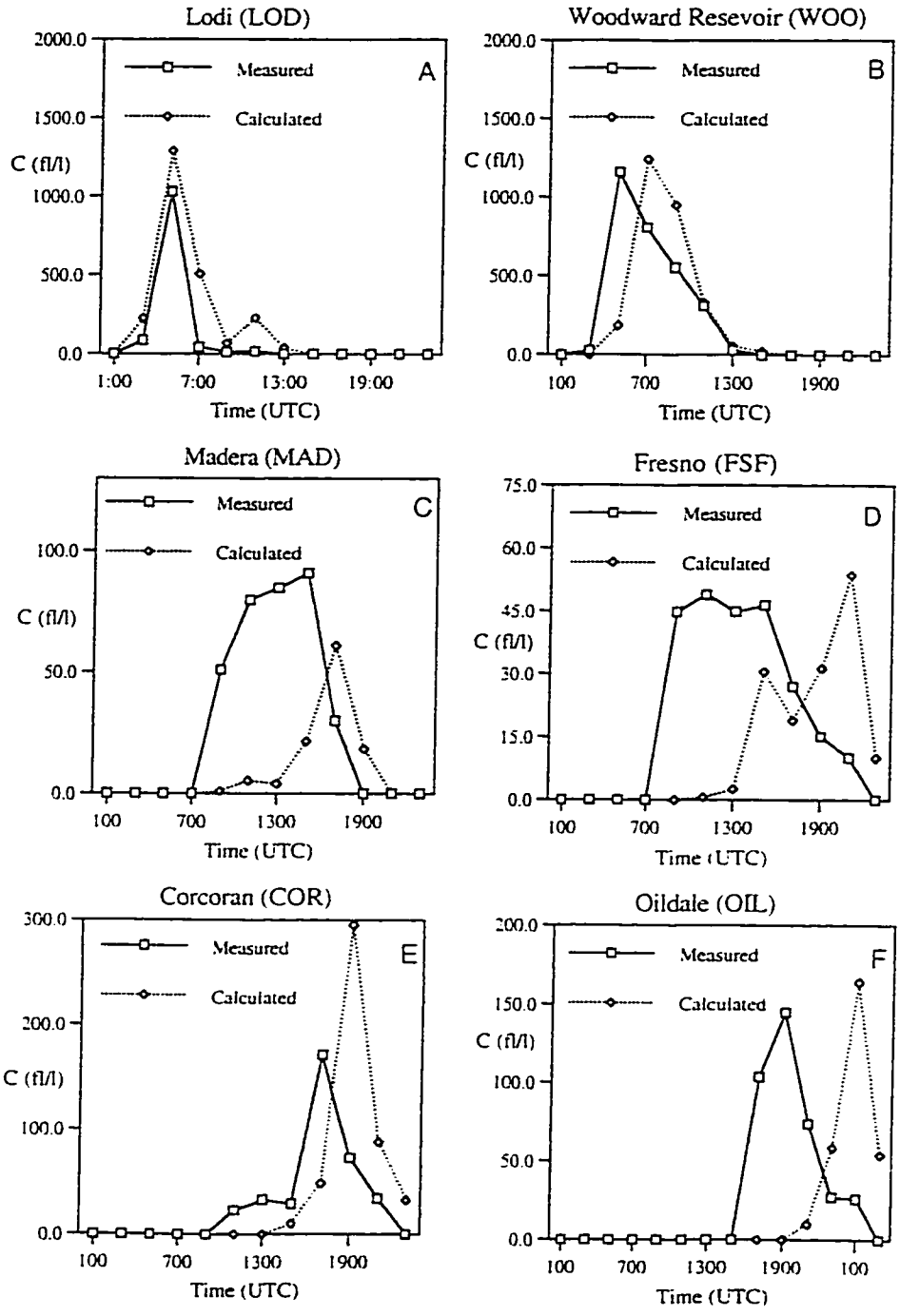
Lodi (LOD)
Measured
Calculated
A
C (fl/l)
2000.0
1500.0
1000.0
500.0
0.0
1:00
7:00
13:00
19:00
Time (UTC)
Woodward Resevoir (WOO)
Measured
Calculated
B
C (fl/l)
2000.0
1500.0
1000.0
500.0
0.0
100
700
1300
1900
Time (UTC)
Madera (MAD)
Measured
Calculated
C
C (fl/l)
100.0
50.0
0.0
100
700
1300
1900
Time (UTC)
Fresno (FSF)
Measured
Calculated
D
C (fl/l)
75.0
60.0
45.0
30.0
15.0
0.0
100
700
1300
1900
Time (UTC)
Corcoran (COR)
Measured
Calculated
E
C (fl/l)
300.0
200.0
100.0
0.0
100
700
1300
1900
Time (UTC)
Oildale (OIL)
Measured
Calculated
F
C (fl/l)
200.0
150.0
100.0
50.0
0.0
100
700
1300
1900
100
Time (UTC)

Fig. 14

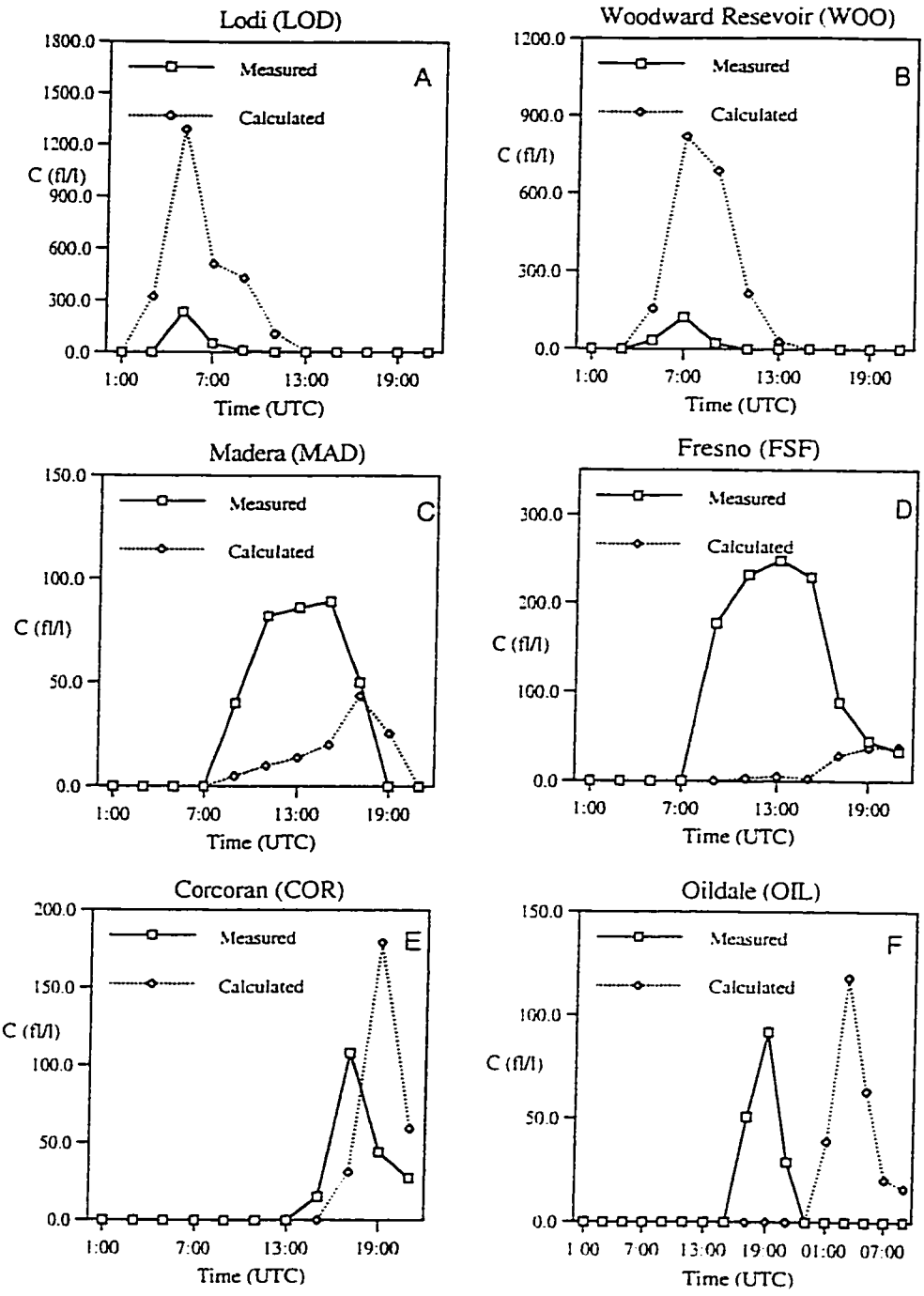
Lodi (LOD)
Measured
Calculated
A
C (fl/l)
Time (UTC)
Woodward Resevoir (WOO)
B
Madera (MAD)
C
Fresno (FSF)
D
Corcoran (COR)
E
Oildale (OIL)
F
1:00
7:00
13:00
19:00
01:00
07:00

Fig. 15

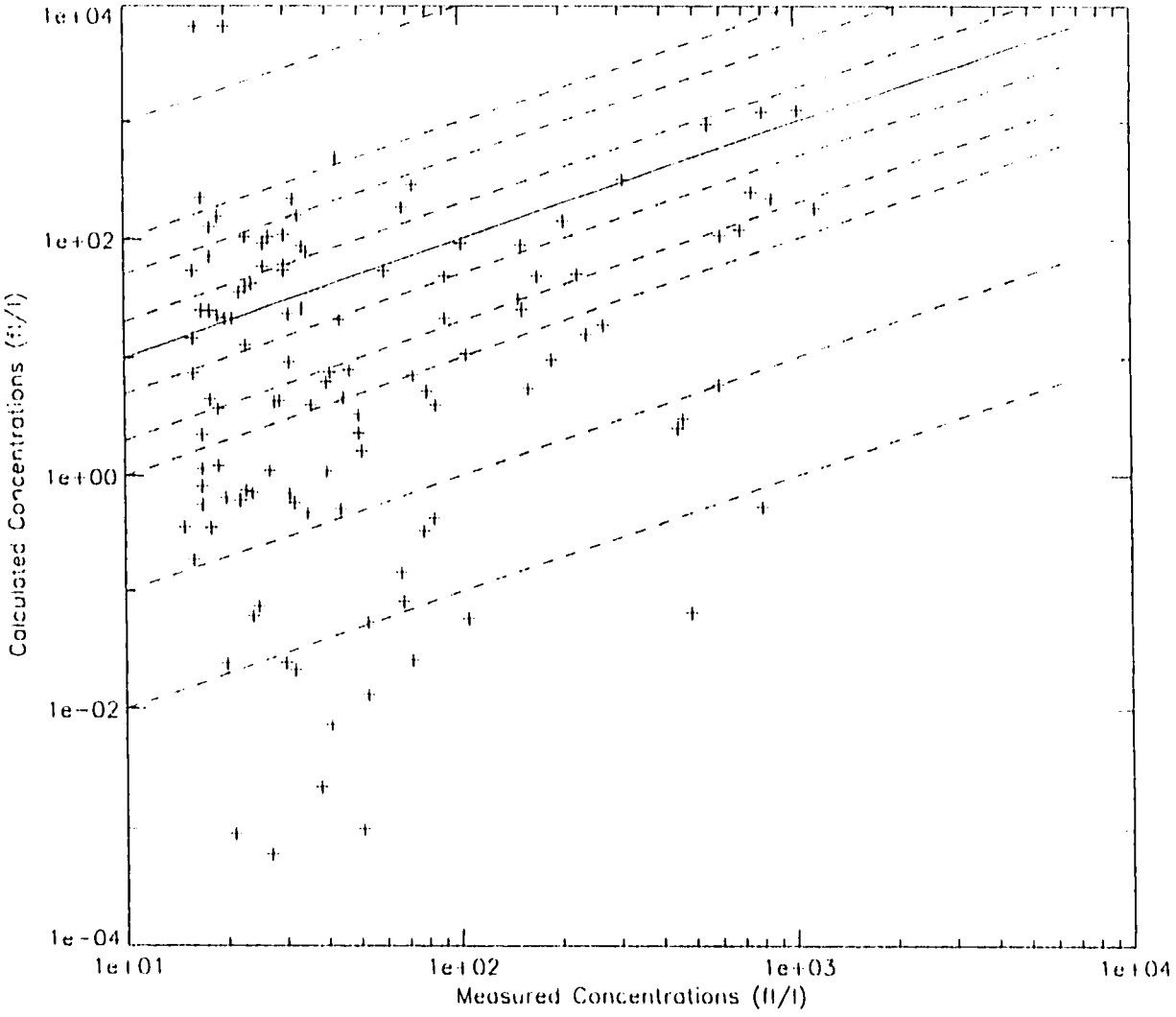
1e+04
1e+02
1e+00
1e-02
1e-04
Calculated Concentrations (ng/l)
1e+01
1e+02
1e+03
1e+04
Measured Concentrations (ng/l)

Fig. 16

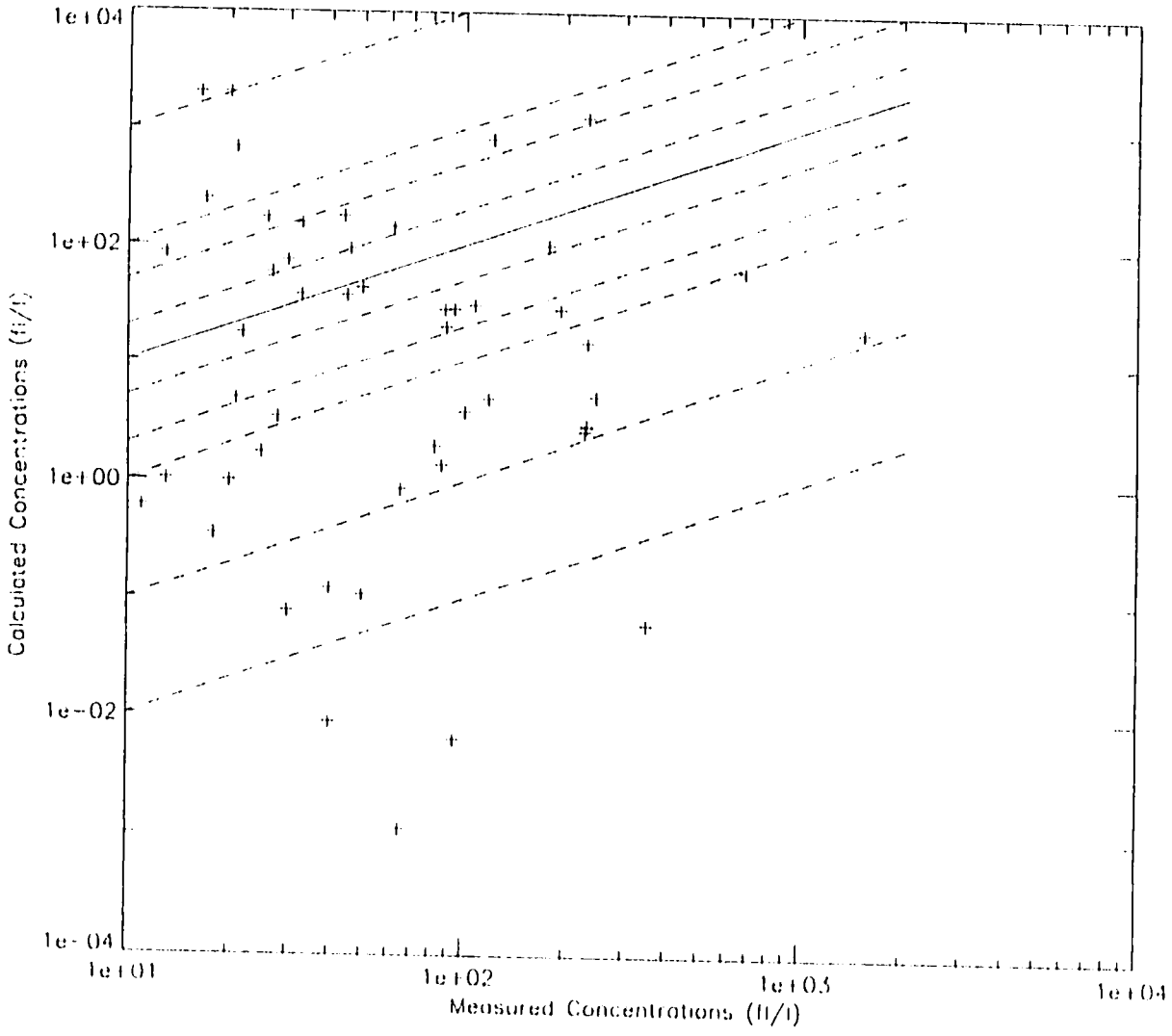
1e+04
1e+02
1e+00
1e-02
1e-04
Calculated Concentrations (ft/l)
1e+01
1e+02
1e+03
1e+04
Measured Concentrations (ft/l)

Fig. 17

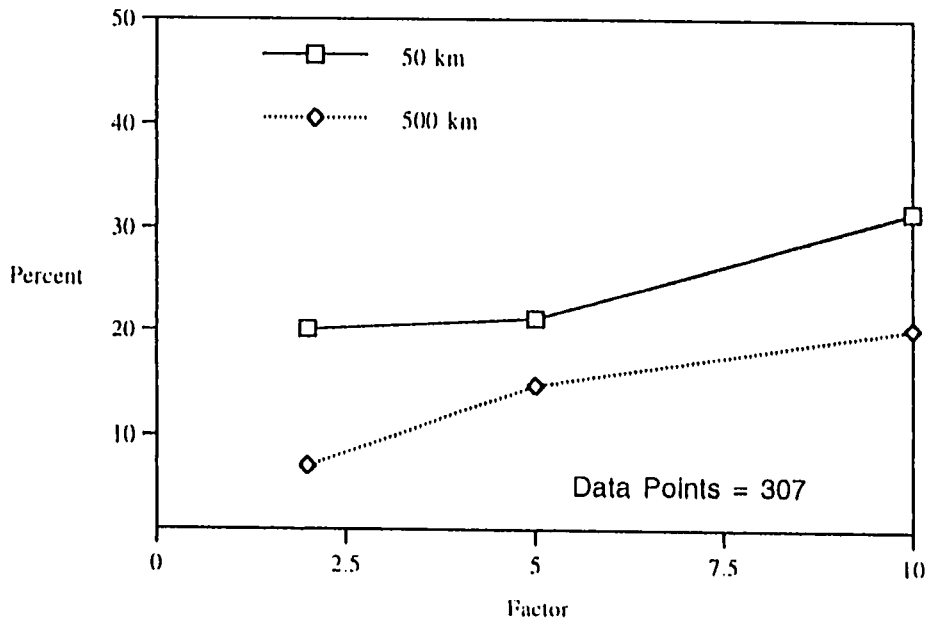
50
40
30
20
10
Percent
50 km
500 km
Data Points = 307
0
2.5
5
7.5
10
Factor

Fig. 18

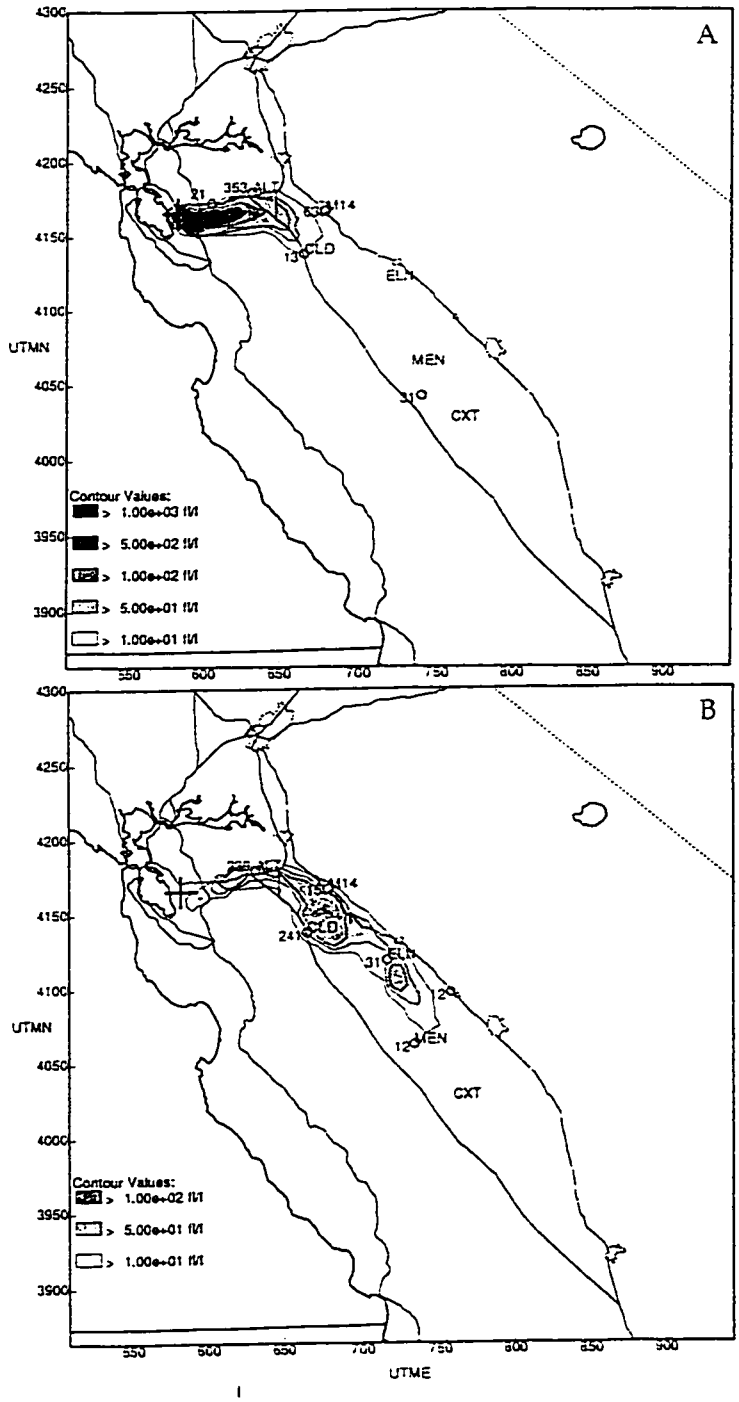
A
B
UTMN
UTME
CLD
ELM
MEN
CXT
Contour Values:
> 1.00e+03 ft/t
> 5.00e+02 ft/t
> 1.00e+02 ft/t
> 5.00e+01 ft/t
> 1.00e+01 ft/t

Fig. 19

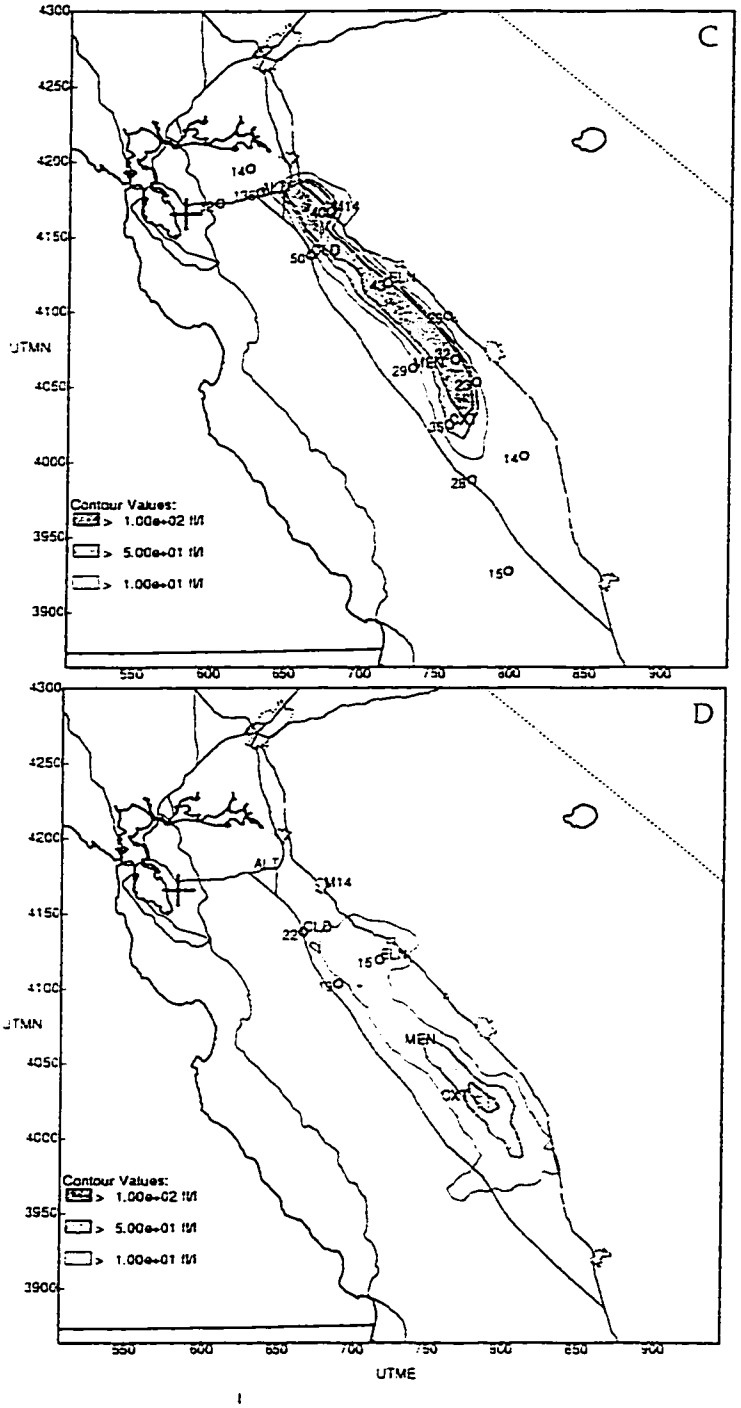

Fig. 19 (continued)

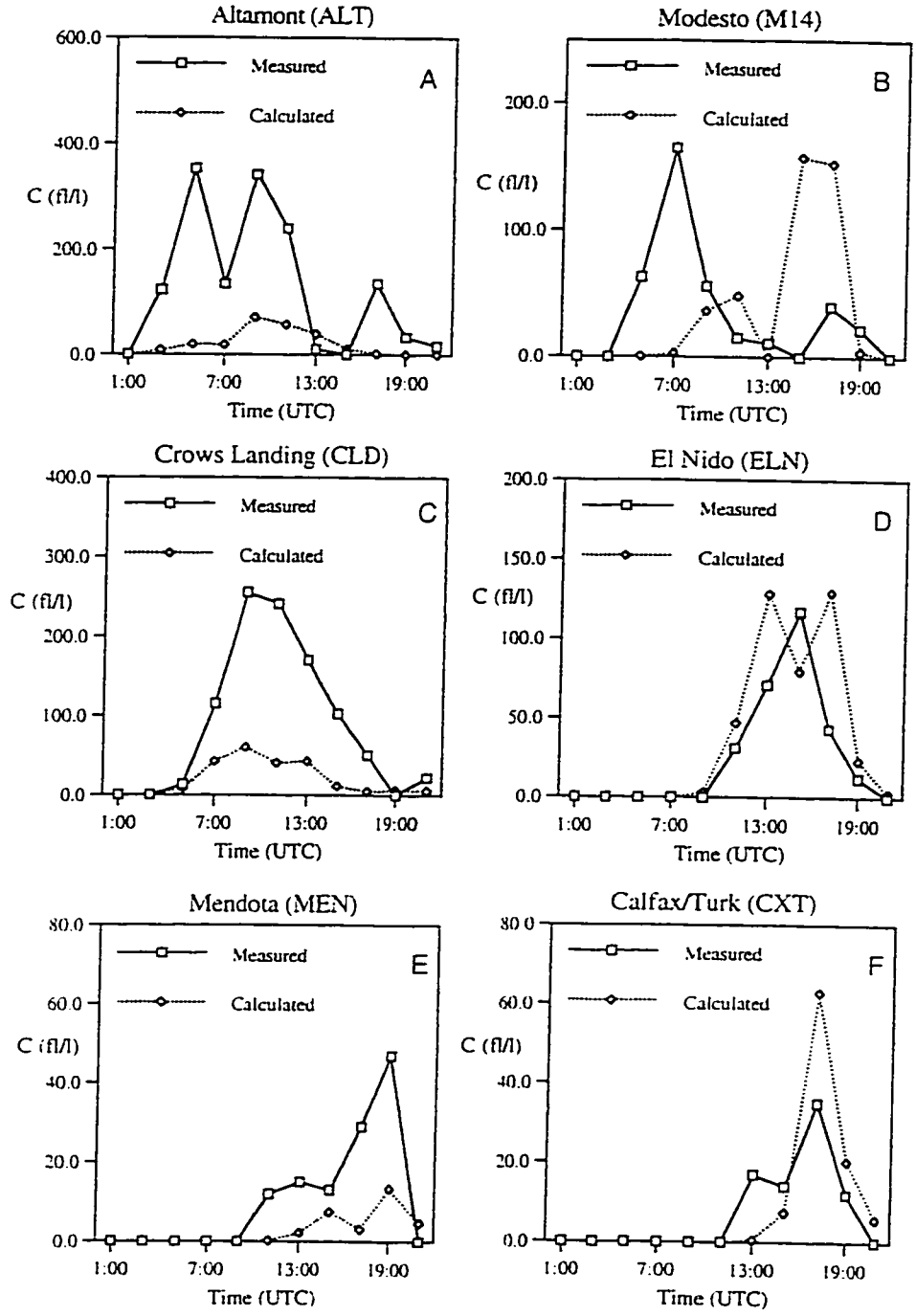
Altamont (ALT)
Measured
Calculated
A
C (fl/l)
600.0
400.0
200.0
0.0
1:00
7:00
13:00
19:00
Time (UTC)
Modesto (M14)
Measured
Calculated
B
C (fl/l)
200.0
100.0
0.0
1:00
7:00
13:00
19:00
Time (UTC)
Crows Landing (CLD)
Measured
Calculated
C
C (fl/l)
400.0
300.0
200.0
100.0
0.0
1:00
7:00
13:00
19:00
Time (UTC)
El Nido (ELN)
Measured
Calculated
D
C (fl/l)
200.0
150.0
100.0
50.0
0.0
1:00
7:00
13:00
19:00
Time (UTC)
Mendota (MEN)
Measured
Calculated
E
C (fl/l)
80.0
60.0
40.0
20.0
0.0
1:00
7:00
13:00
19:00
Time (UTC)
Calfax/Turk (CXT)
Measured
Calculated
F
C (fl/l)
80.0
60.0
40.0
20.0
0.0
1:00
7:00
13:00
19:00
Time (UTC)

Fig. 20

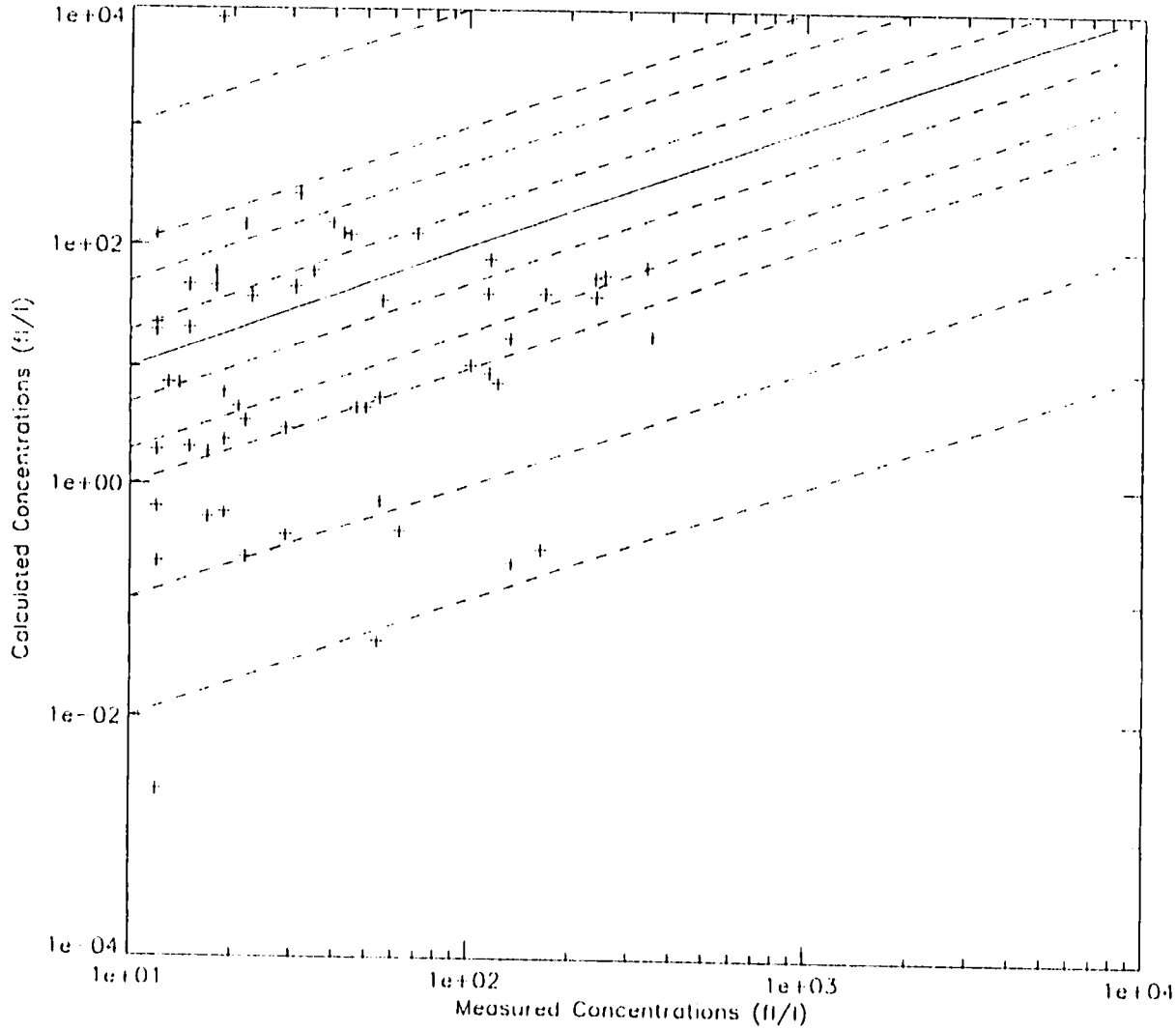
1e+04
1e+02
1e+00
1e-02
1e-04
Calculated Concentrations (ug/l)
1e+01
1e+02
1e+03
1e+04
Measured Concentrations (ug/l)

Fig. 21

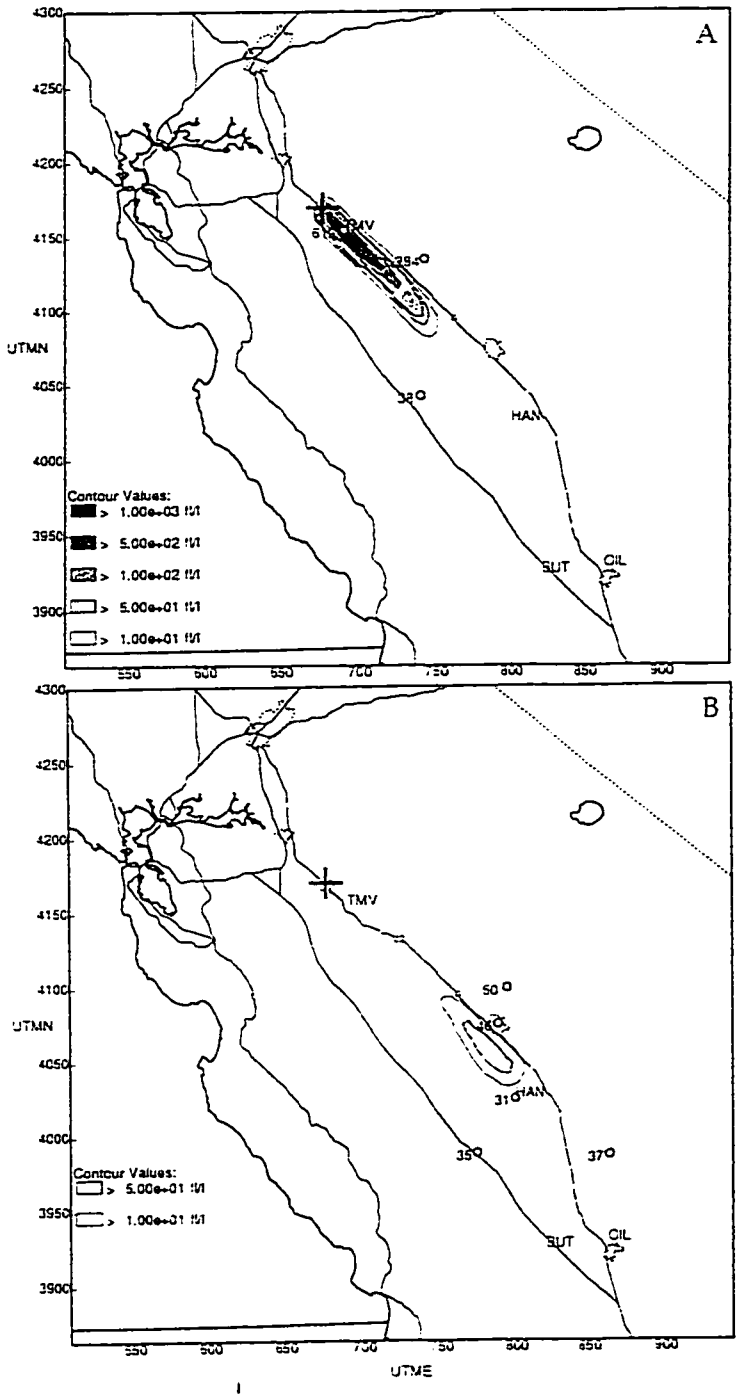
A
B
TMV
HAN
SUT
OIL
UTMN
UTME
Contour Values:
> 1.00e+03 ft/t
> 5.00e+02 ft/t
> 1.00e+02 ft/t
> 5.00e+01 ft/t
> 1.00e+01 ft/t

Fig. 22

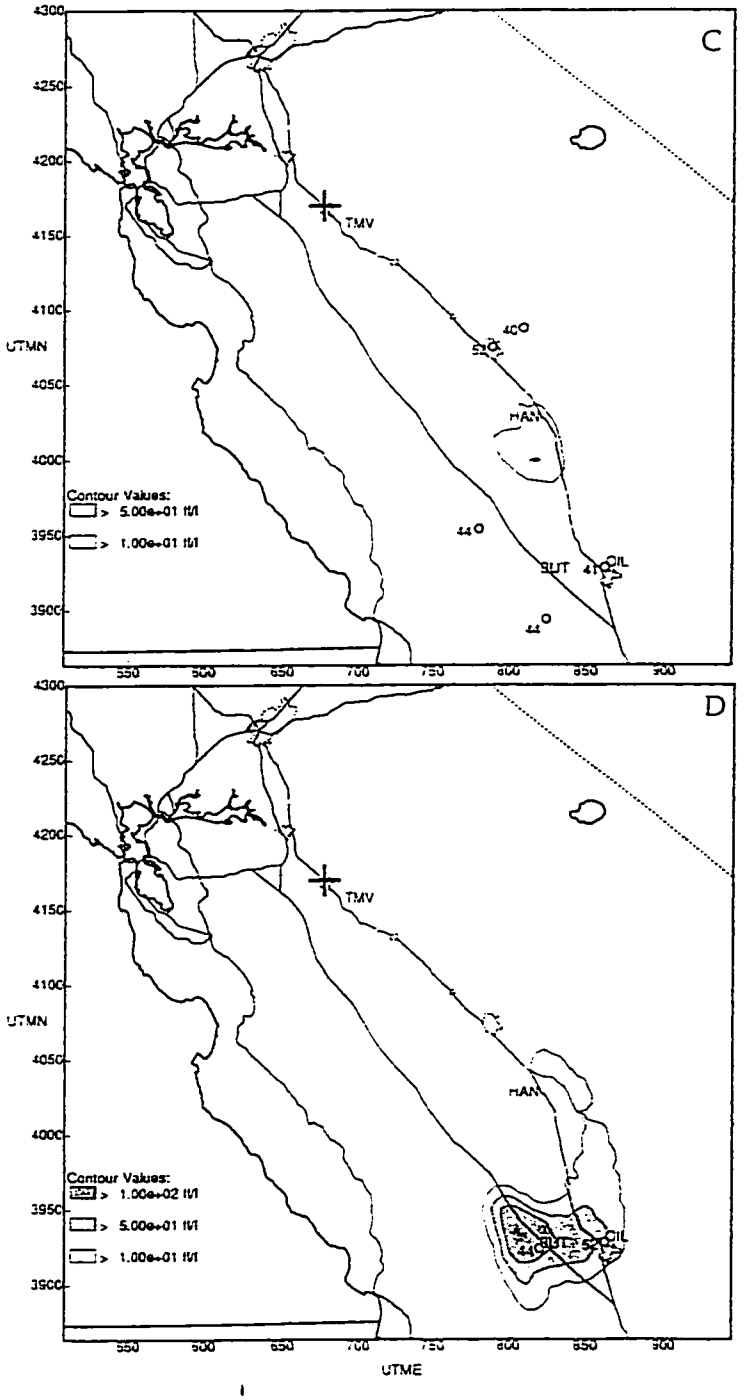

Fig. 22 (continued)

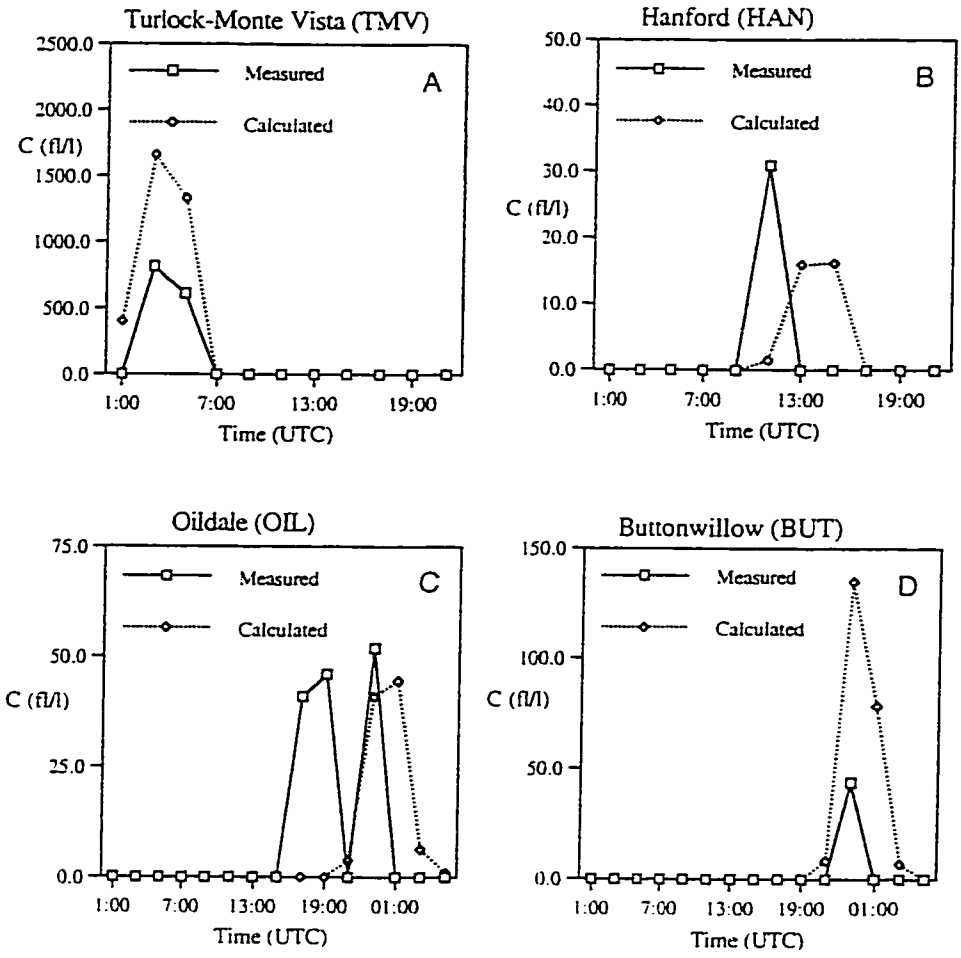
Turlock-Monte Vista (TMV)
Measured
Calculated
A
C (fl/l)
2500.0
2000.0
1500.0
1000.0
500.0
0.0
1:00
7:00
13:00
19:00
Time (UTC)
Hanford (HAN)
Measured
Calculated
B
C (fl/l)
50.0
40.0
30.0
20.0
10.0
0.0
1:00
7:00
13:00
19:00
Time (UTC)
Oildale (OIL)
Measured
Calculated
C
C (fl/l)
75.0
50.0
25.0
0.0
1:00
7:00
13:00
19:00
01:00
Time (UTC)
Buttonwillow (BUT)
Measured
Calculated
D
C (fl/l)
150.0
100.0
50.0
0.0
1:00
7:00
13:00
19:00
01:00
Time (UTC)

Fig. 23

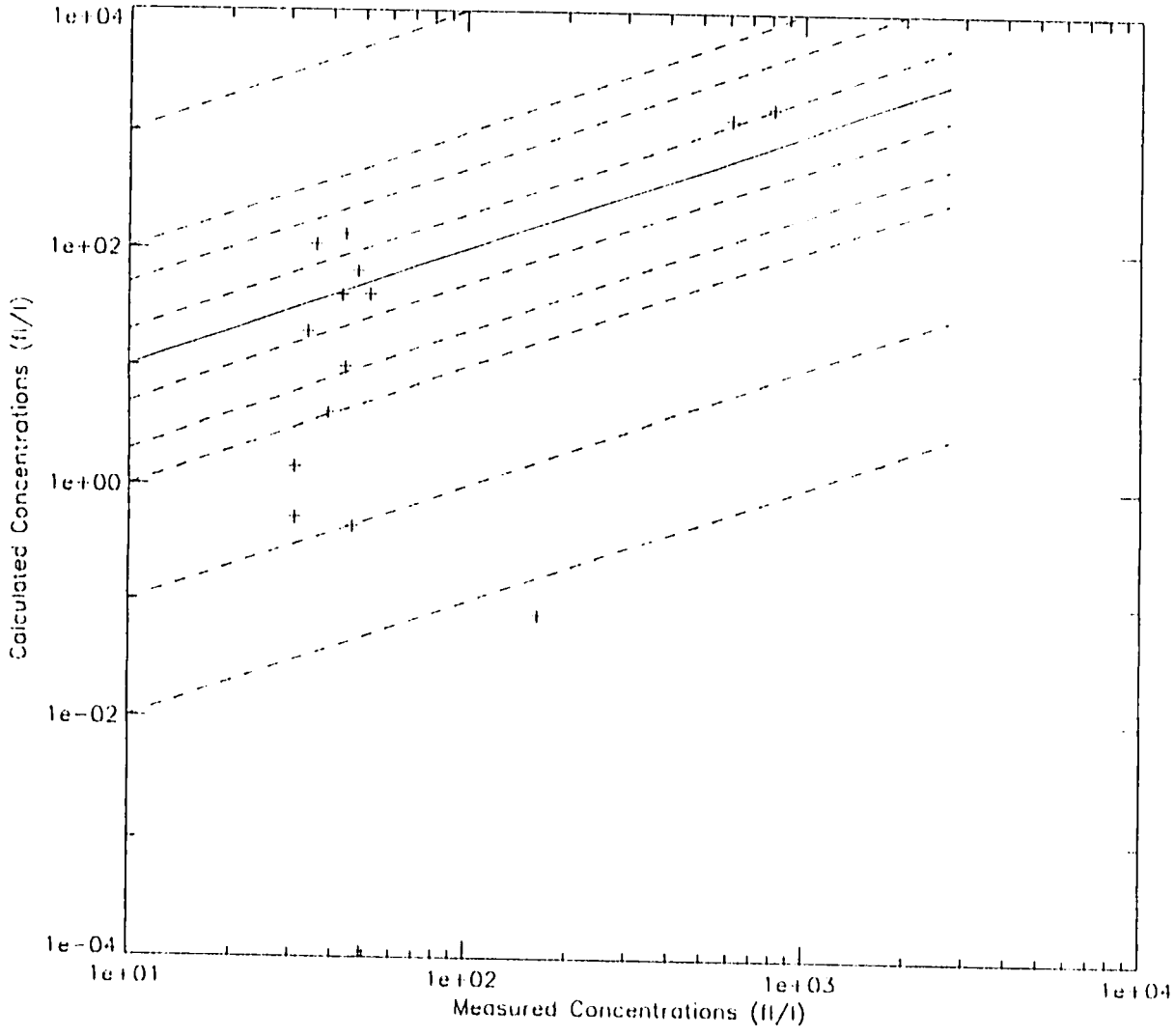
1e+04
1e+02
1e+00
1e-02
1e-04
Calculated Concentrations (fl/l)
1e+01
1e+02
1e+03
1e+04
Measured Concentrations (fl/l)

Fig. 24

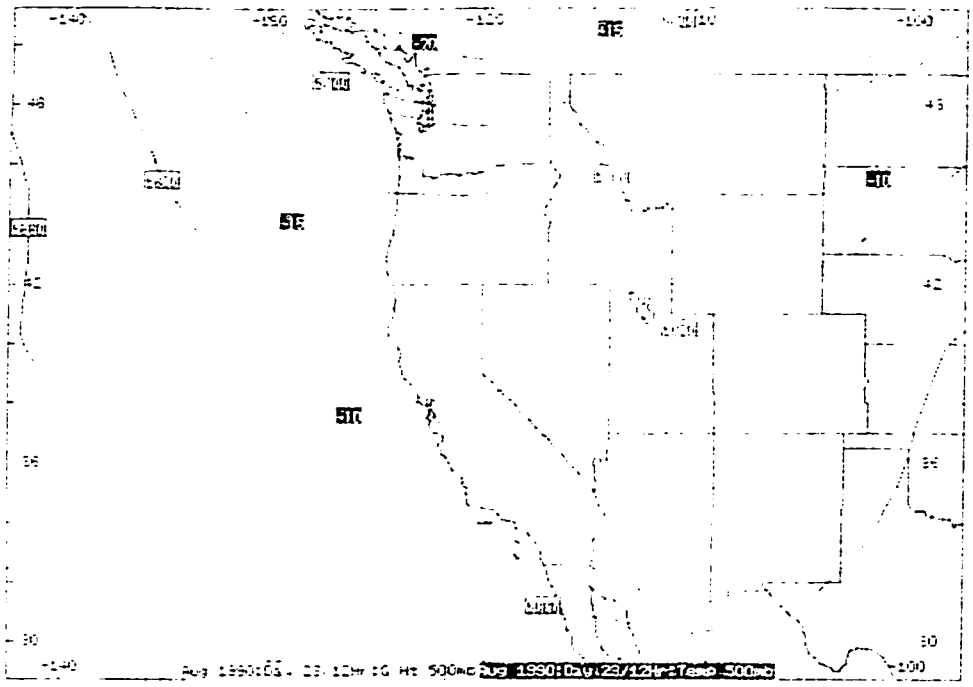

A

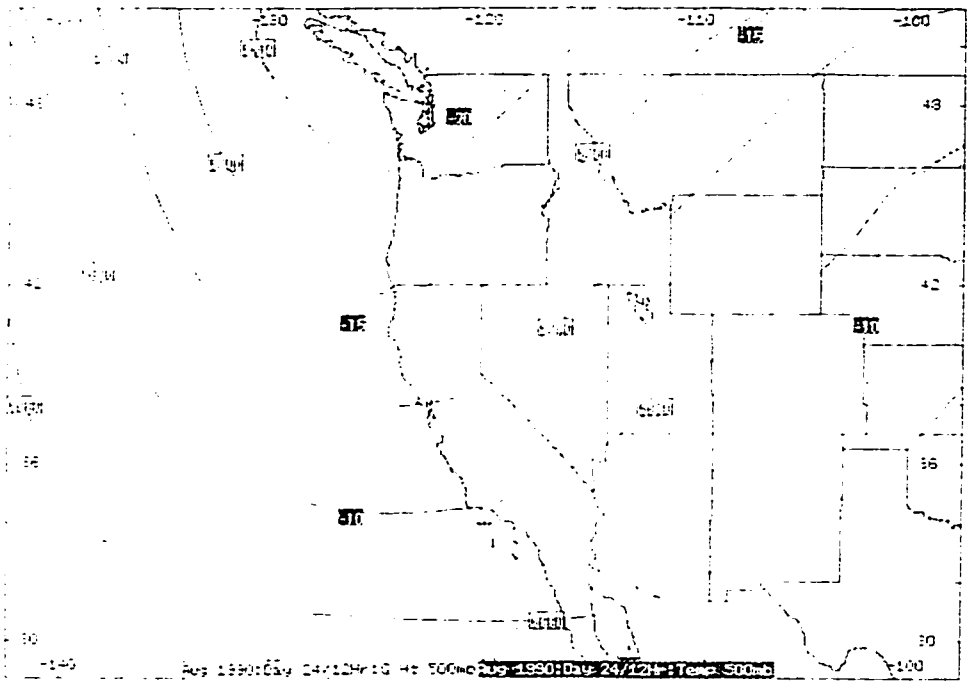

B

Fig. 25

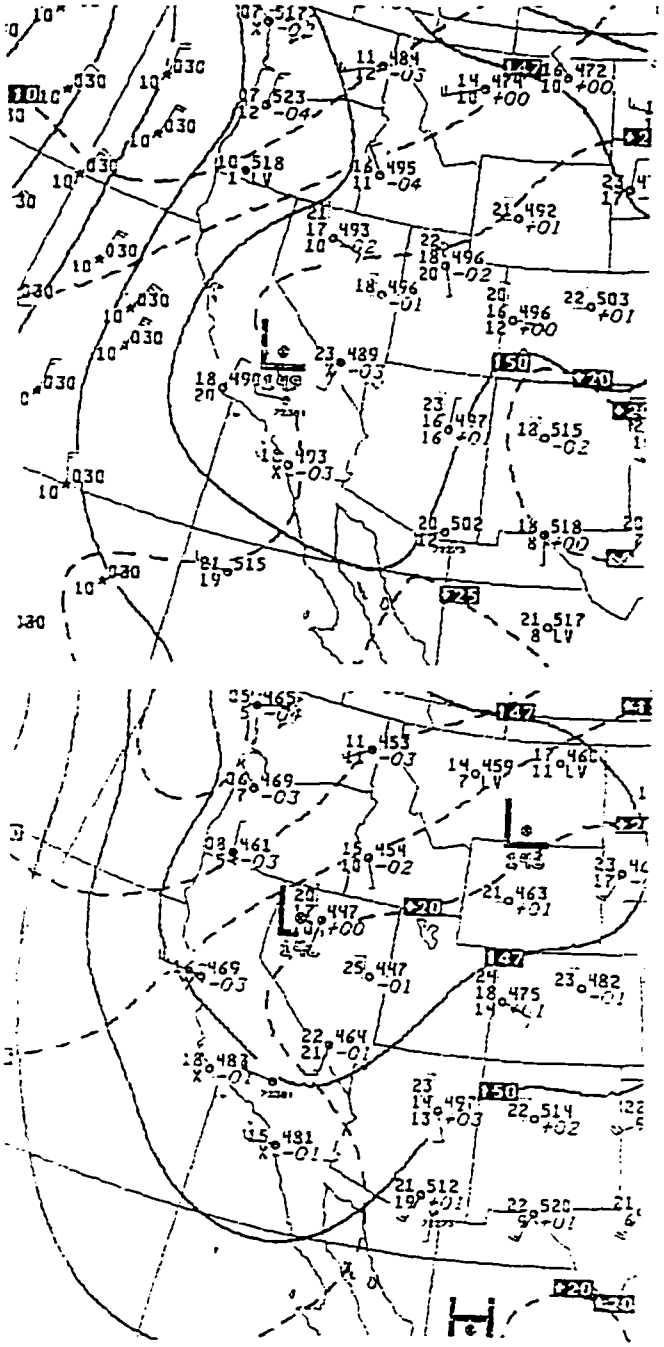

Fig. 26

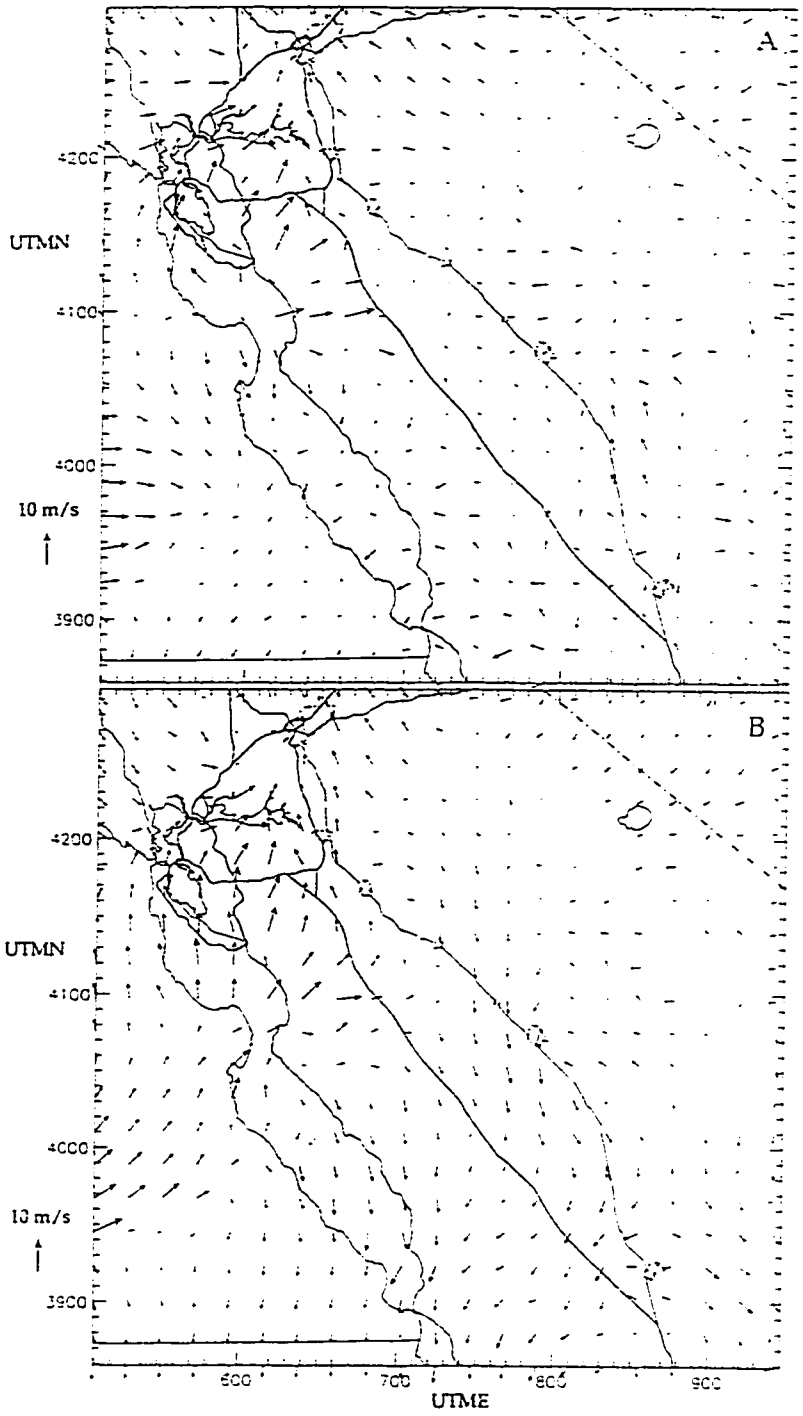

Fig. 27

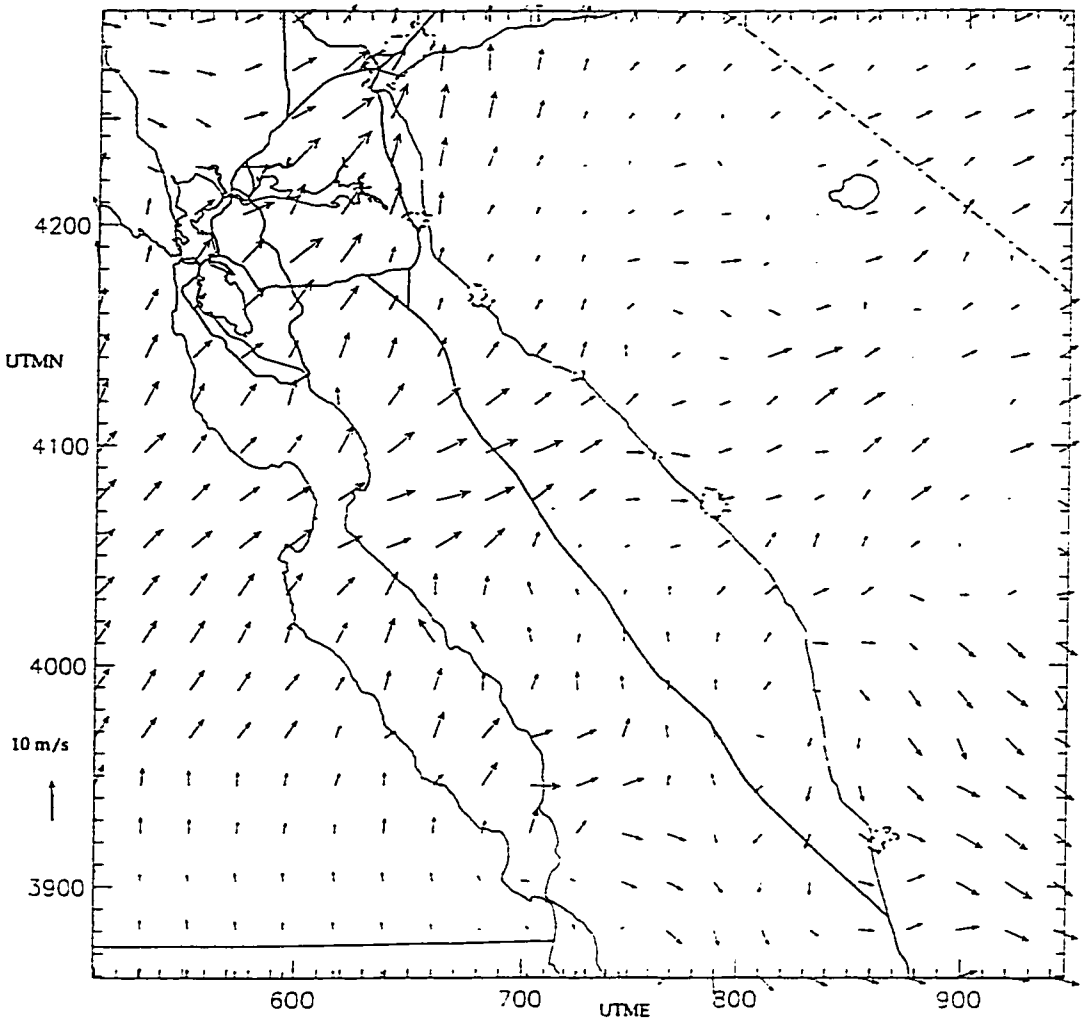

Fig. 28

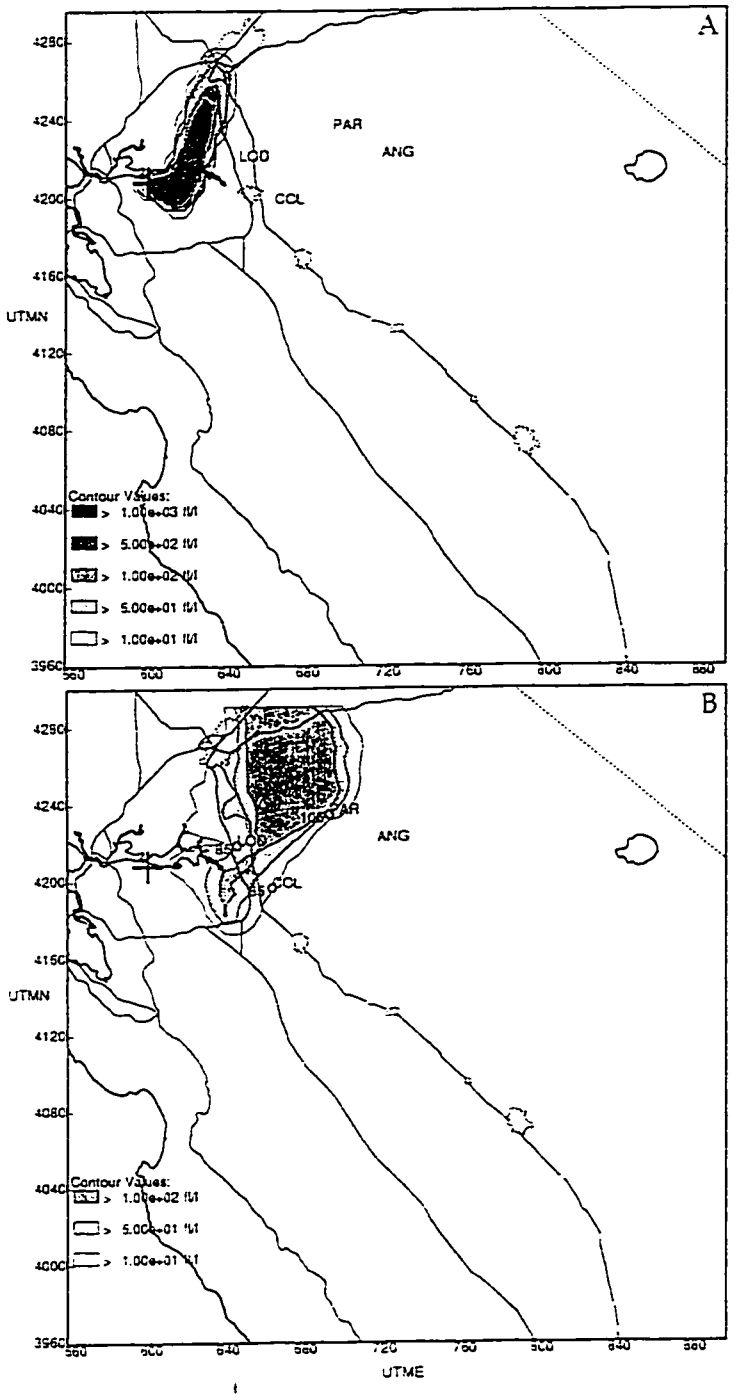
A
PAR
ANG
LOD
CCL
UTMN
Contour Values:
> 1.00e+03 ft/t
> 5.00e+02 ft/t
> 1.00e+02 ft/t
> 5.00e+01 ft/t
> 1.00e+01 ft/t
B
PAR
ANG
LOD
CCL
UTMN
Contour Values:
> 1.00e+02 ft/t
> 5.00e+01 ft/t
> 1.00e+01 ft/t
UTME

Fig. 29

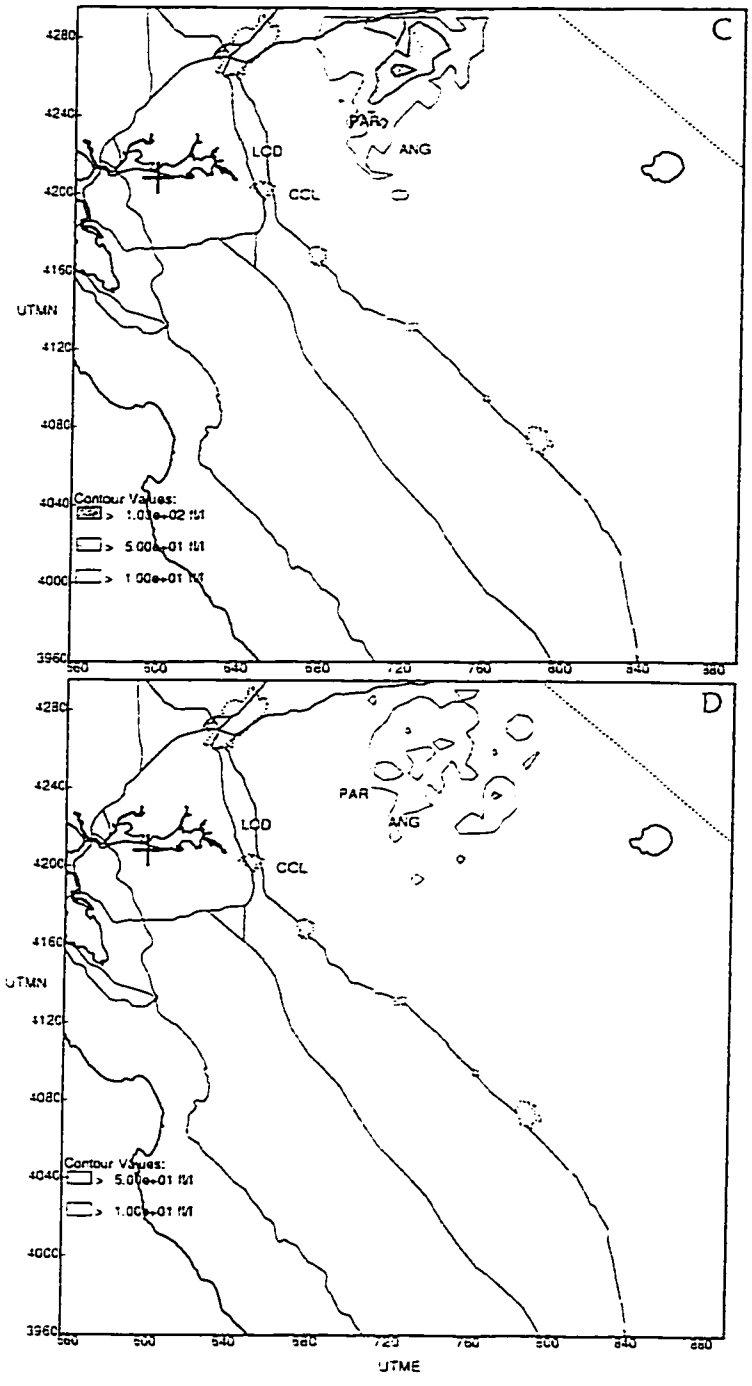

Fig. 29 (continued)

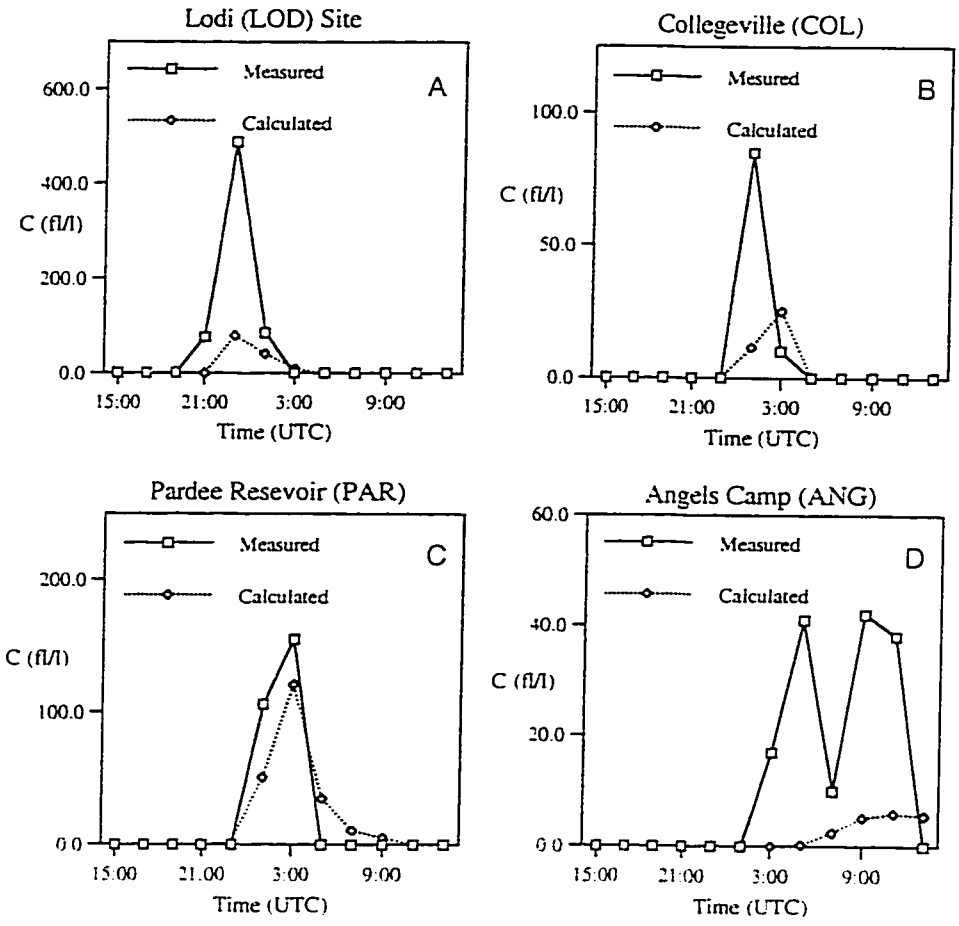
Lodi (LOD) Site
Measured
Calculated
A
600.0
400.0
200.0
0.0
C (fl/l)
15:00
21:00
3:00
9:00
Time (UTC)
Collegeville (COL)
Mesured
Calculated
B
100.0
50.0
0.0
C (fl/l)
15:00
21:00
3:00
9:00
Time (UTC)
Pardee Resevoir (PAR)
Measured
Calculated
C
200.0
100.0
0.0
C (fl/l)
15:00
21.00
3:00
9:00
Time (UTC)
Angels Camp (ANG)
Measured
Calculated
D
60.0
40.0
20.0
0.0
C (fl/l)
15:00
21:00
3:00
9:00
Time (UTC)

Fig. 30

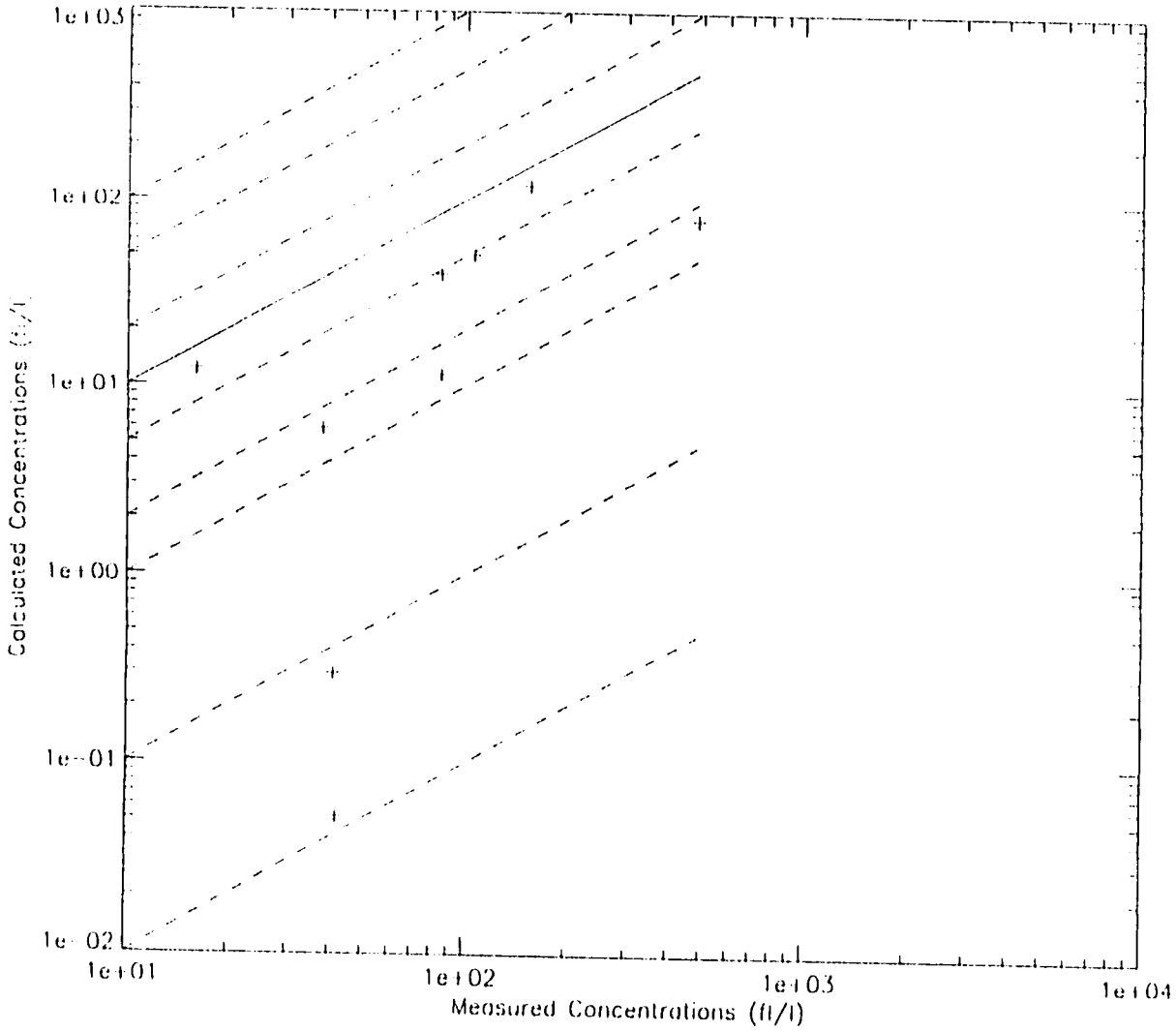
1e+03
1e+02
1e+01
1e+00
1e-01
1e-02
Calculated Concentrations (fl/l)
1e+01
1e+02
1e+03
1e+04
Measured Concentrations (fl/l)

Fig. 31

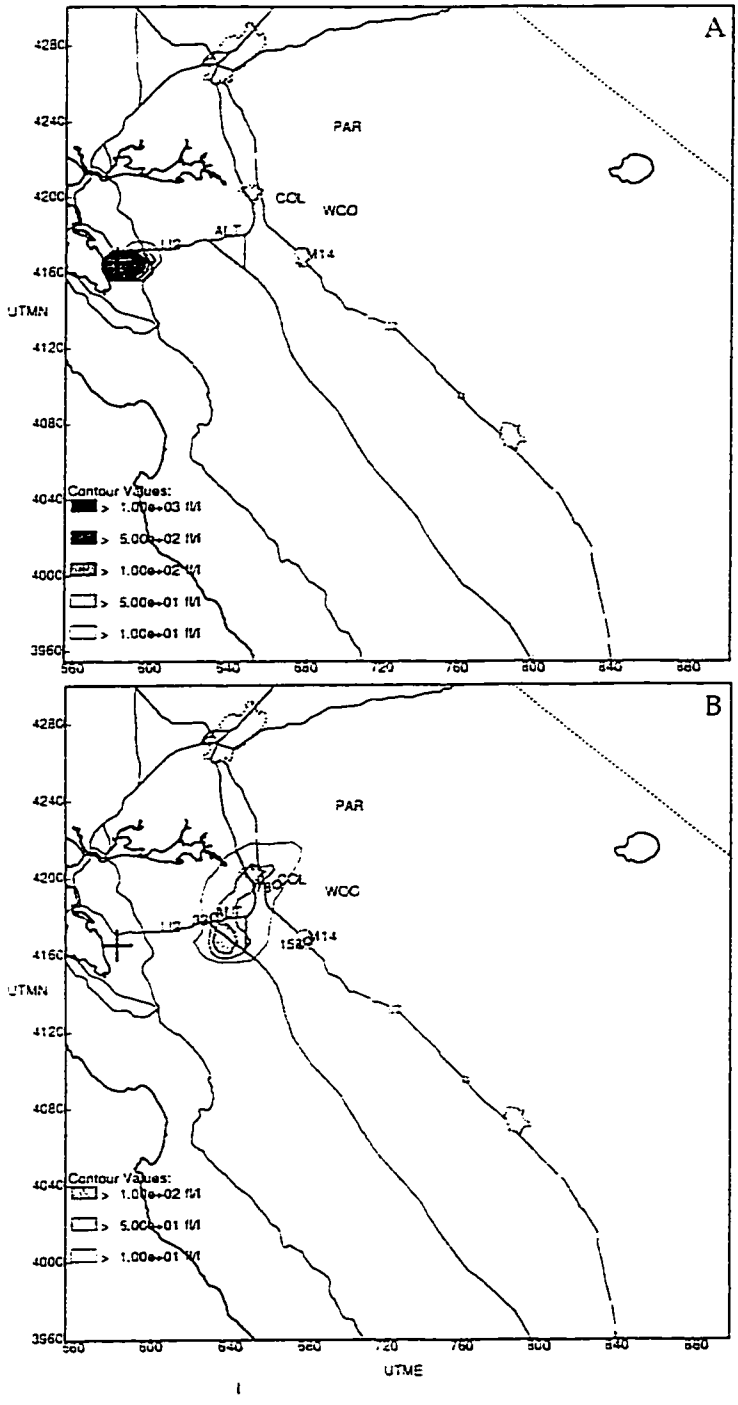
A
PAR
CCL
WCO
M14
UTMN
Contour Values:
> 1.00e+03 ft/t
> 5.00e+02 ft/t
> 1.00e+02 ft/t
> 5.00e+01 ft/t
> 1.00e+01 ft/t
B
PAR
CCL
WCO
M14
UTMN
Contour Values:
> 1.00e+02 ft/t
> 5.00e+01 ft/t
> 1.00e+01 ft/t
UTME

Fig. 32

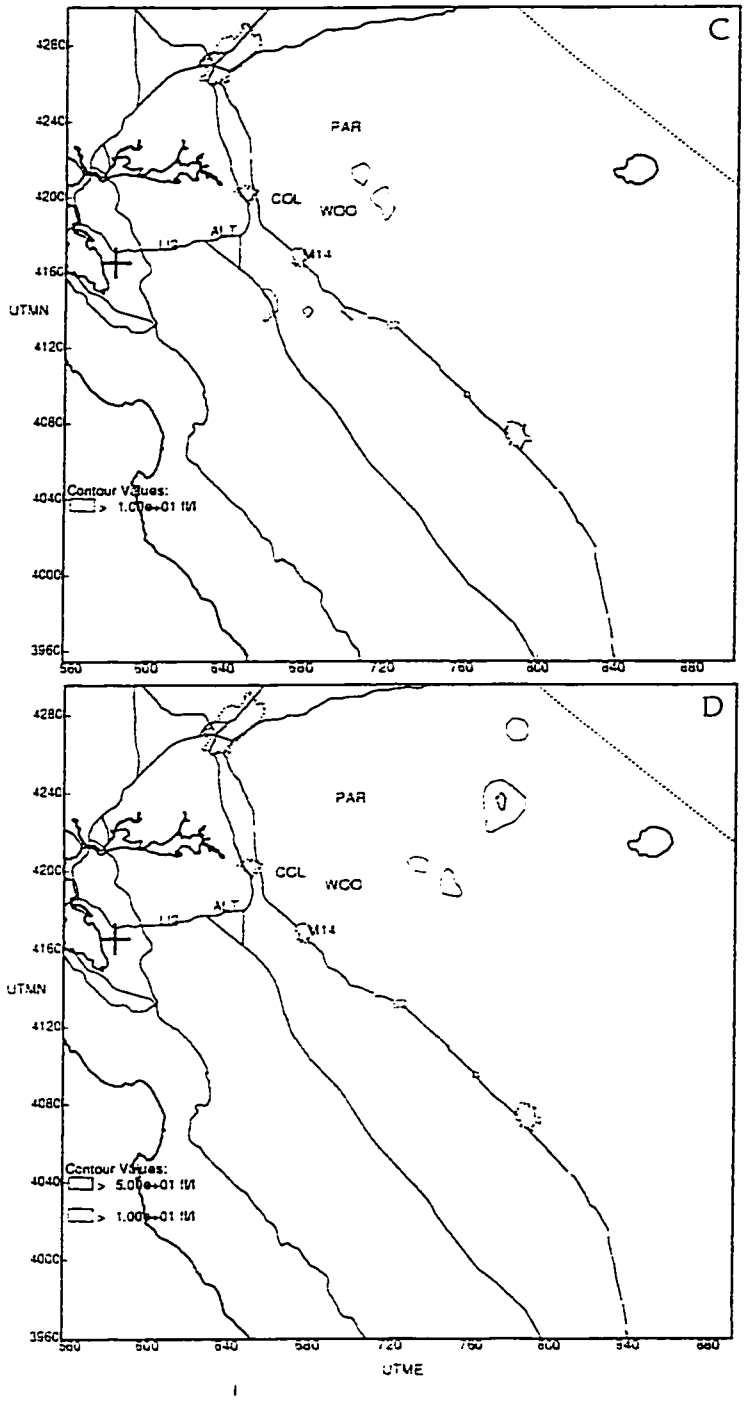

Fig. 32 (continued)

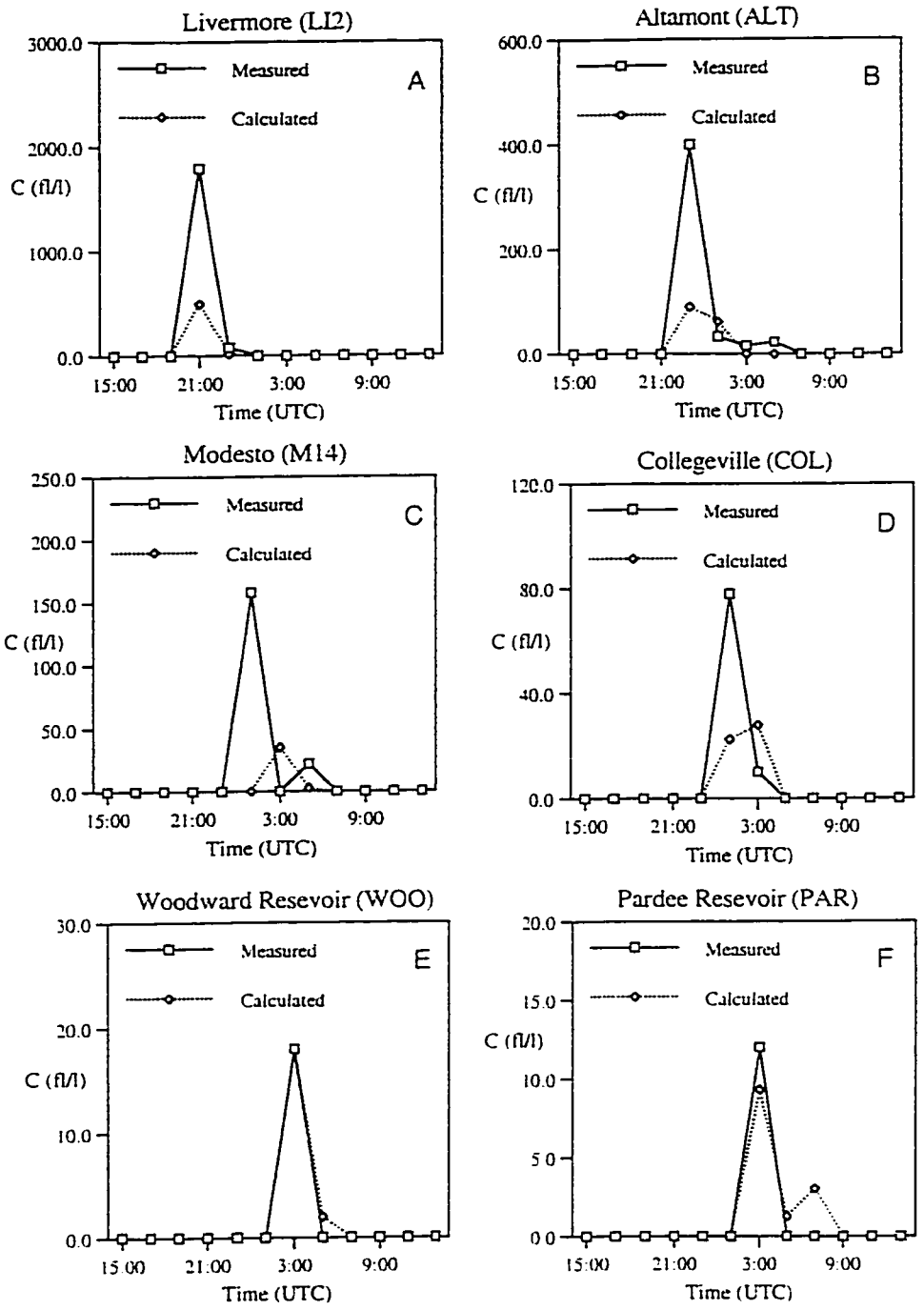
Livermore (LI2)
A
Measured
Calculated
C (fl/l)
3000.0
2000.0
1000.0
0.0
15:00
21:00
3:00
9:00
Time (UTC)
Altamont (ALT)
B
Measured
Calculated
C (fl/l)
600.0
400.0
200.0
0.0
15:00
21:00
3:00
9:00
Time (UTC)
Modesto (M14)
C
Measured
Calculated
C (fl/l)
250.0
200.0
150.0
100.0
50.0
0.0
15:00
21:00
3:00
9:00
Time (UTC)
Collegeville (COL)
D
Measured
Calculated
C (fl/l)
120.0
80.0
40.0
0.0
15:00
21:00
3:00
9:00
Time (UTC)
Woodward Resevoir (WOO)
E
Measured
Calculated
C (fl/l)
30.0
20.0
10.0
0.0
15:00
21:00
3:00
9:00
Time (UTC)
Pardee Resevoir (PAR)
F
Measured
Calculated
C (fl/l)
20.0
15.0
10.0
5.0
0.0
15:00
21:00
3:00
9:00
Time (UTC)

Fig. 33

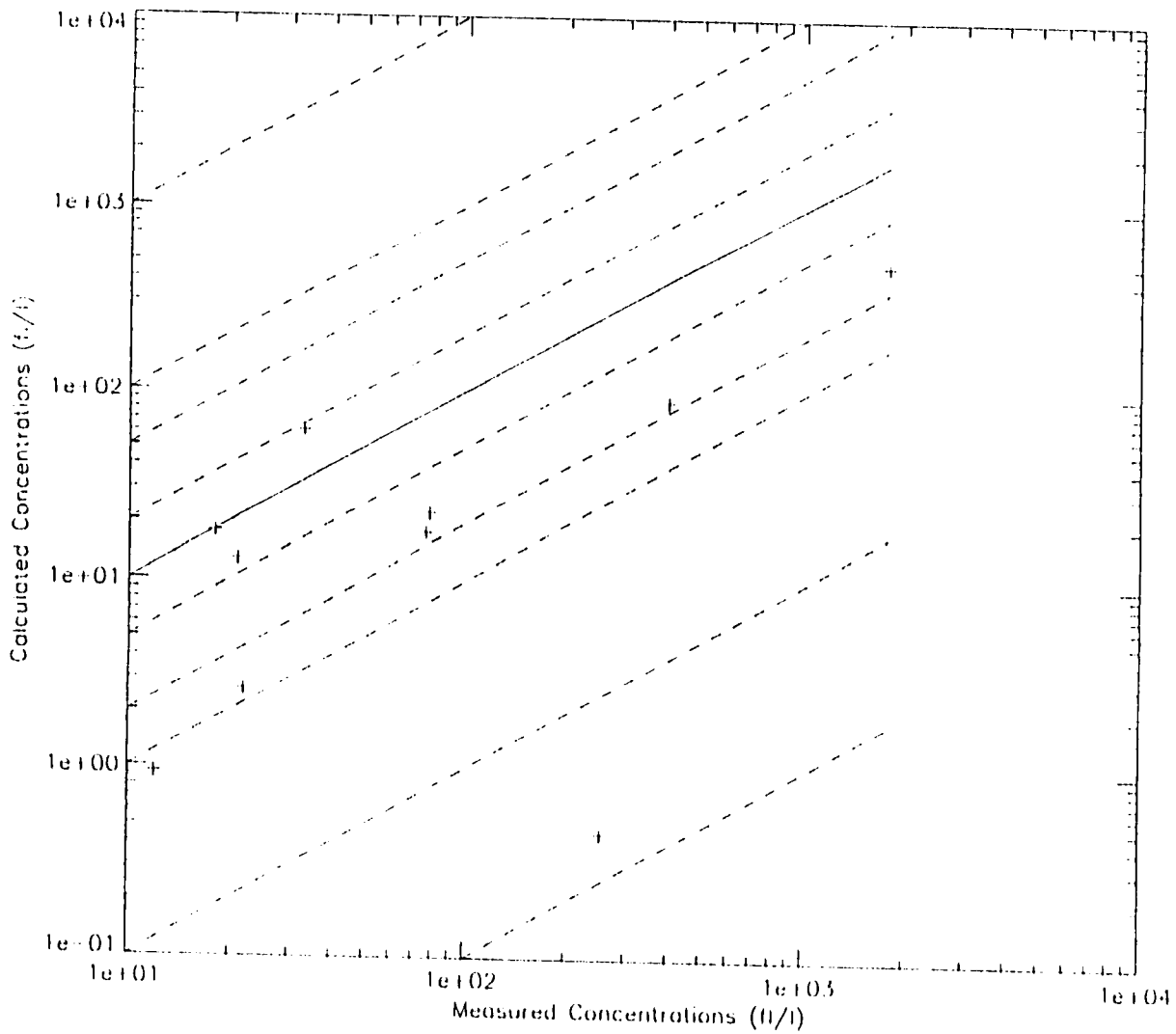
1e+04
1e+03
1e+02
1e+01
1e+00
1e-01
Calculated Concentrations (ug/l)
1e+01
1e+02
1e+03
1e+04
Measured Concentrations (ug/l)

Fig. 34

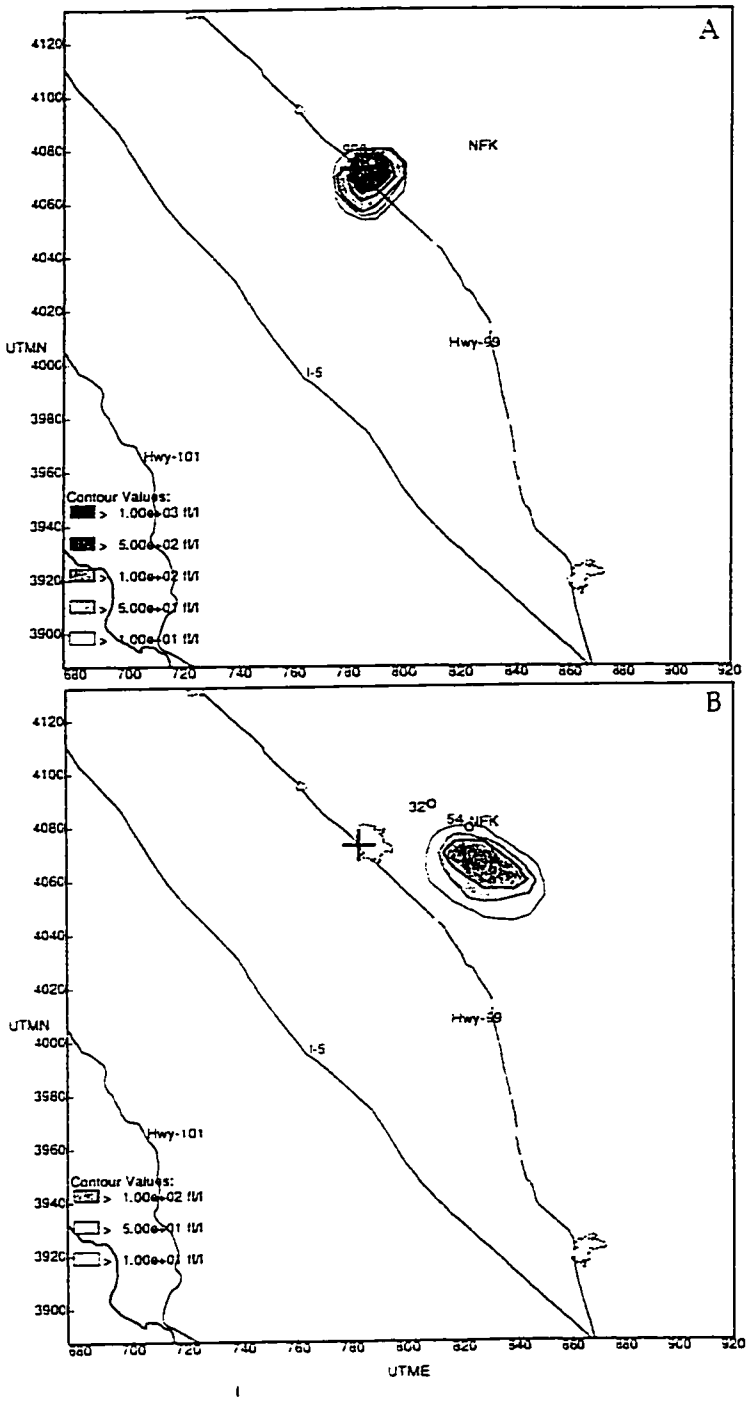
A
NFK
Hwy-99
I-5
Hwy-101
UTMN
Contour Values:
> 1.00e+03 ft/t
> 5.00e+02 ft/t
> 1.00e+02 ft/t
> 5.00e+01 ft/t
> 1.00e+01 ft/t
B
32
54
NFK
Hwy-99
I-5
Hwy-101
UTMN
Contour Values:
> 1.00e+02 ft/t
> 5.00e+01 ft/t
> 1.00e+01 ft/t
UTME

Fig. 35

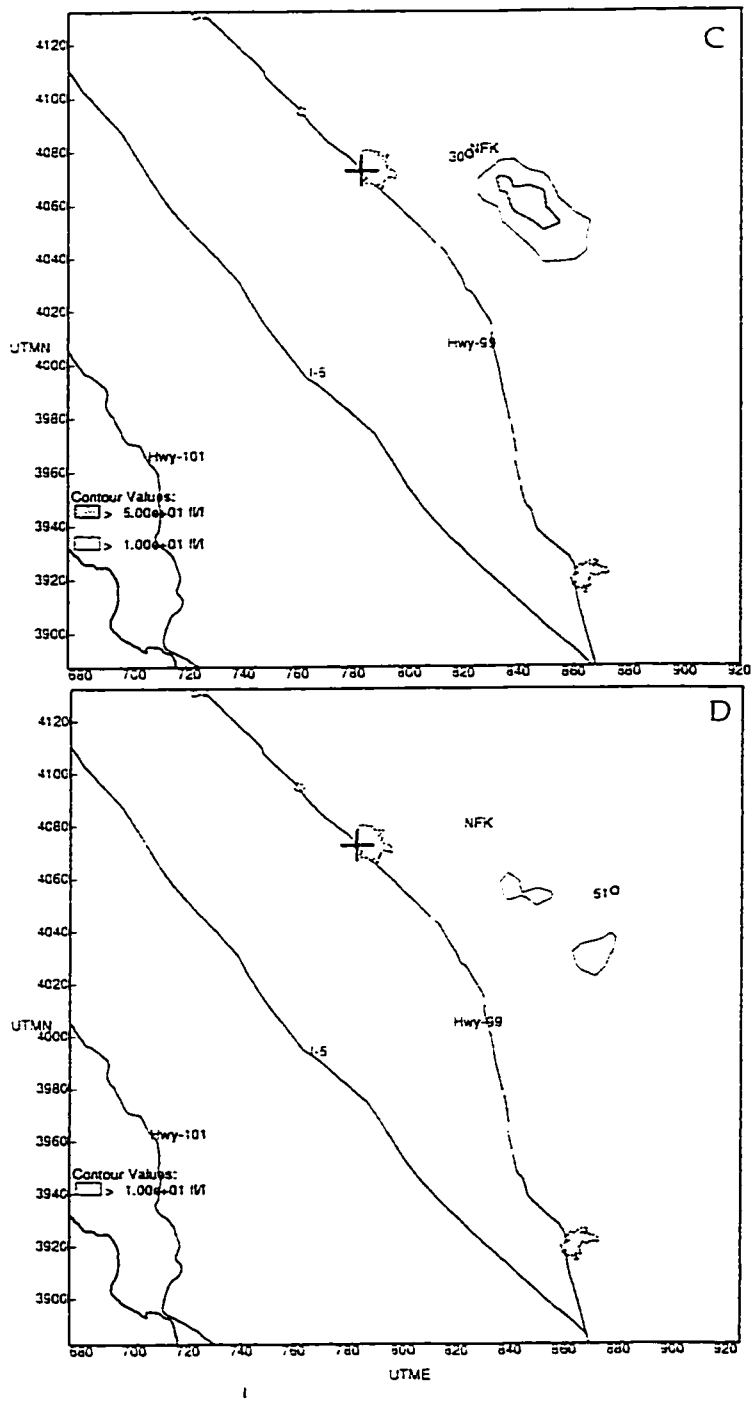

Fig. 35 (continued)

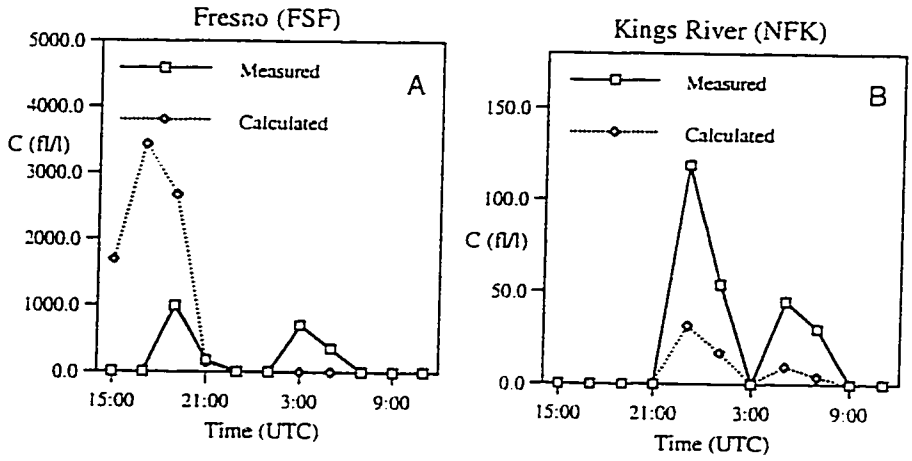
Fresno (FSF)
5000.0
4000.0
3000.0
2000.0
1000.0
0.0
C (fl/l)
Measured
Calculated
A
15:00
21:00
3:00
9:00
Time (UTC)
Kings River (NFK)
150.0
100.0
50.0
0.0
C (fl/l)
Measured
Calculated
B
15:00
21:00
3:00
9:00
Time (UTC)

Fig. 36

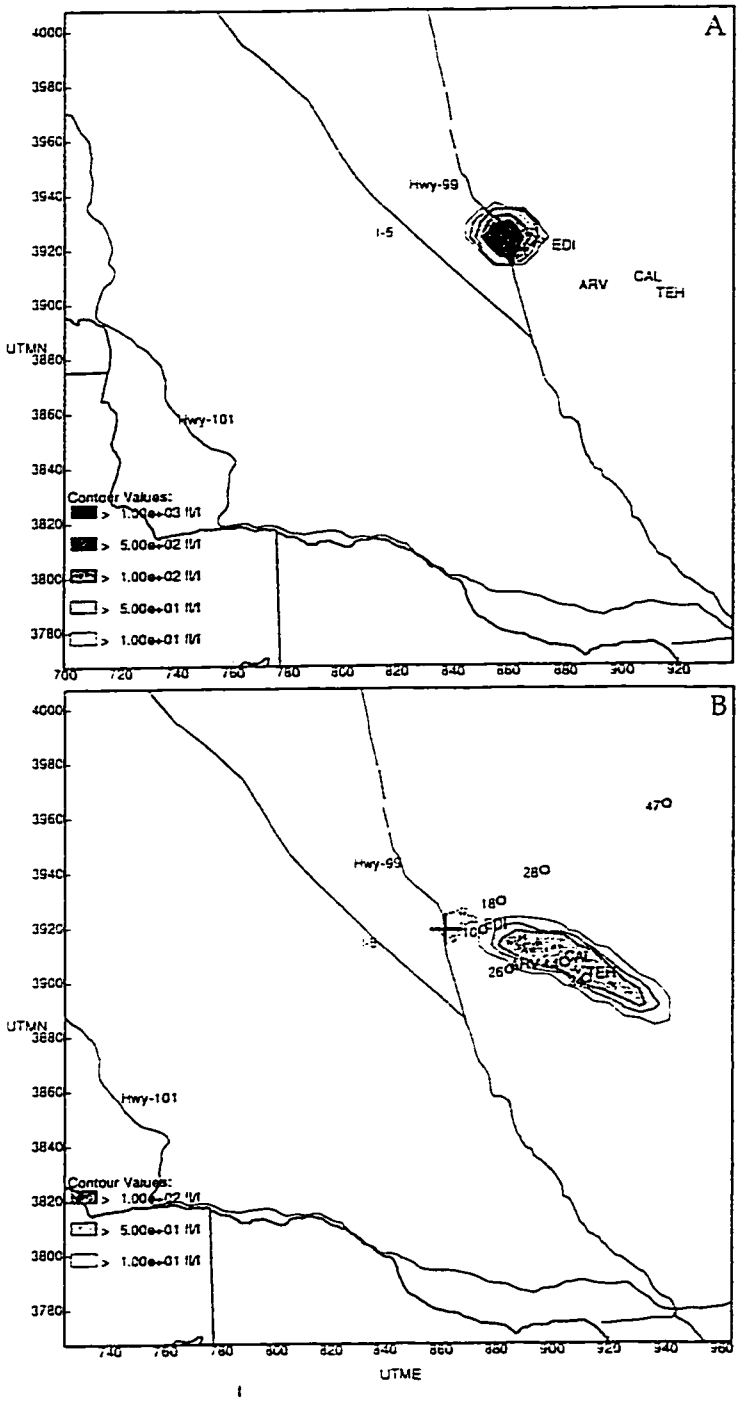
A
Hwy-99
I-5
EDI
ARV
CAL
TEH
UTMN
Hwy-101
Contour Values:
> 1.00e+03 ft/t
> 5.00e+02 ft/t
> 1.00e+02 ft/t
> 5.00e+01 ft/t
> 1.00e+01 ft/t
B
Hwy-99
EDI
CAL
ARV
TEH
Hwy-101
Contour Values:
> 5.00e+01 ft/t
> 1.00e+01 ft/t
UTME

Fig. 37

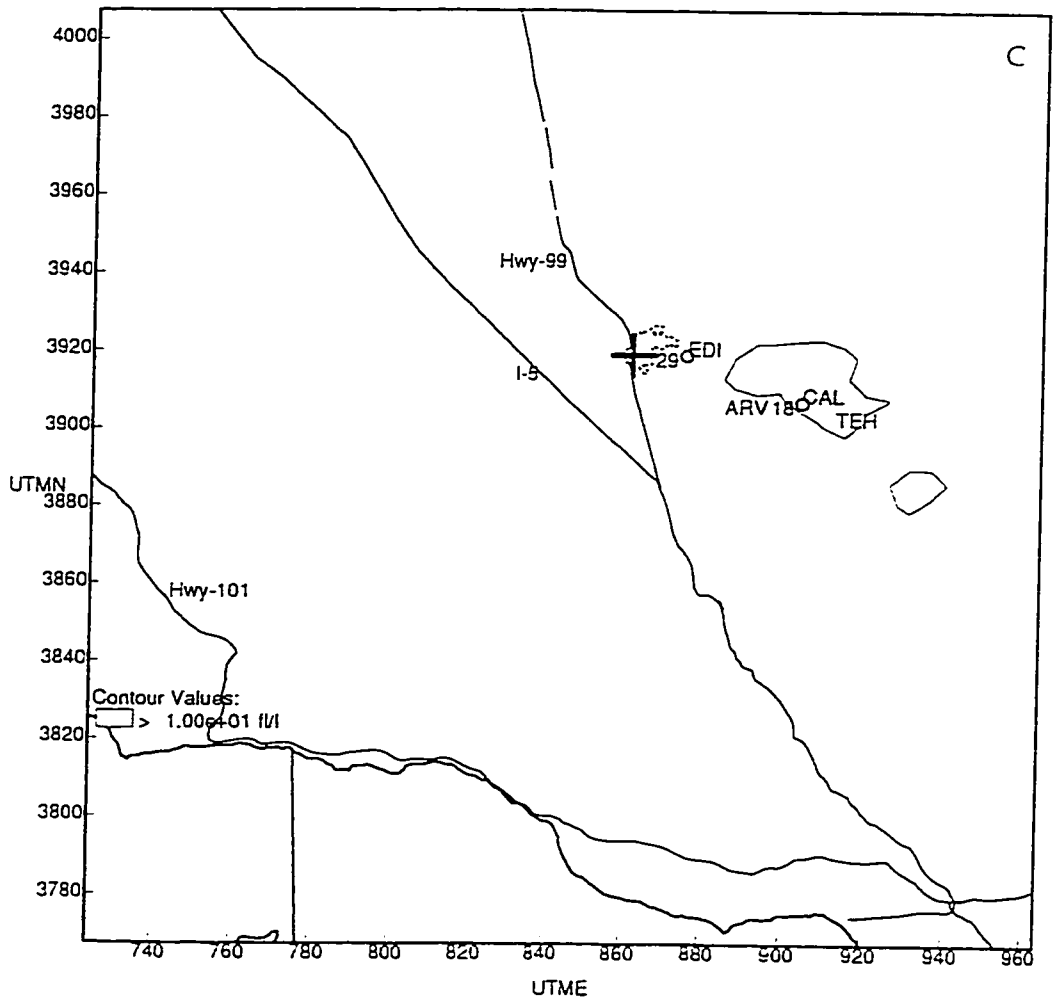

Fig. 37 (continued)

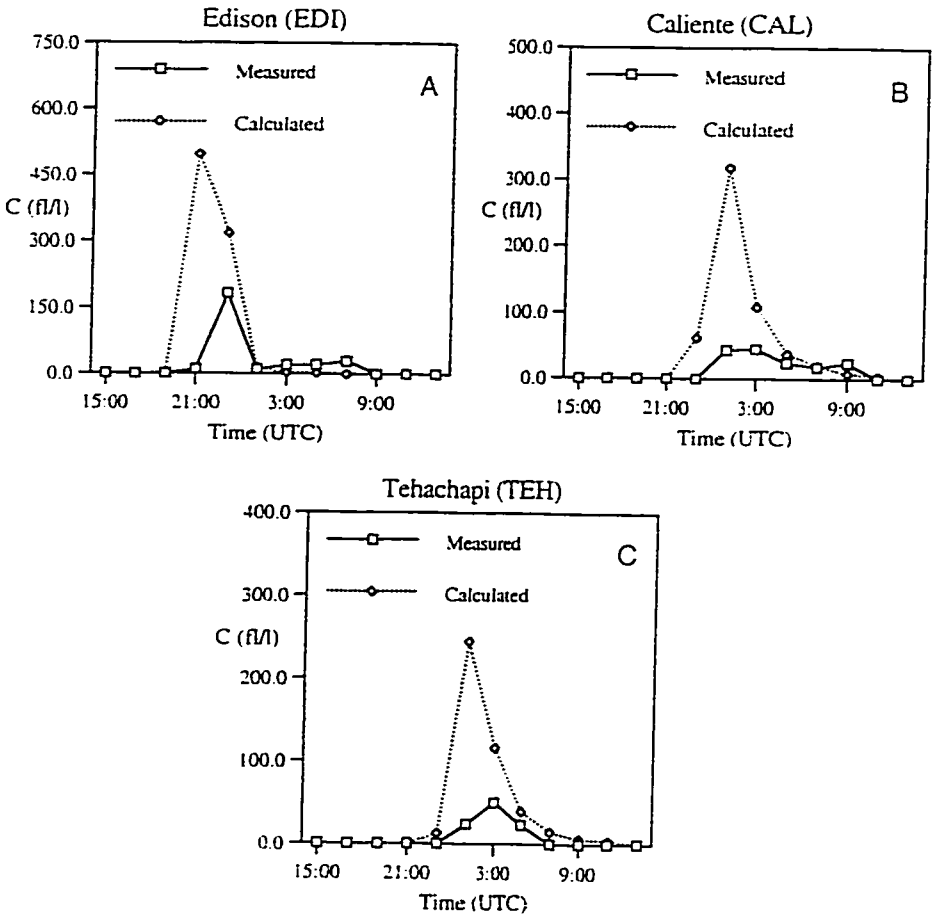
Edison (EDI)
750.0
600.0
450.0
300.0
150.0
0.0
C (fl/l)
Measured
Calculated
A
15:00
21:00
3:00
9:00
Time (UTC)
Caliente (CAL)
500.0
400.0
300.0
200.0
100.0
0.0
C (fl/l)
Measured
Calculated
B
15:00
21:00
3:00
9:00
Time (UTC)
Tehachapi (TEH)
400.0
300.0
200.0
100.0
0.0
C (fl/l)
Measured
Calculated
C
15:00
21:00
3:00
9:00
Time (UTC)

Fig. 38

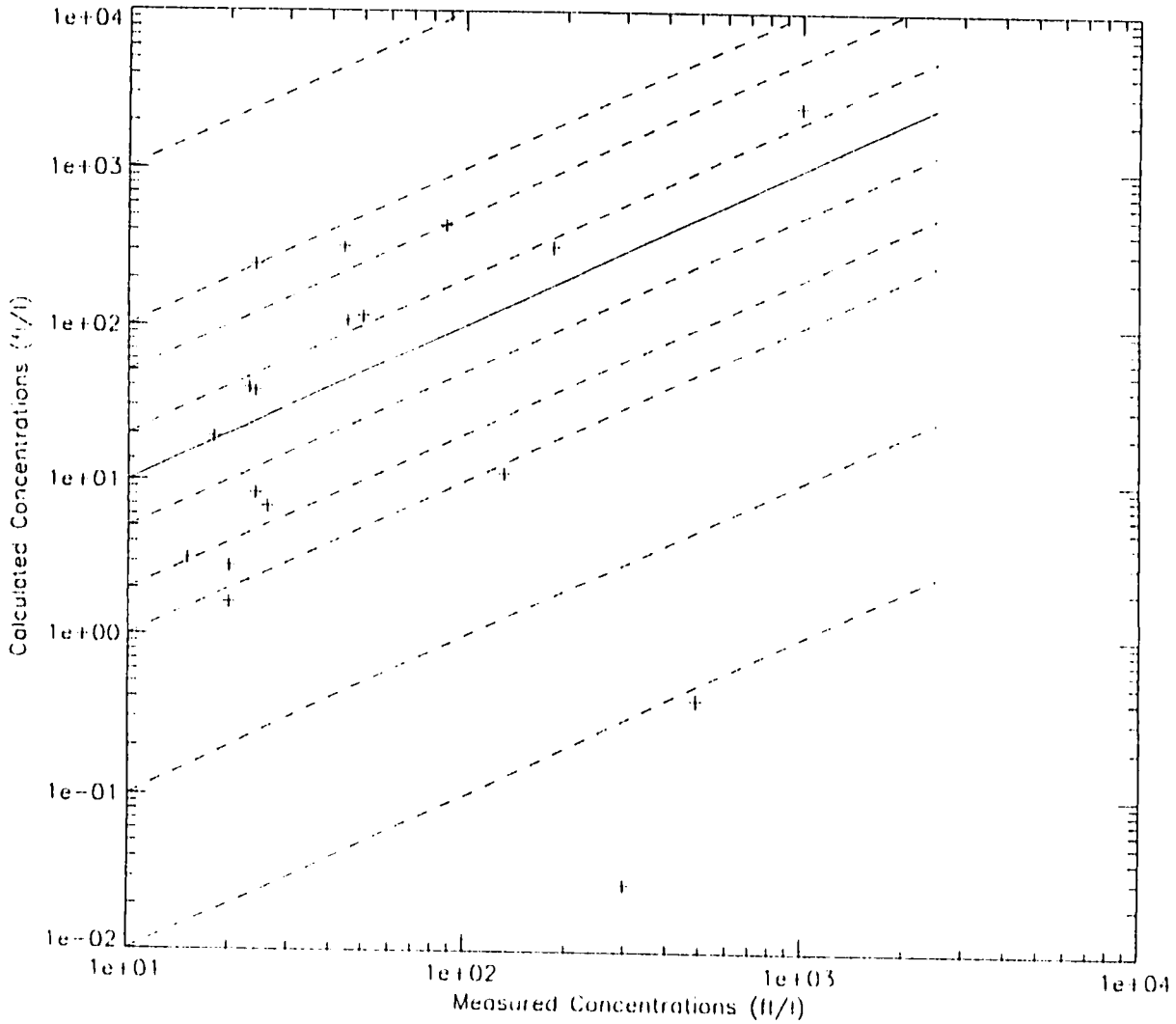
1e+04
1e+03
1e+02
1e+01
1e+00
1e-01
1e-02
Calculated Concentrations (ft/l)
1e+01
1e+02
1e+03
1e+04
Measured Concentrations (ft/l)

Fig. 39

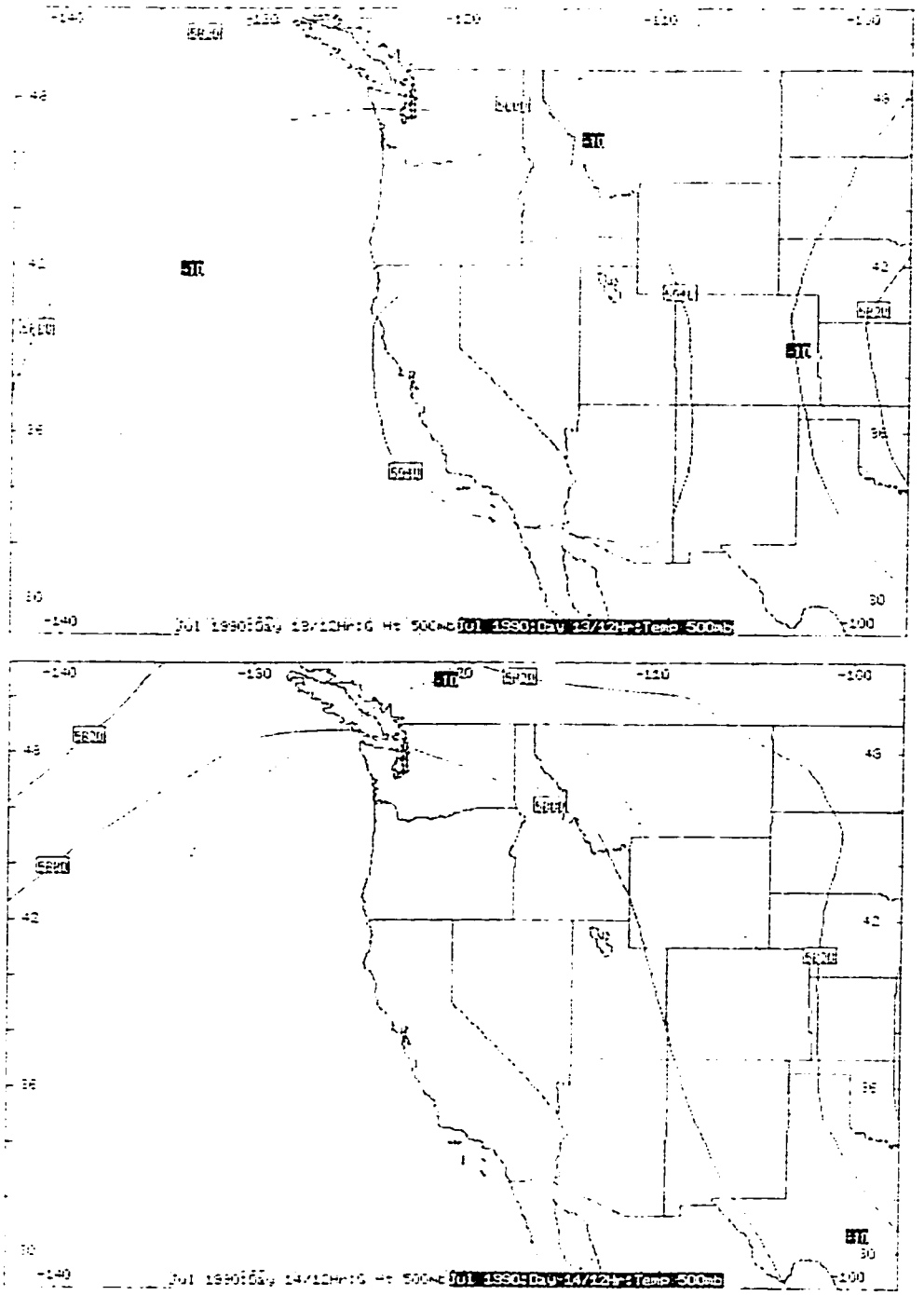

Fig. 40

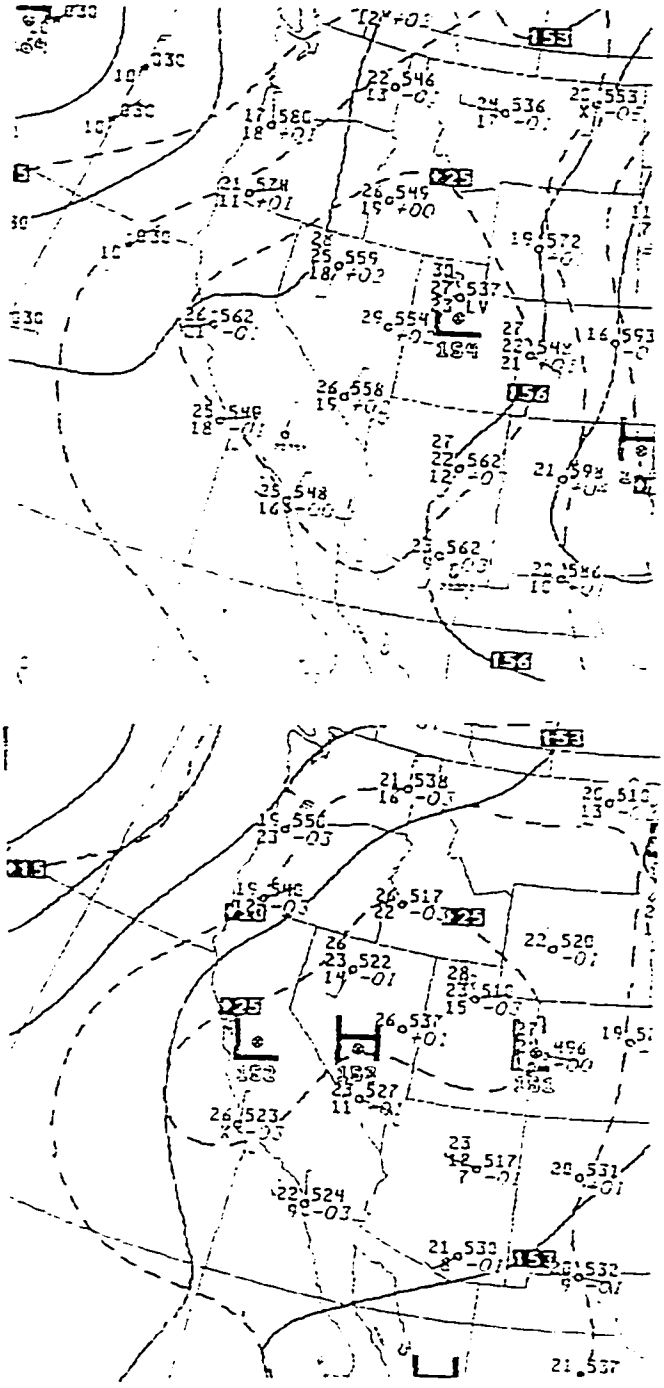

Fig. 41

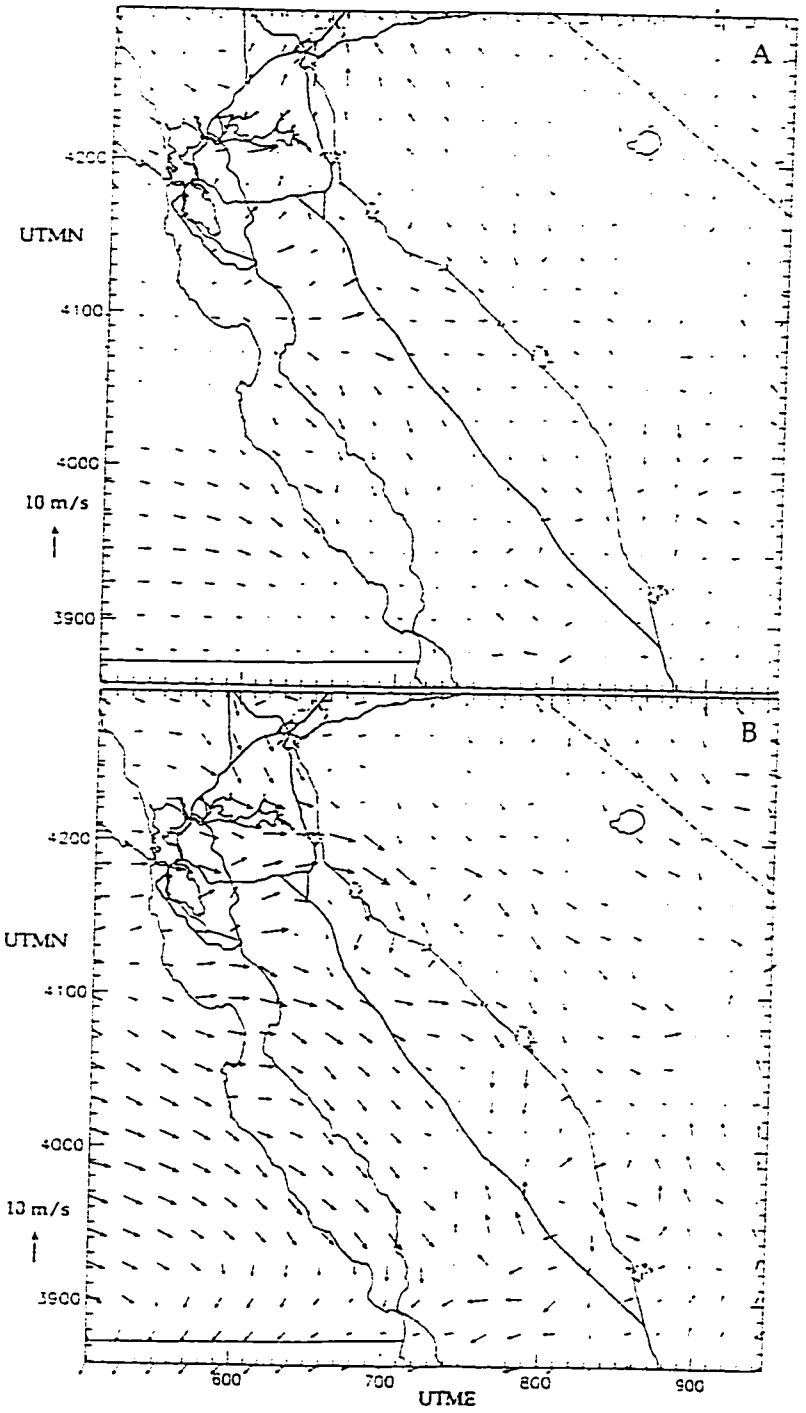
A
4200
UTMN
4100
4000
10 m/s
3900
B
4200
UTMN
4100
4000
10 m/s
3900
600
700
800
900
UTME

Fig. 42

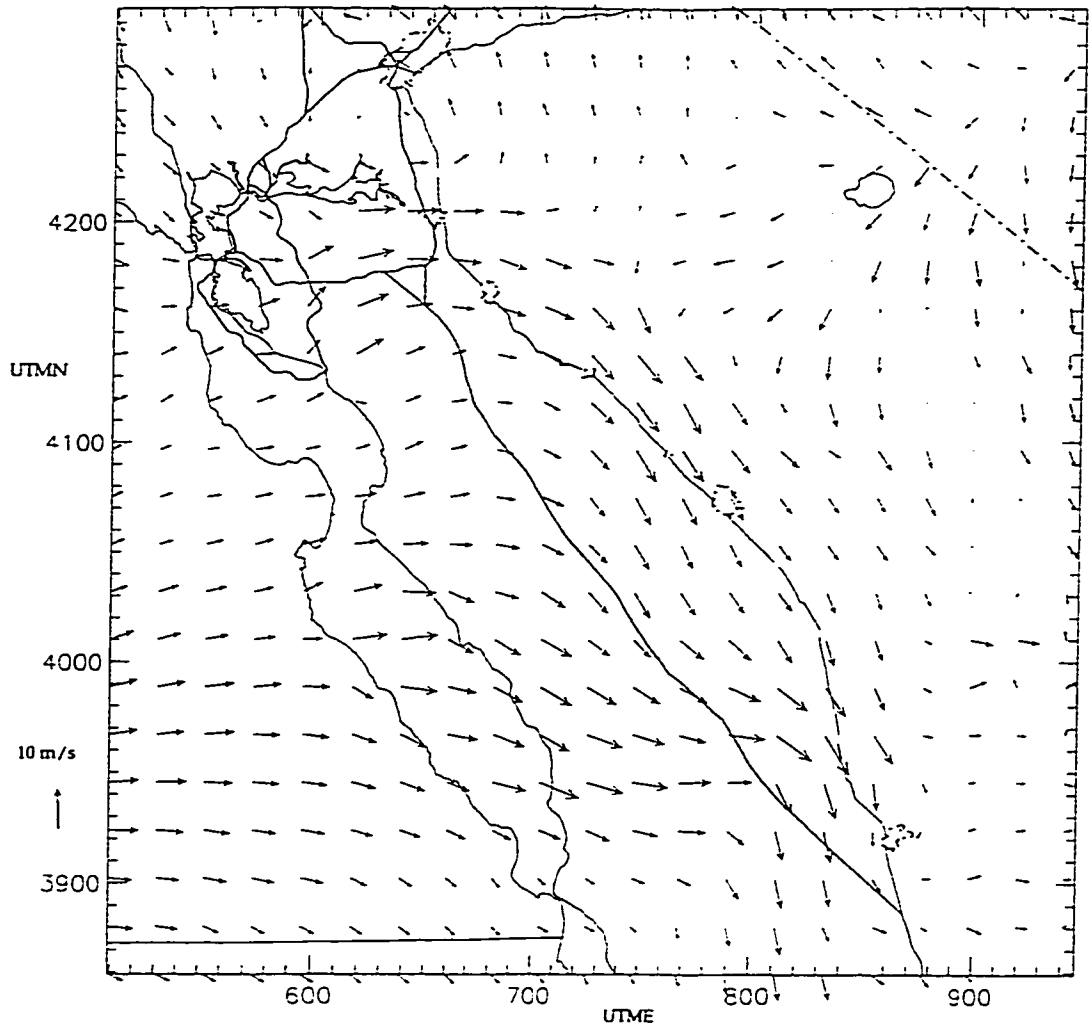

Fig. 43

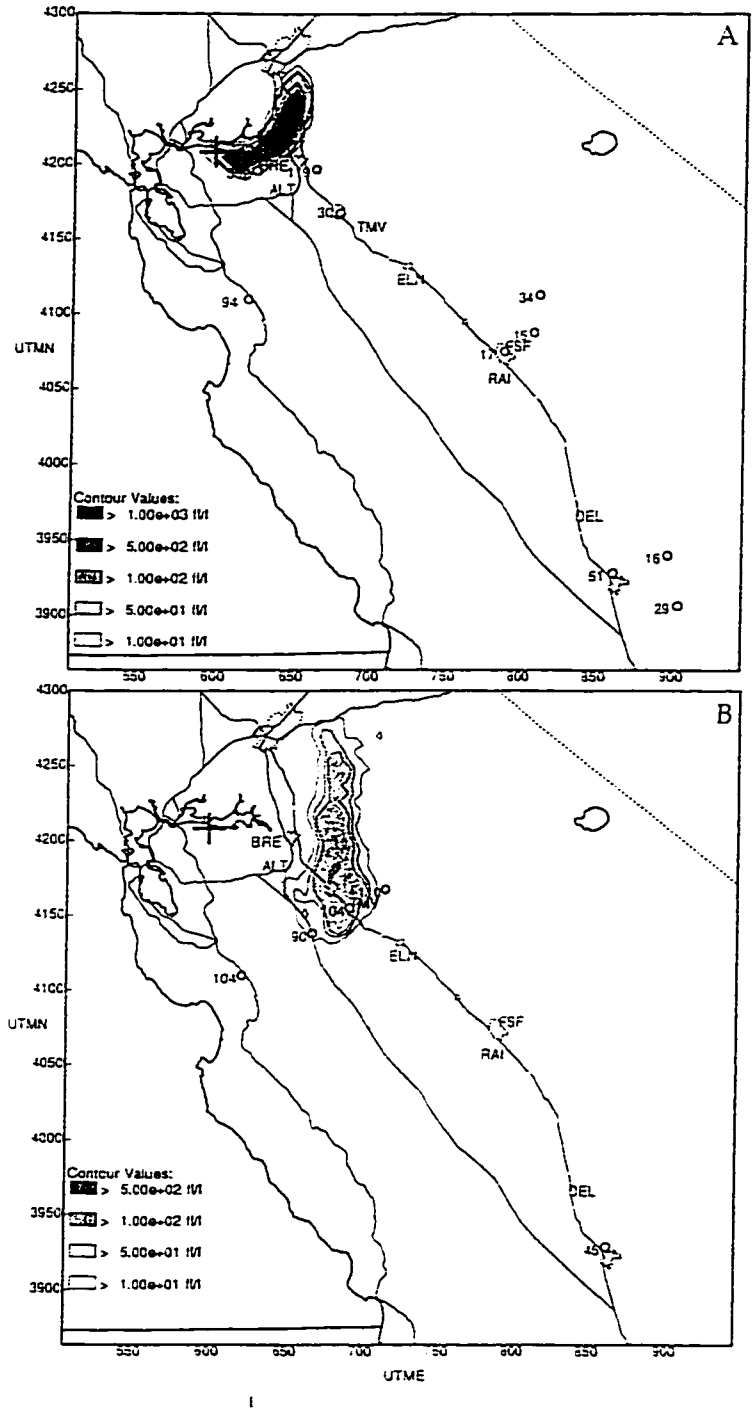
A
B
UTMN
UTME
BRE
ALT
TMV
ELY
RAI
DEL
ESF
Contour Values:
> 1.00e+03 f/l
> 5.00e+02 f/l
> 1.00e+02 f/l
> 5.00e+01 f/l
> 1.00e+01 f/l

Fig. 11

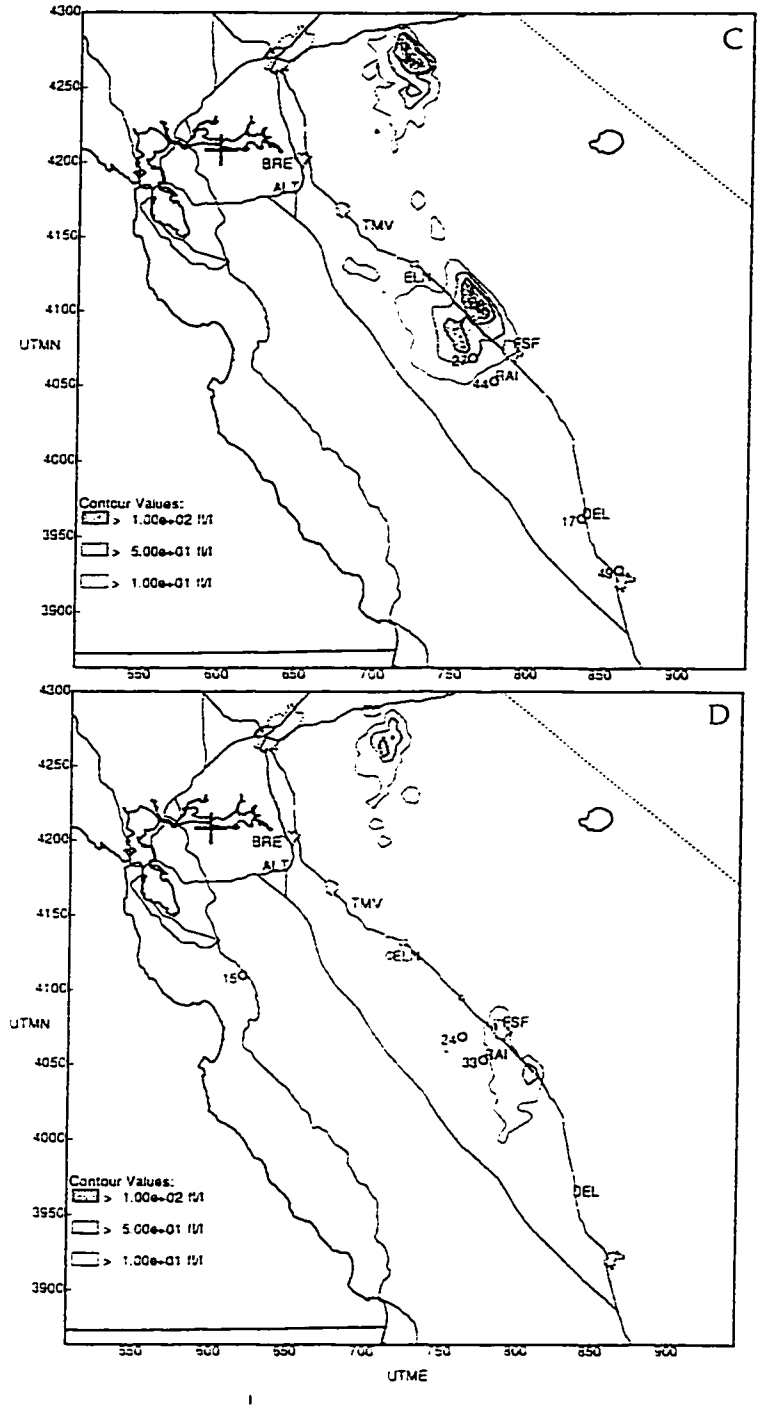

Fig. ~~11~~ (continued)

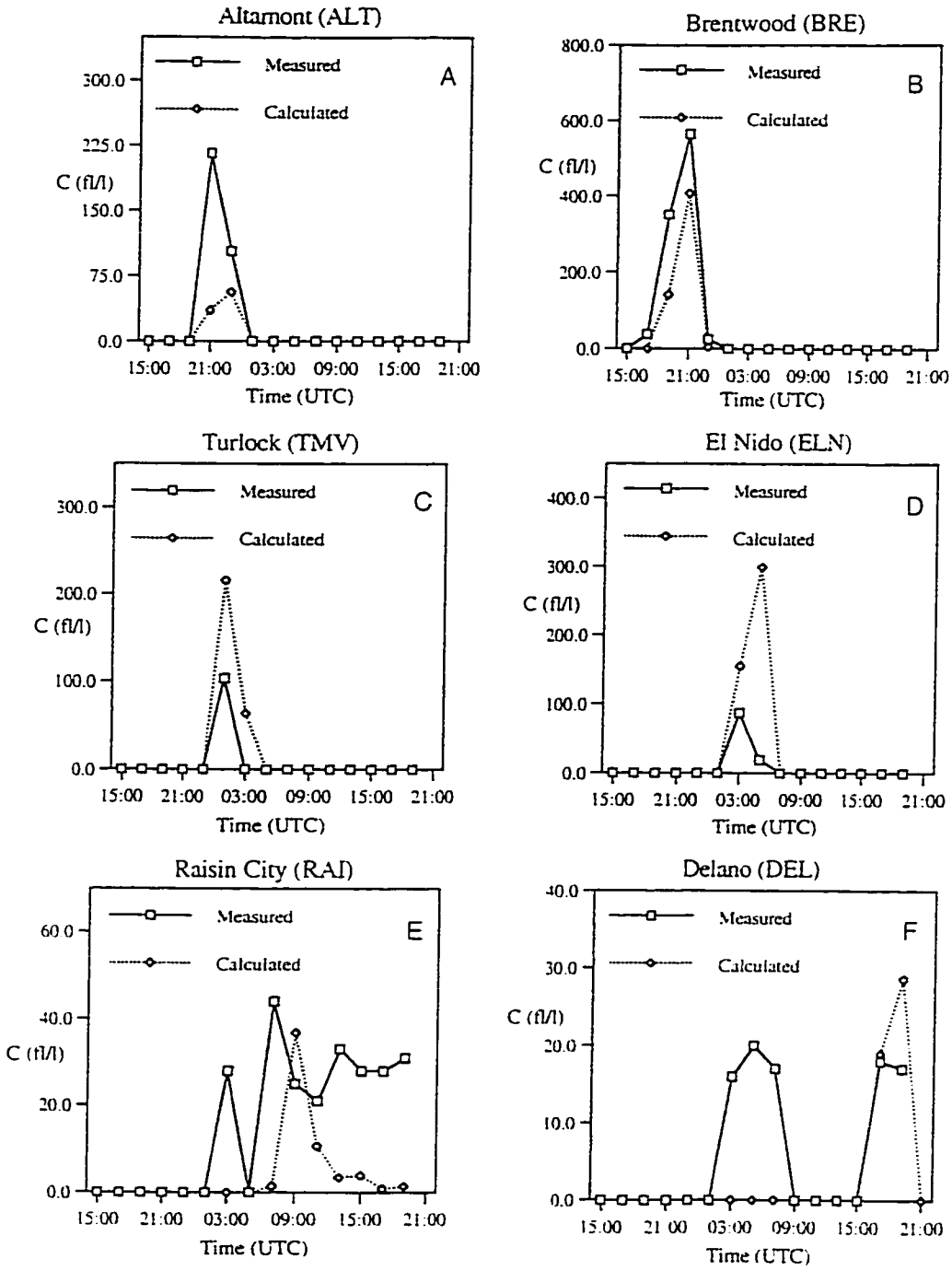
Altamont (ALT)
Measured
Calculated
A
300.0
225.0
C (fl/l)
150.0
75.0
0.0
15:00 21:00 03:00 09:00 15:00 21:00
Time (UTC)
Brentwood (BRE)
Measured
Calculated
B
800.0
600.0
C (fl/l)
400.0
200.0
0.0
15:00 21:00 03:00 09:00 15:00 21:00
Time (UTC)
Turlock (TMV)
Measured
Calculated
C
300.0
200.0
C (fl/l)
100.0
0.0
15:00 21:00 03:00 09:00 15:00 21:00
Time (UTC)
El Nido (ELN)
Measured
Calculated
D
400.0
300.0
C (fl/l)
200.0
100.0
0.0
15:00 21:00 03:00 09:00 15:00 21:00
Time (UTC)
Raisin City (RAI)
Measured
Calculated
E
60.0
40.0
C (fl/l)
20.0
0.0
15:00 21:00 03:00 09:00 15:00 21:00
Time (UTC)
Delano (DEL)
Measured
Calculated
F
40.0
30.0
C (fl/l)
20.0
10.0
0.0
15:00 21:00 03:00 09:00 15:00 21:00
Time (UTC)

Fig. 45

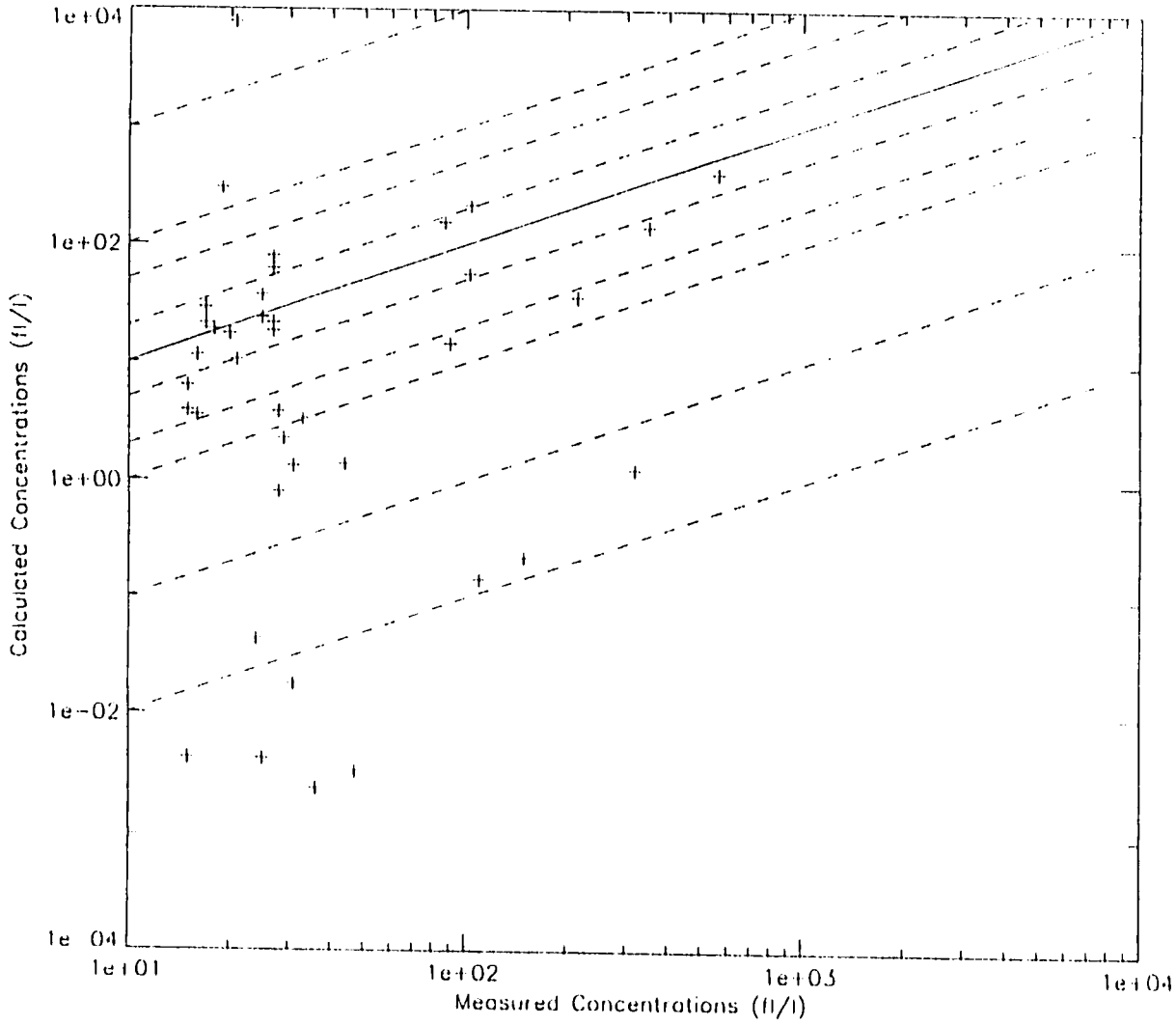
1e+04
1e+02
1e+00
1e-02
1e-04
Calculated Concentrations (fl/l)
1e+01
1e+02
1e+03
1e+04
Measured Concentrations (fl/l)

Fig. 46

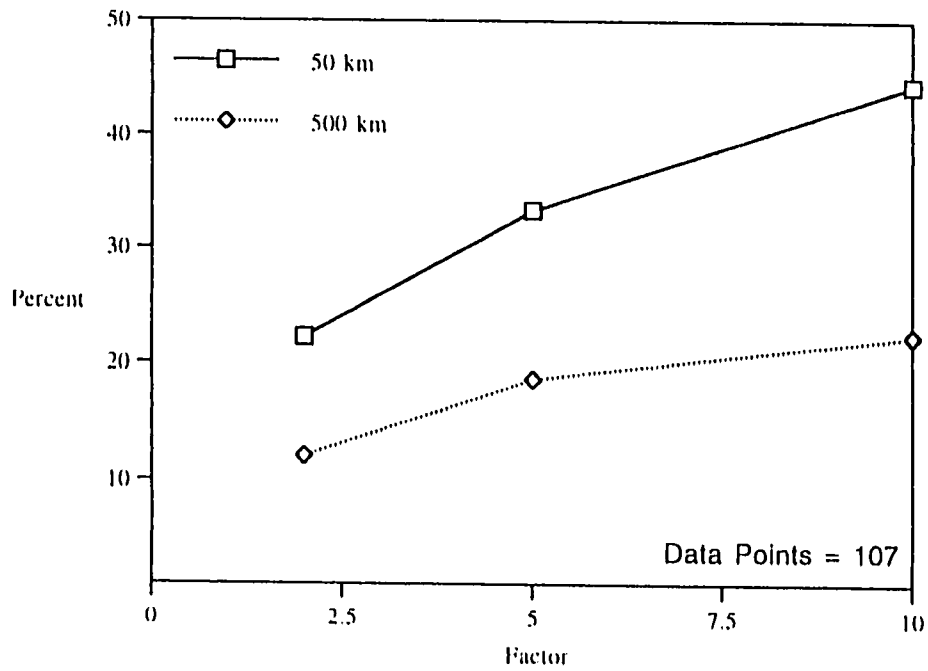
50
40
30
20
10
Percent
50 km
500 km
Data Points = 107
0
2.5
5
7.5
10
Factor

Fig. 47

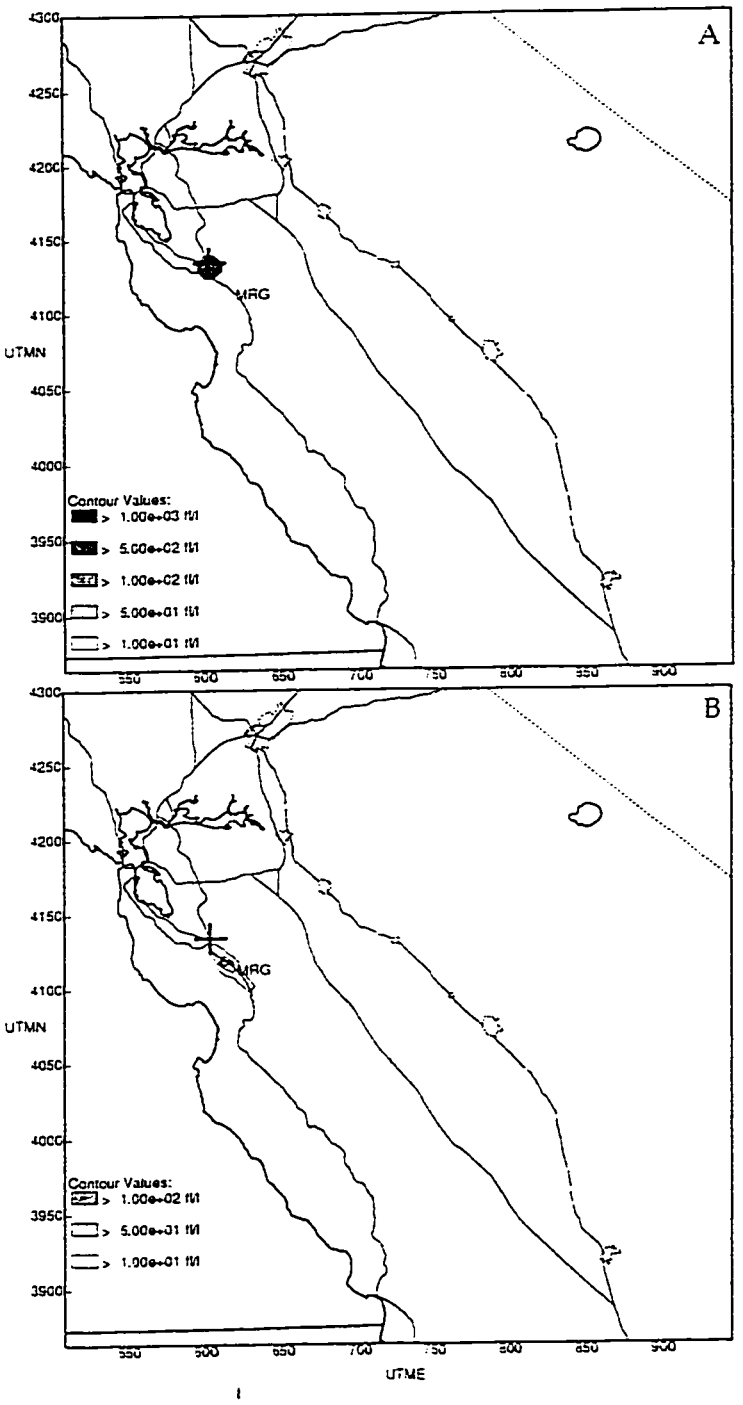
A
B
MRG
MRG
UTMN
UTMN
UTME
Contour Values:
> 1.00e+03 ft/t
> 5.00e+02 ft/t
> 1.00e+02 ft/t
> 5.00e+01 ft/t
> 1.00e+01 ft/t
Contour Values:
> 1.00e+02 ft/t
> 5.00e+01 ft/t
> 1.00e+01 ft/t

Fig. 48

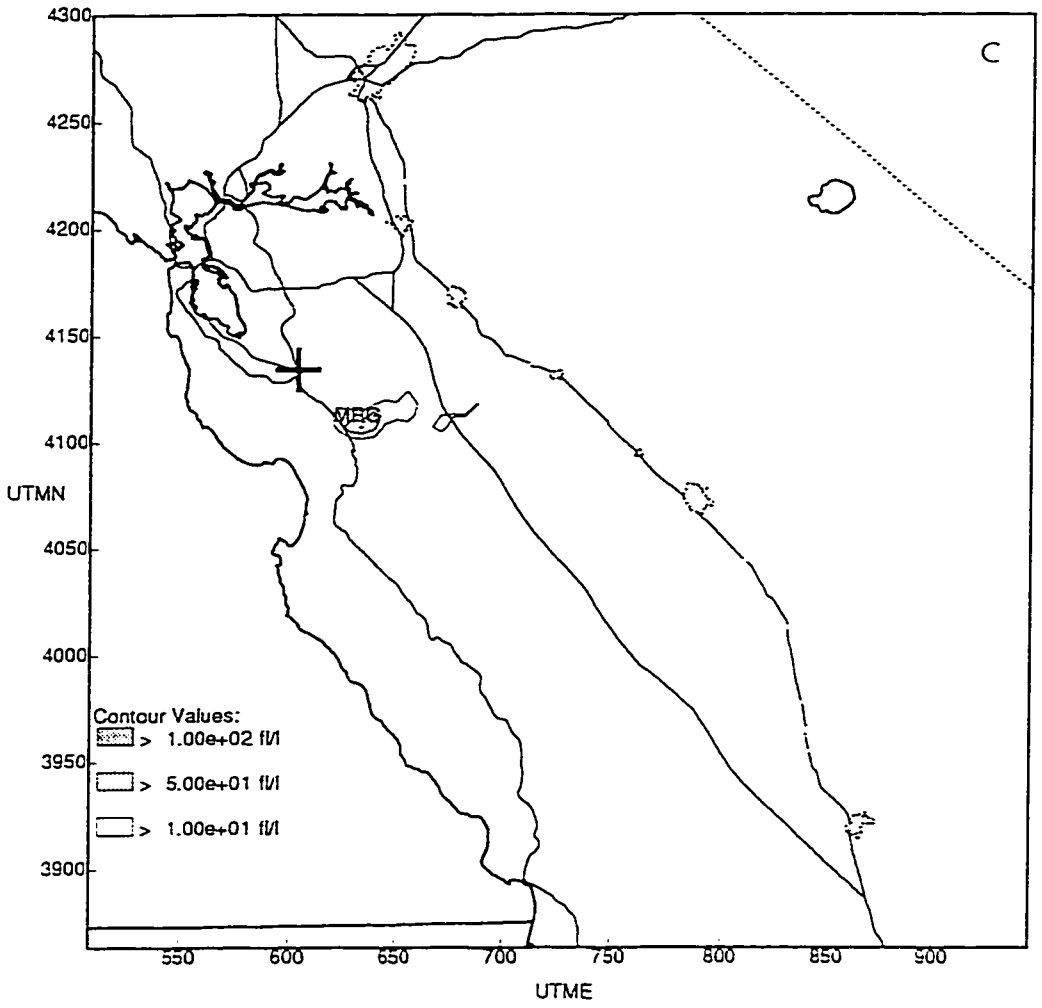

Fig. 48 (continued)

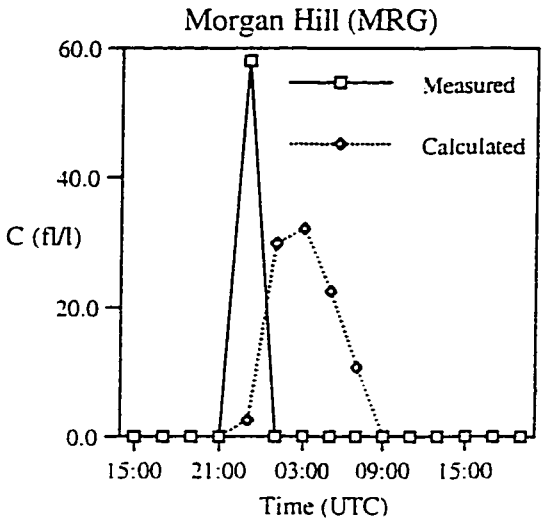
Morgan Hill (MRG)
60.0
40.0
20.0
0.0
C (fl/l)
Measured
Calculated
15:00
21:00
03:00
09:00
15:00
Time (UTC)

Fig. 49

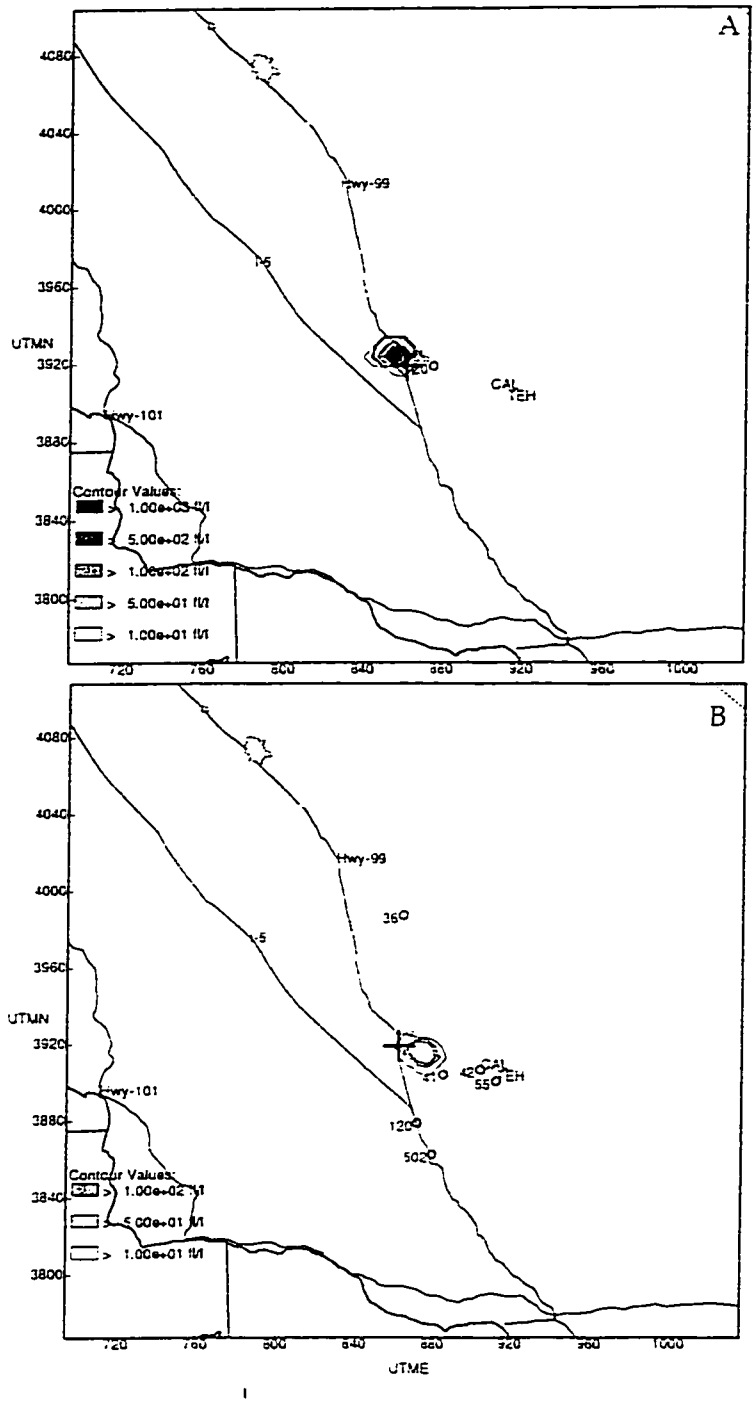
A
B
Hwy-99
I-5
Hwy-101
UTMN
UTME
Contour Values:
> 1.00e+03 f/l
> 5.00e+02 f/l
> 1.00e+02 f/l
> 5.00e+01 f/l
> 1.00e+01 f/l
4080
4040
4000
3960
3920
3880
3840
3800
720
760
800
840
880
920
960
1000

Fig. 50

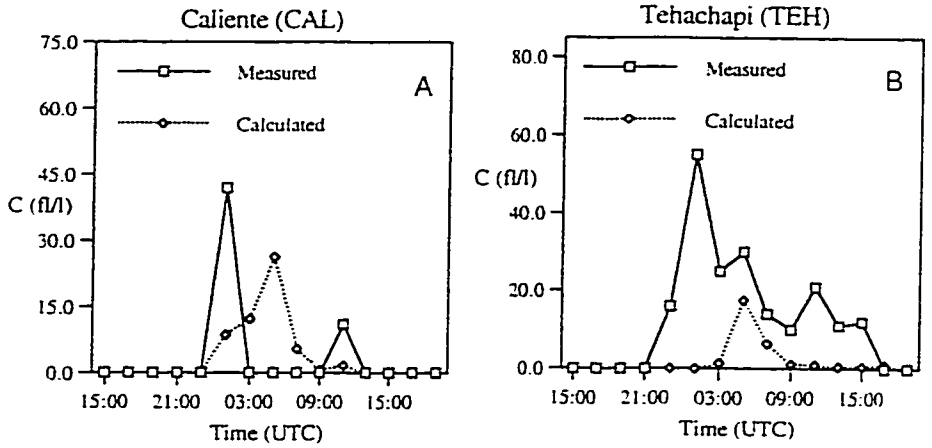
Caliente (CAL)
75.0
60.0
45.0
30.0
15.0
0.0
C (fl/l)
Measured
Calculated
A
15:00
21:00
03:00
09:00
15:00
Time (UTC)
Tehachapi (TEH)
80.0
60.0
40.0
20.0
0.0
C (fl/l)
Measured
Calculated
B
15:00
21:00
03:00
09:00
15:00
Time (UTC)

Fig. 51

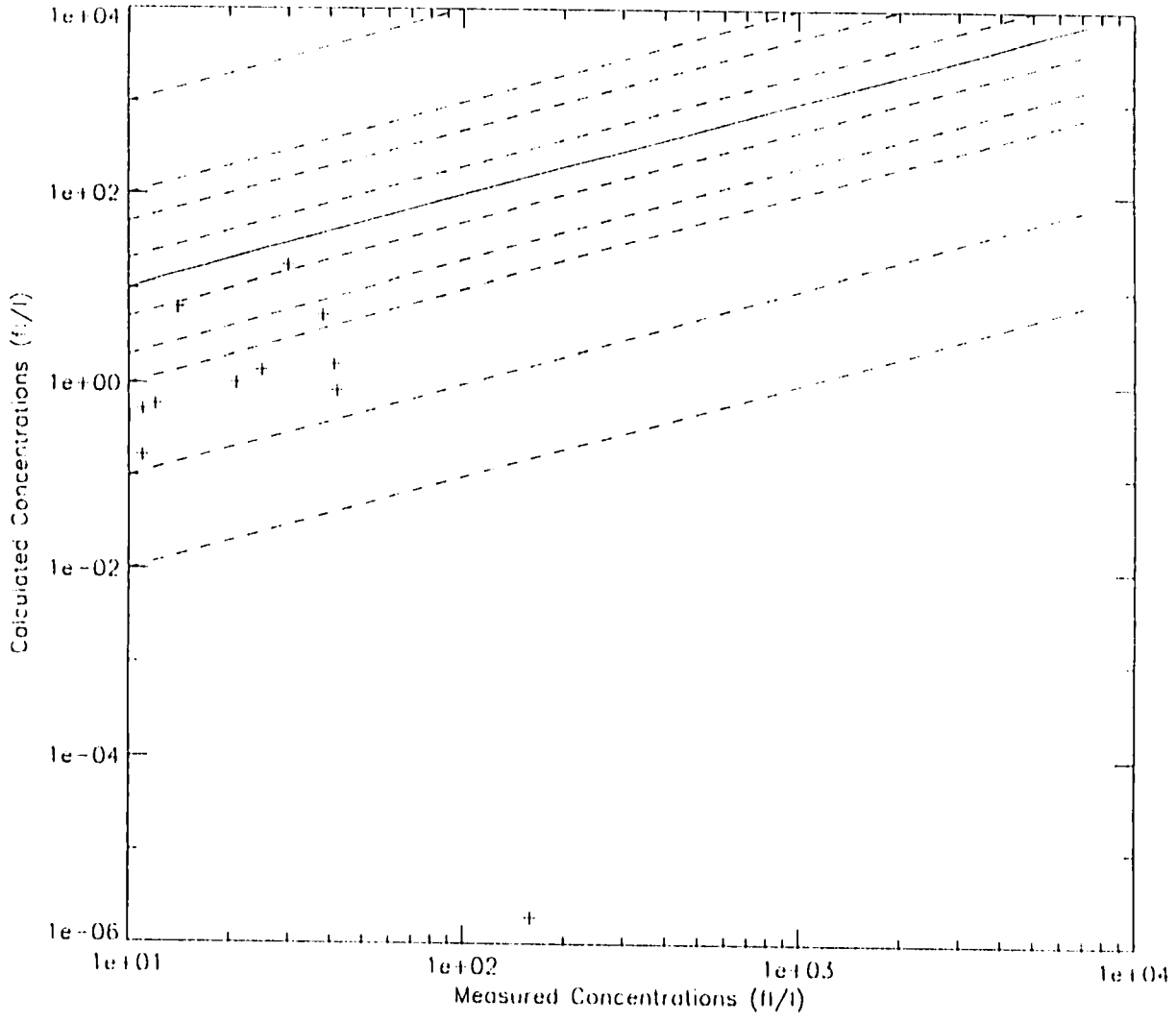
1e+04
1e+02
1e+00
1e-02
1e-04
1e-06
Calculated Concentrations (ft/l)
1e+01
1e+02
1e+03
1e+04
Measured Concentrations (ft/l)

Fig. 52

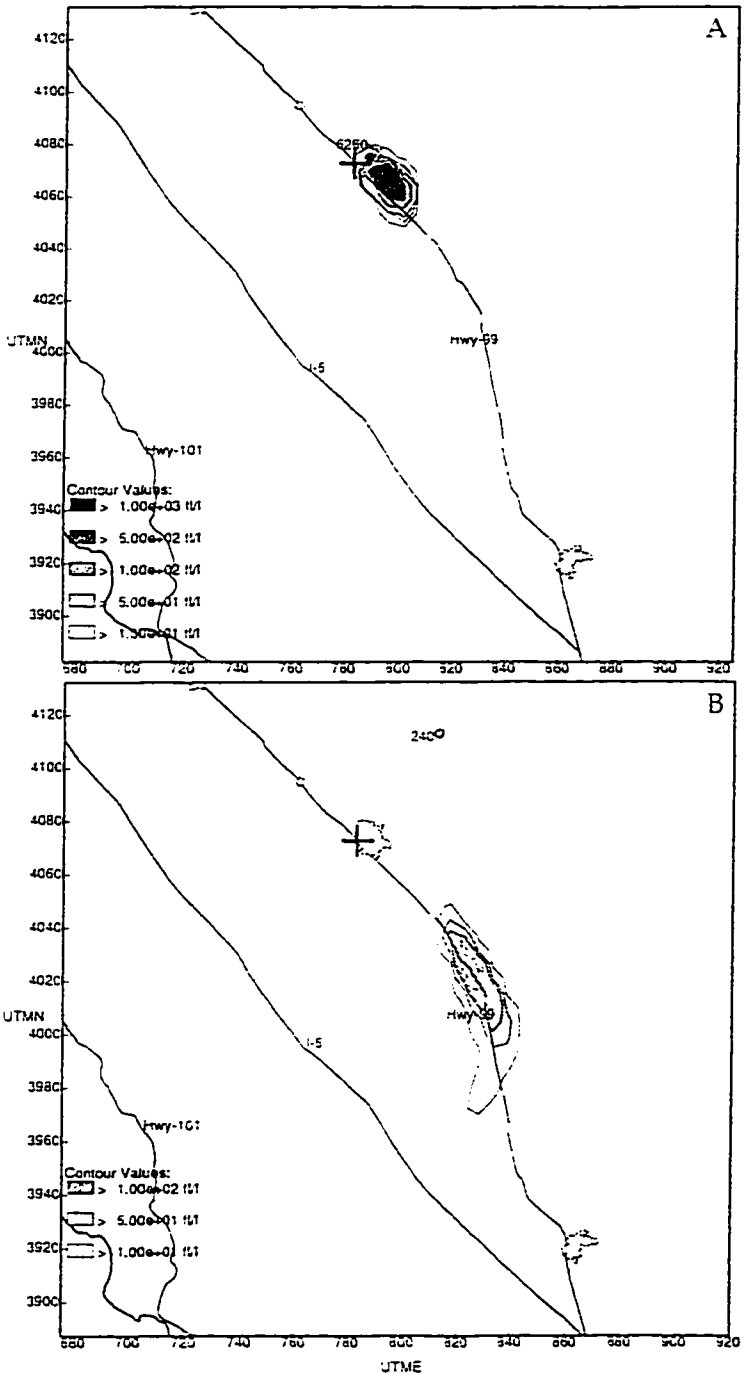
A
B
UTMN
UTME
Hwy-99
I-5
Hwy-101
Contour Values:
> 1.00e+03 ft/t
> 5.00e+02 ft/t
> 1.00e+02 ft/t
> 5.00e+01 ft/t
> 1.00e+01 ft/t
> 1.00e+02 ft/t
> 5.00e+01 ft/t
> 1.00e+01 ft/t

Fig. 53

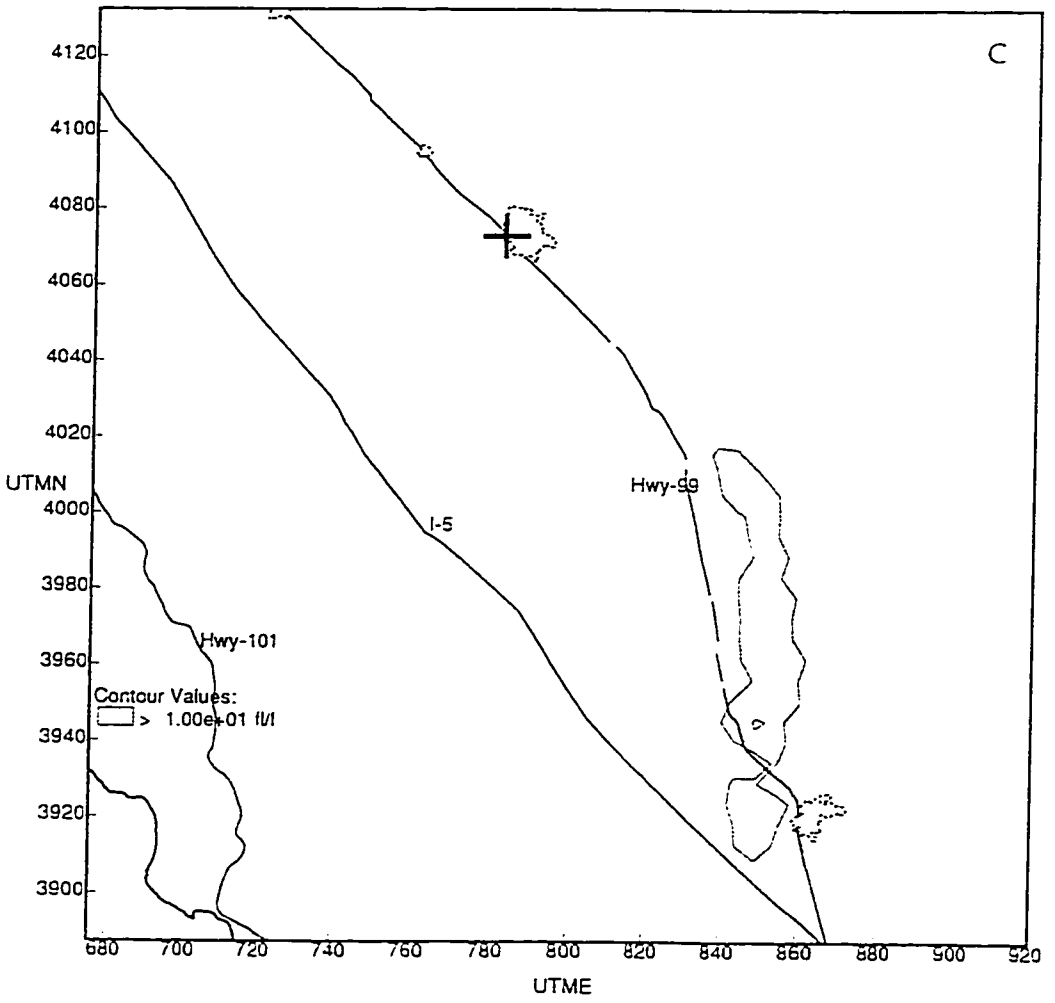

Fig. 53 (continued)

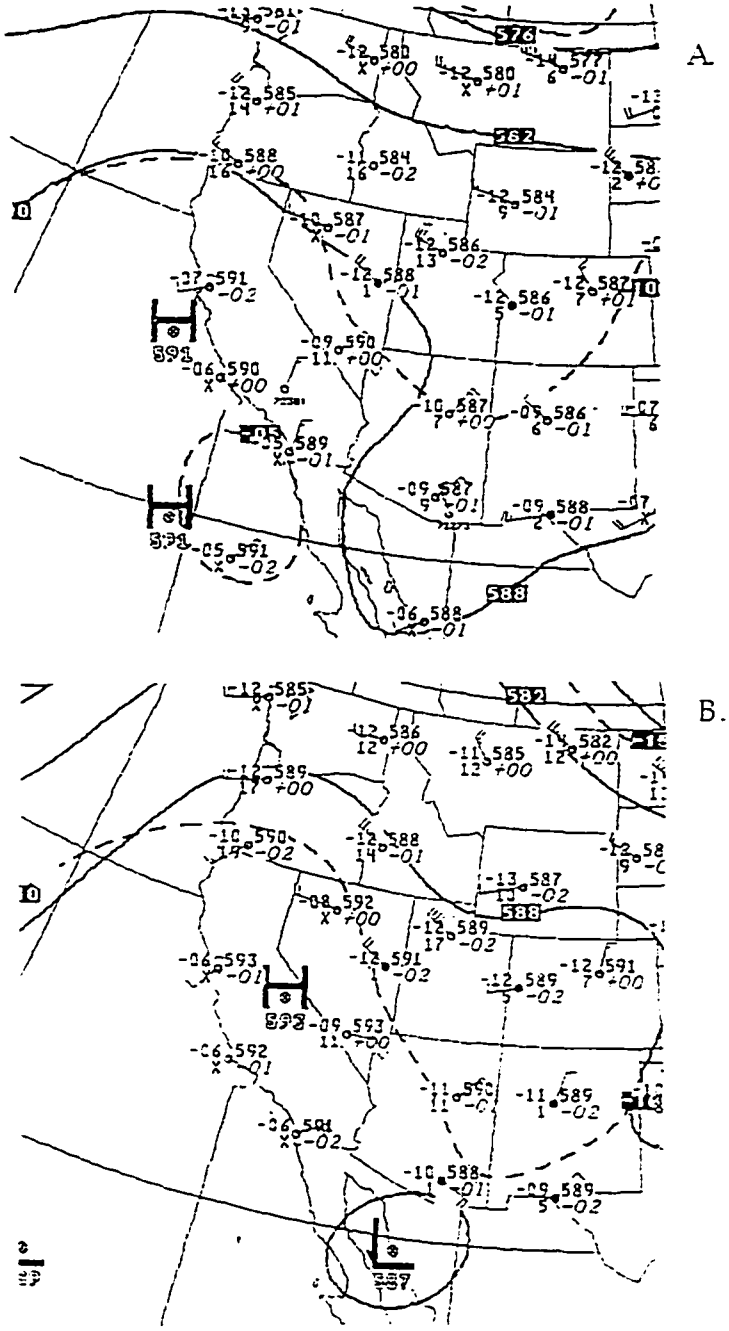

Fig. 54

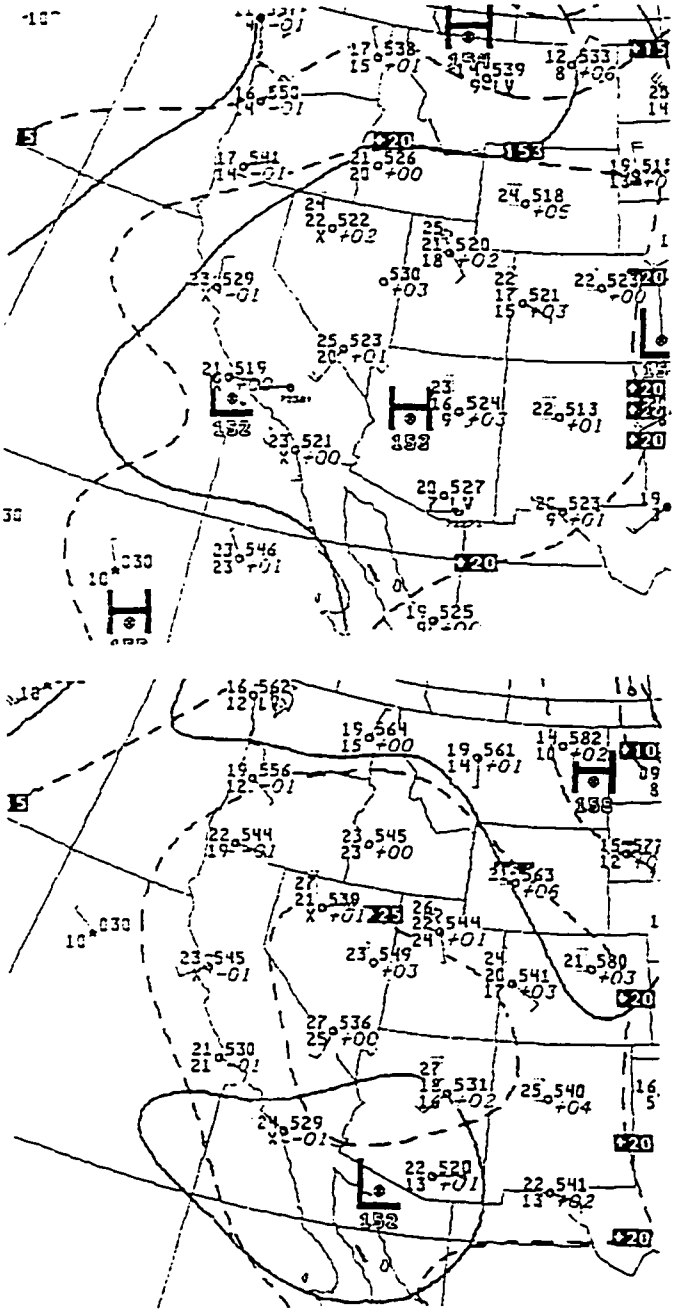

Fig. 55

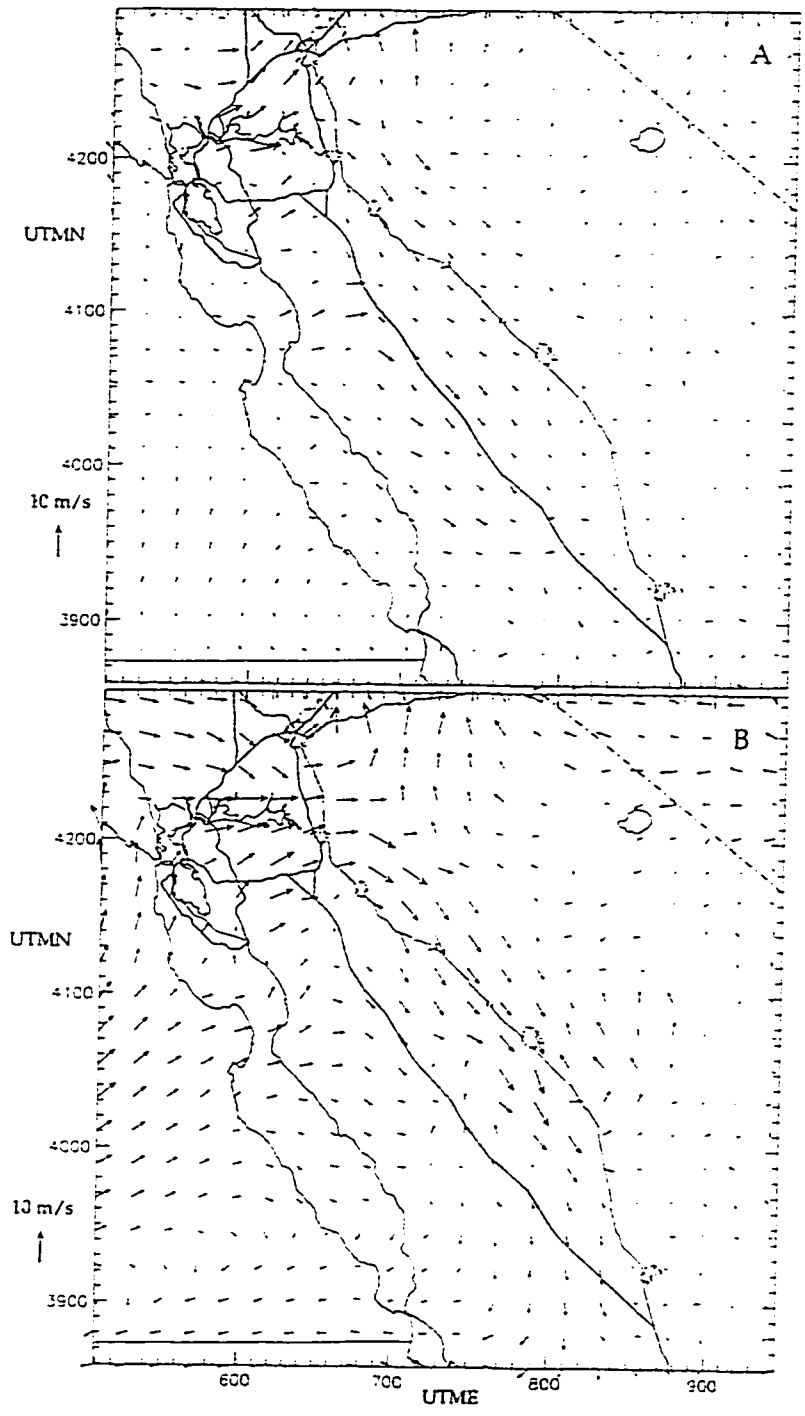
A
4200
UTMN
4100
4000
10 m/s
3900
B
4200
UTMN
4100
4000
10 m/s
3900
600
700
800
900
UTME

Fig. 56

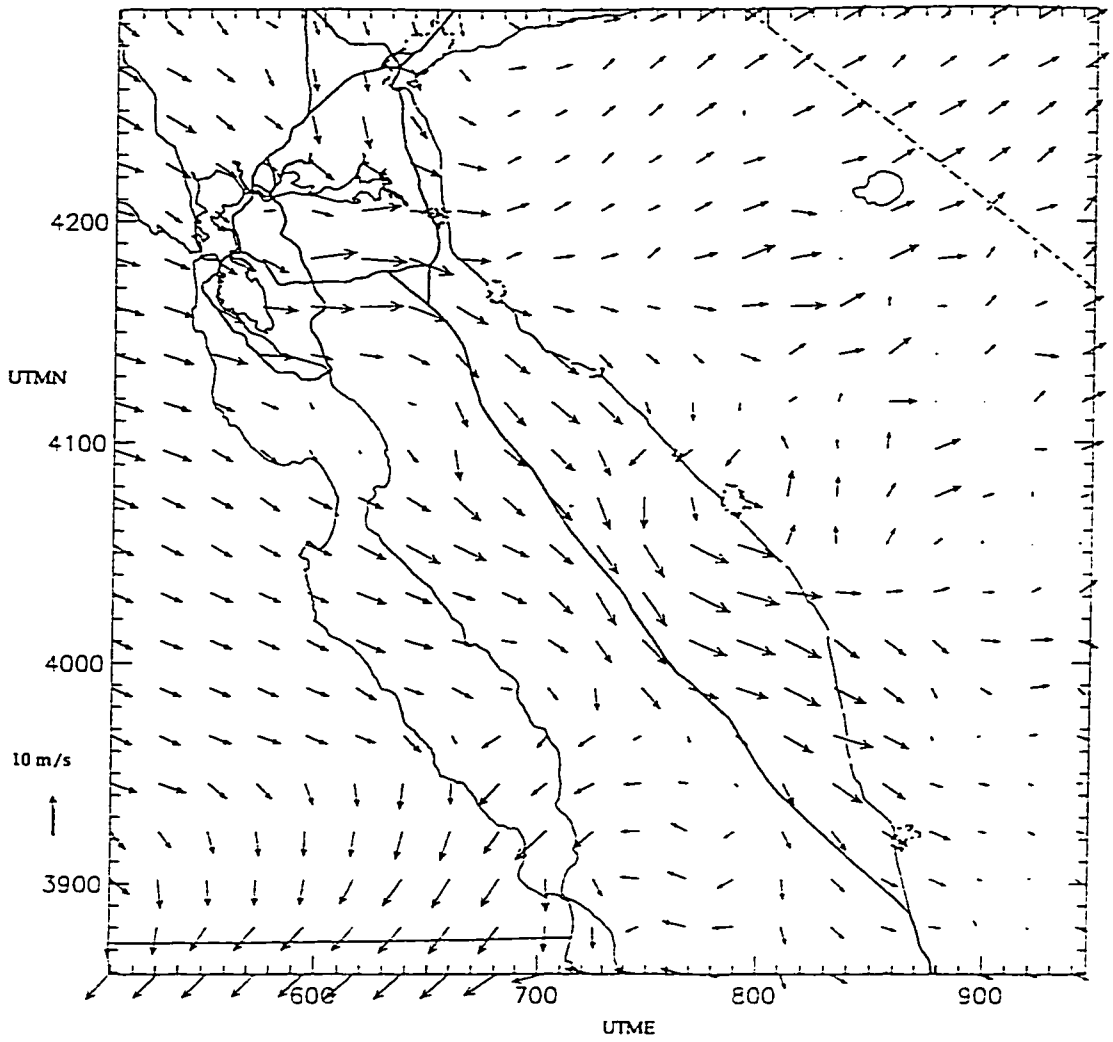

Fig. 57

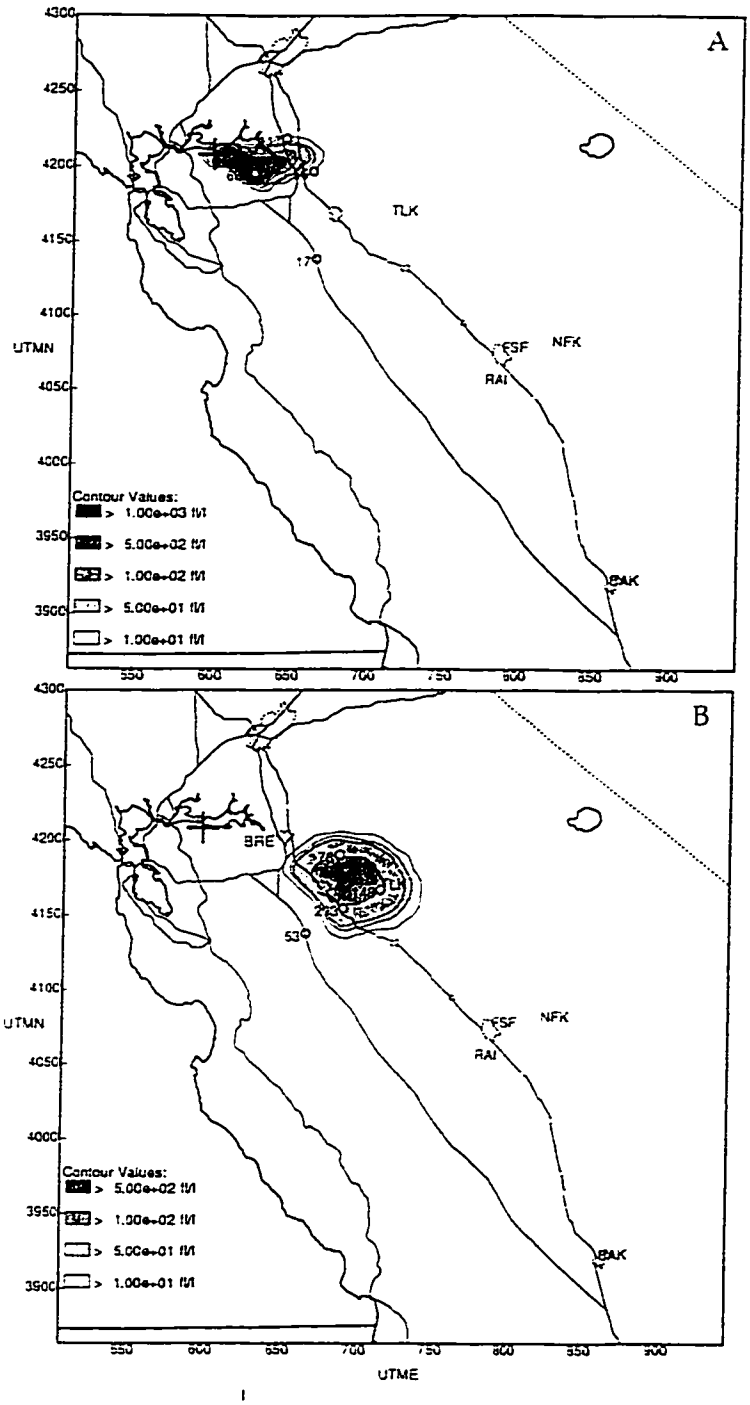
A
TLK
FSF
NFK
RAI
BAK
UTMN
Contour Values:
> 1.00e+03 f/l
> 5.00e+02 f/l
> 1.00e+02 f/l
> 5.00e+01 f/l
> 1.00e+01 f/l
B
BRE
FSF
NFK
RAI
BAK
UTMN
UTME
Contour Values:
> 5.00e+02 f/l
> 1.00e+02 f/l
> 5.00e+01 f/l
> 1.00e+01 f/l

Fig. 58

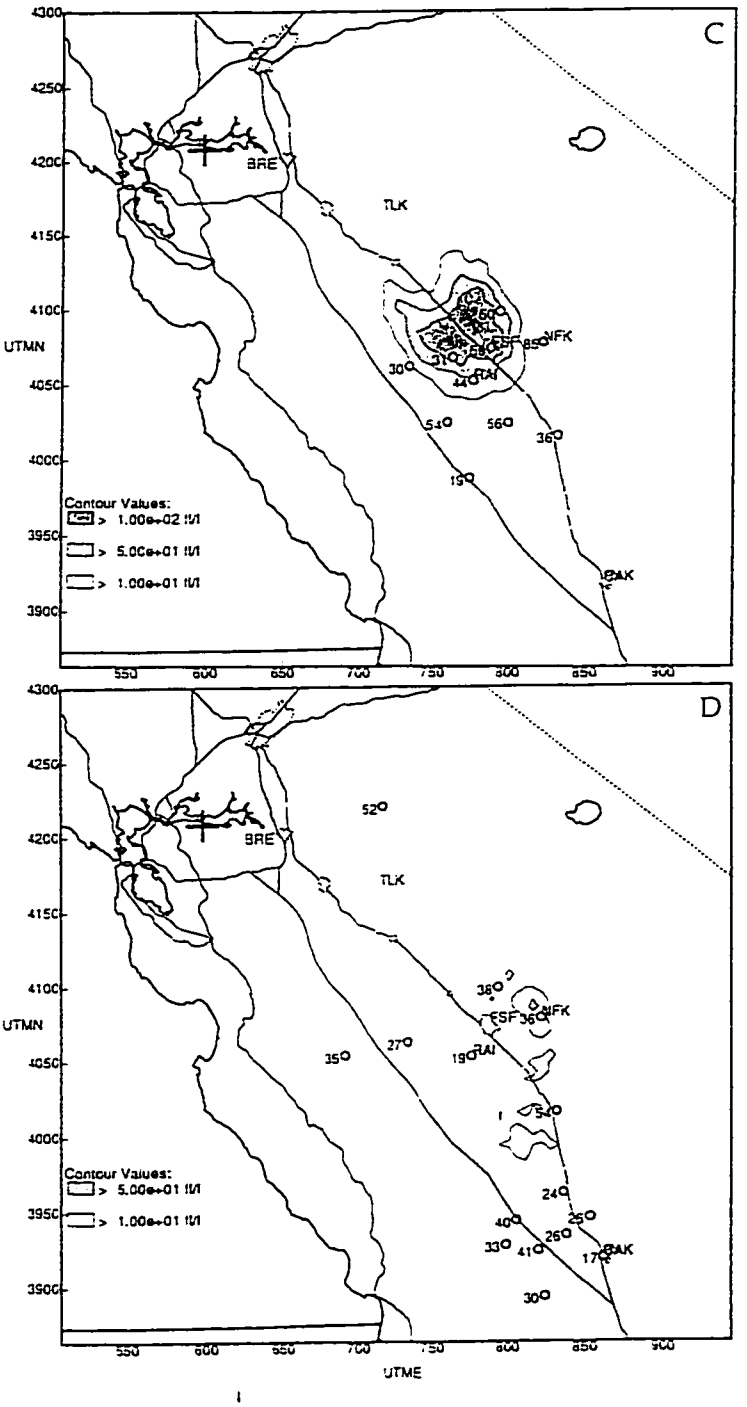

Fig. 58 (continued)

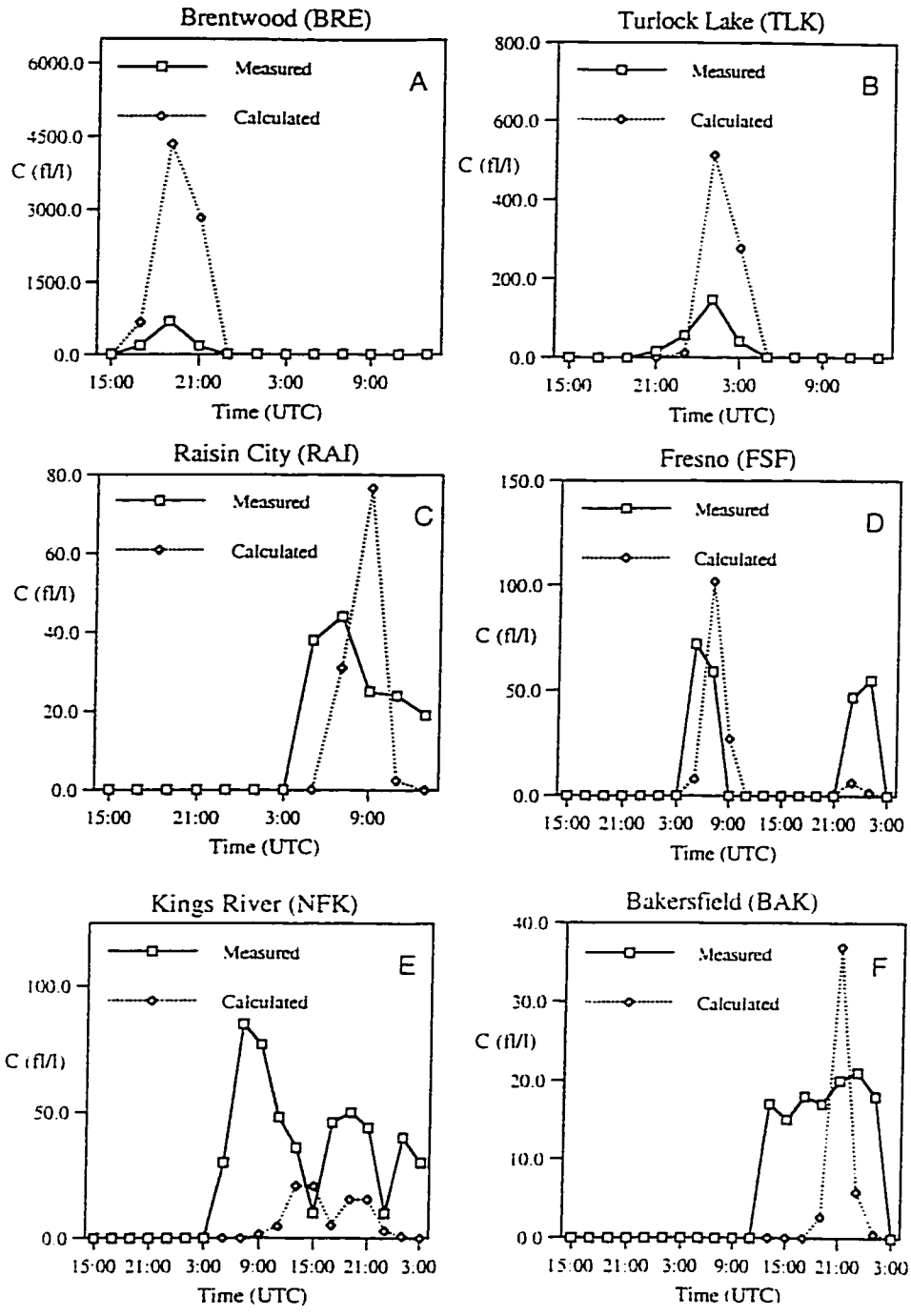
Brentwood (BRE)
Measured
Calculated
A
C (fl/l)
6000.0
4500.0
3000.0
1500.0
0.0
15:00
21:00
3:00
9:00
Time (UTC)
Turlock Lake (TLK)
B
800.0
600.0
400.0
200.0
Raisin City (RAI)
C
80.0
60.0
40.0
20.0
Fresno (FSF)
D
150.0
100.0
50.0
Kings River (NFK)
E
Bakersfield (BAK)
F
40.0
30.0
20.0
10.0

Fig. 59

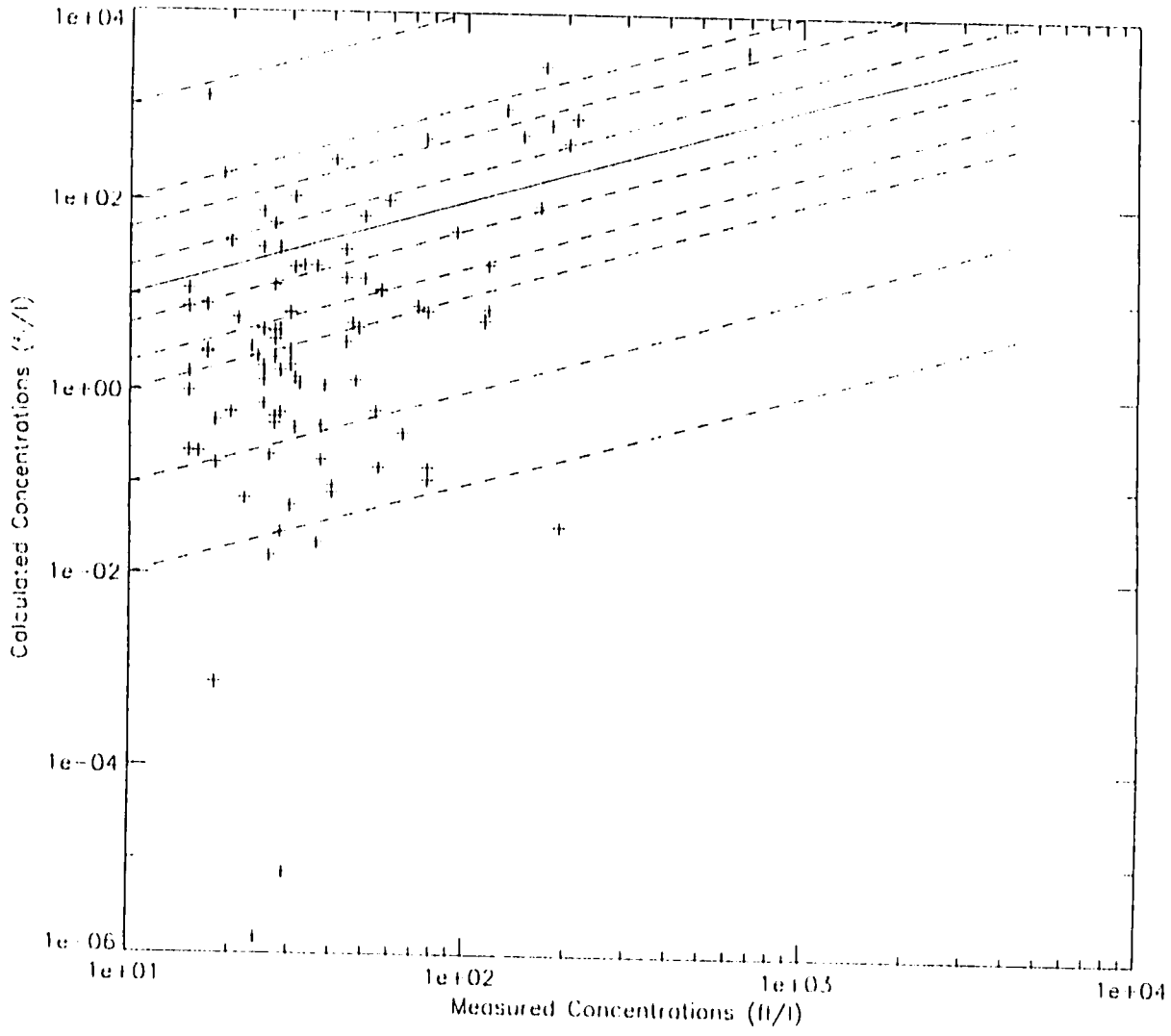
1e+04
1e+02
1e+00
1e-02
1e-04
1e-06
Calculated Concentrations (f/l)
1e+01
1e+02
1e+03
1e+04
Measured Concentrations (f/l)

Fig. 60

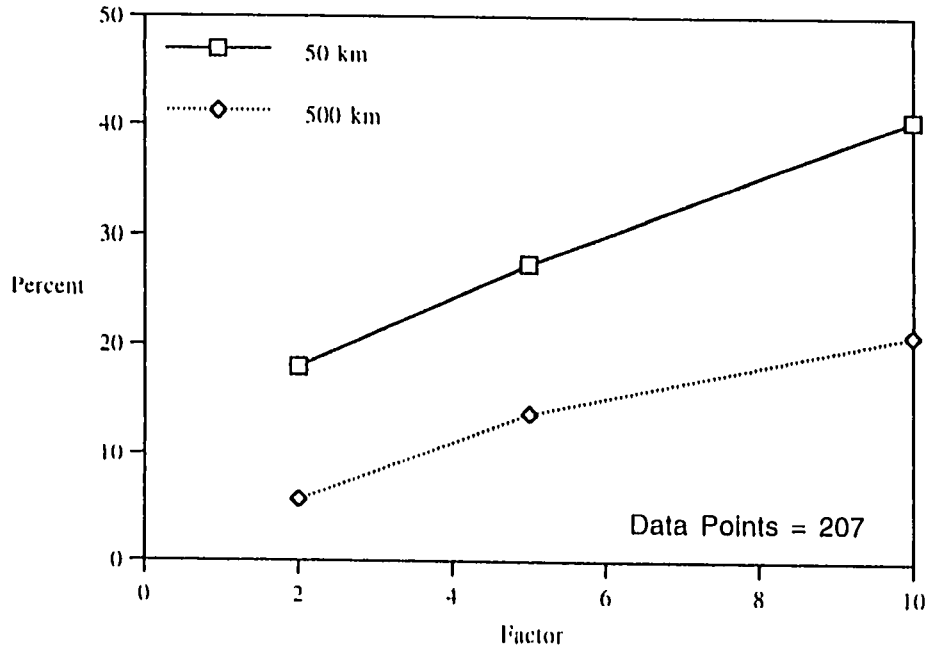
50
40
30
20
10
0
Percent
50 km
500 km
Data Points = 207
0
2
4
6
8
10
Factor

Fig. 61

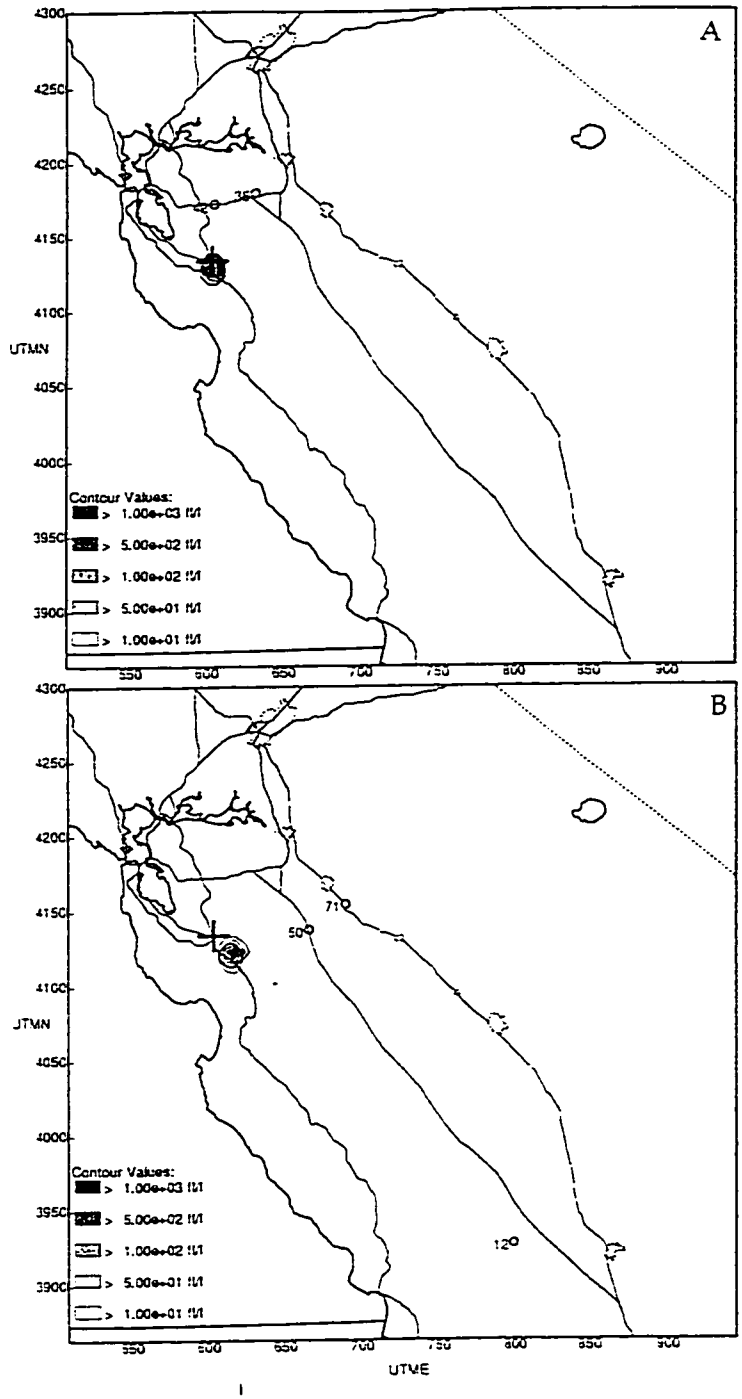
A
B
UTMN
UTME
Contour Values:
> 1.00e+03 ft/t
> 5.00e+02 ft/t
> 1.00e+02 ft/t
> 5.00e+01 ft/t
> 1.00e+01 ft/t
4300
4250
4200
4150
4100
4050
4000
3950
3900
550
600
650
700
750
800
850
900
360
71
50
12

Fig. 62

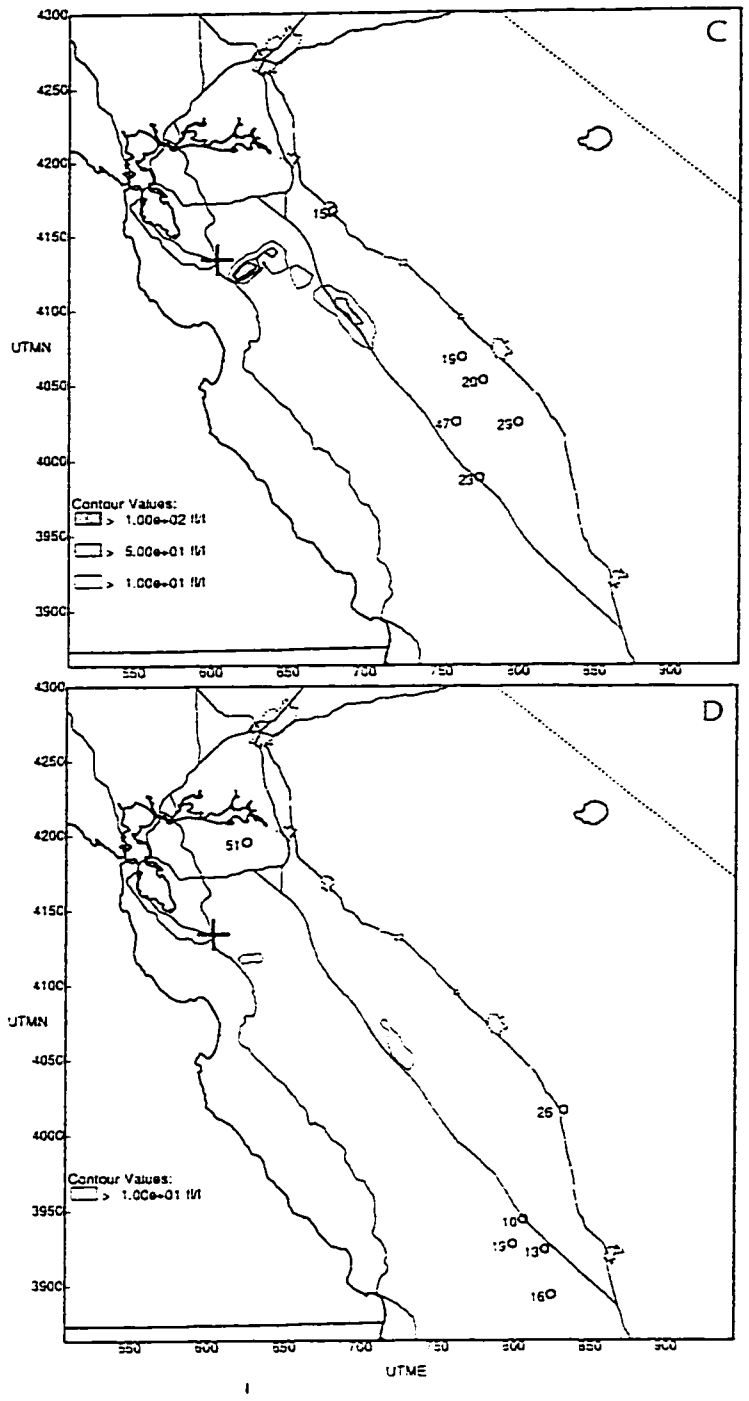

Fig. 62 (continued)

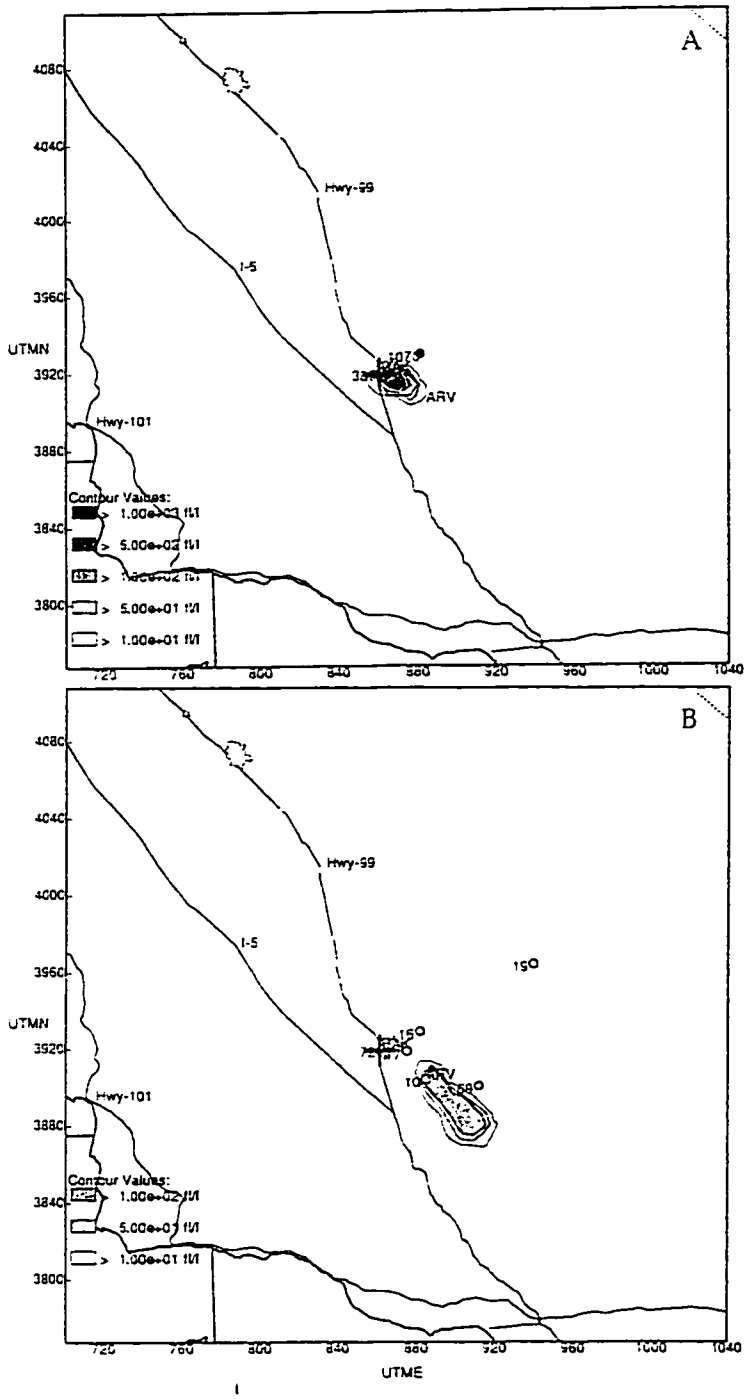
A
Hwy-99
I-5
ARV
Hwy-101
Contour Values:
> 1.00e+02 ft/l
> 5.00e+02 ft/l
> 5.00e+01 ft/l
> 1.00e+01 ft/l
UTMN
4080
4040
4000
3960
3920
3880
3840
3800
720
760
800
840
880
920
960
1000
1040
B
Hwy-99
I-5
ARV
Hwy-101
Contour Values:
> 1.00e+02 ft/l
> 5.00e+01 ft/l
> 1.00e+01 ft/l
UTMN
UTME

Fig. 63

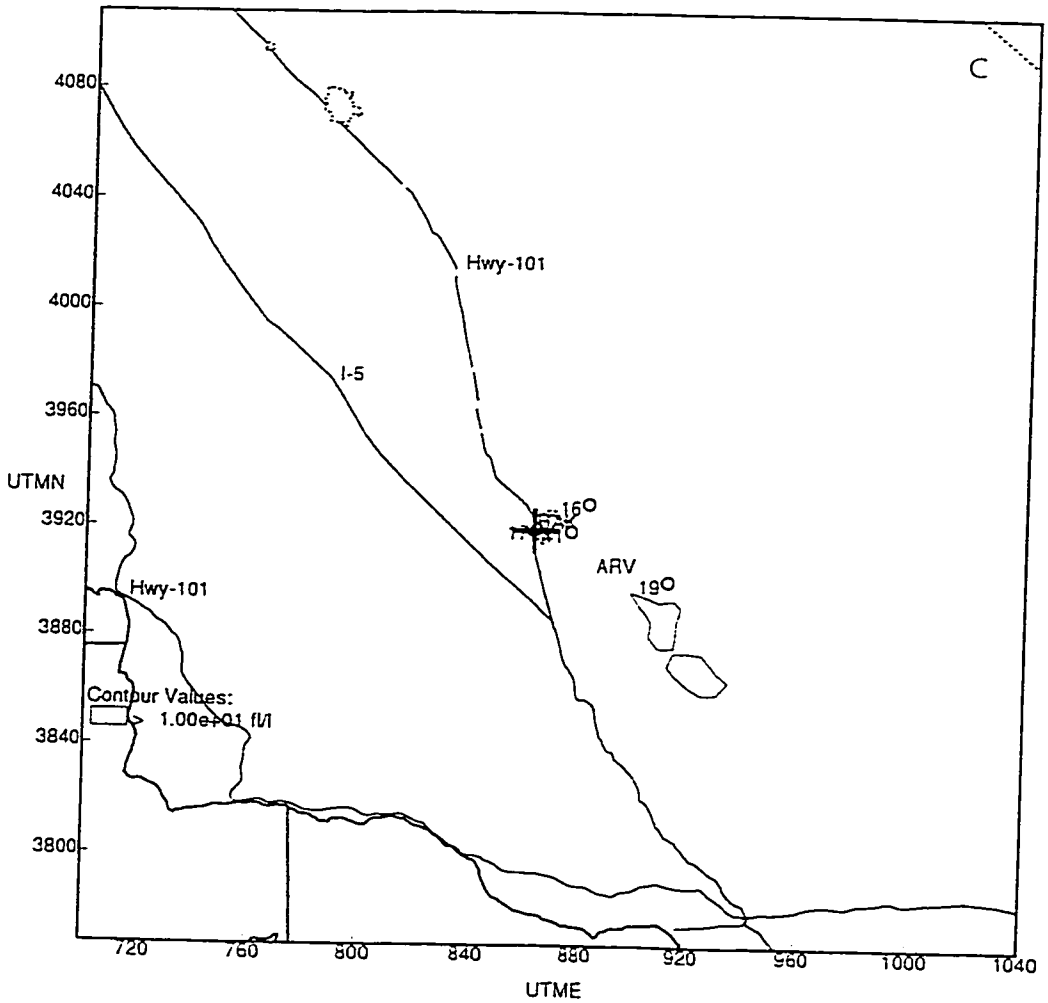

Fig. 63 (continued)

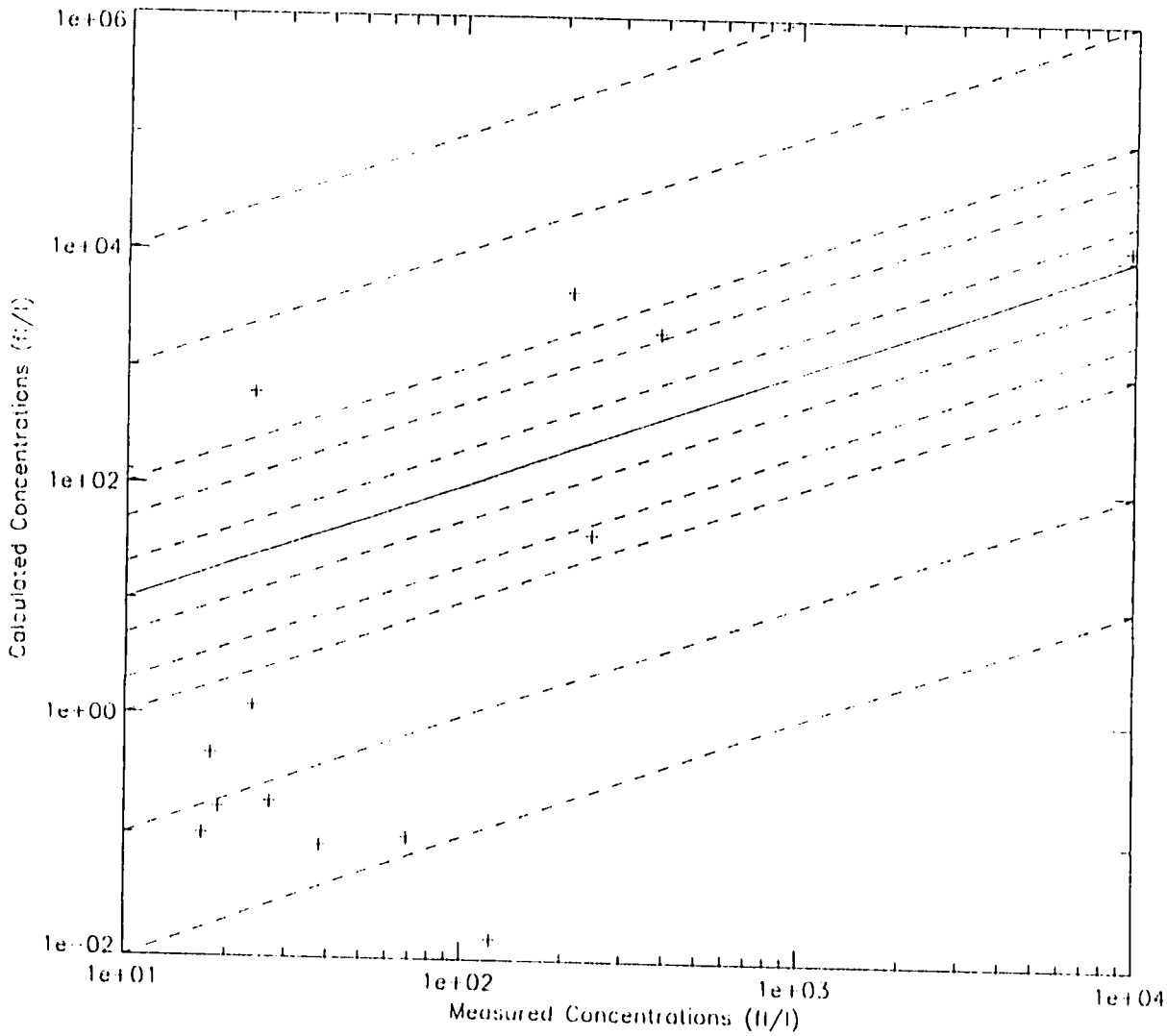
1e+06
1e+04
1e+02
1e+00
1e-02
Calculated Concentrations (ft/l)
1e+01
1e+02
1e+03
1e+04
Measured Concentrations (ft/l)

Fig. 64

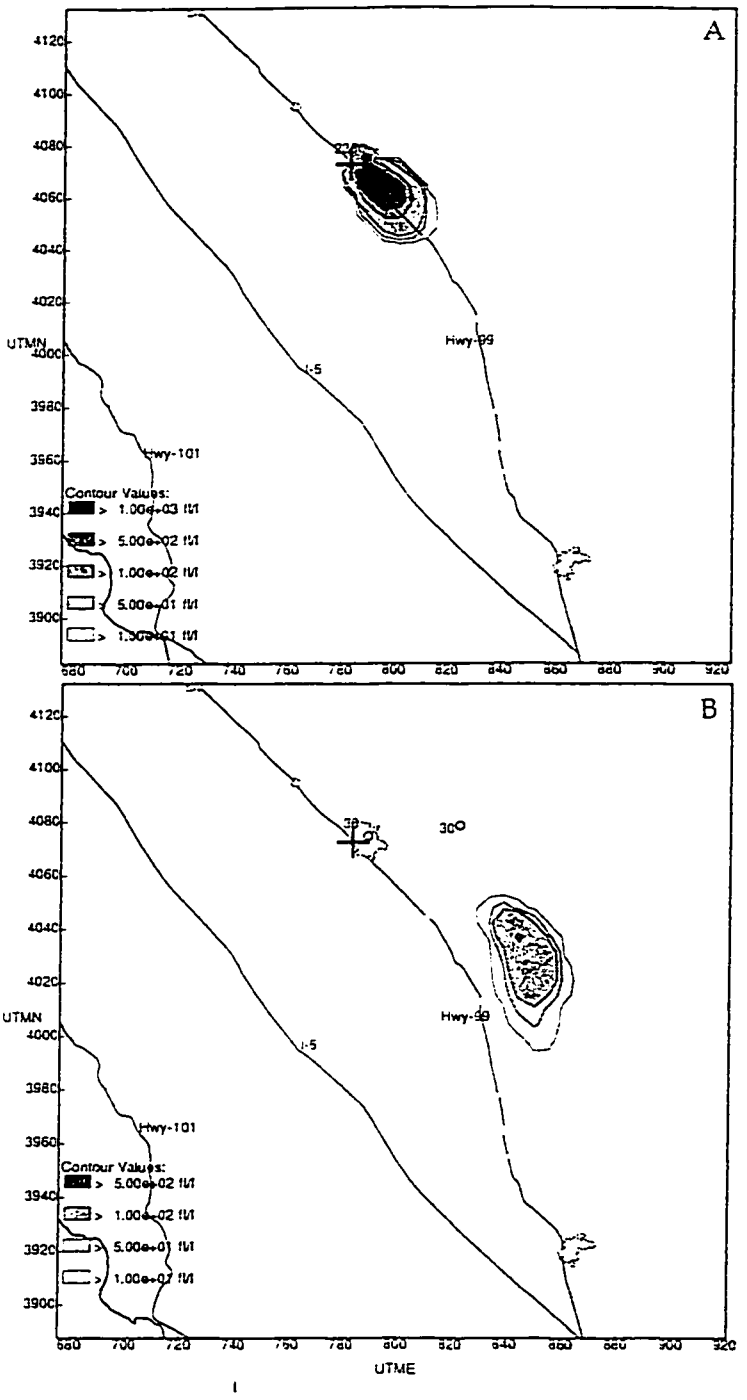
A
B
UTMN
UTME
Hwy-99
I-5
Hwy-101
Contour Values:
> 1.00e+03 ft/t
> 5.00e+02 ft/t
> 1.00e+02 ft/t
> 5.00e+01 ft/t
> 1.00e+01 ft/t
> 5.00e+02 ft/t
> 1.00e+02 ft/t
> 5.00e+01 ft/t
> 1.00e+01 ft/t

Fig. 65

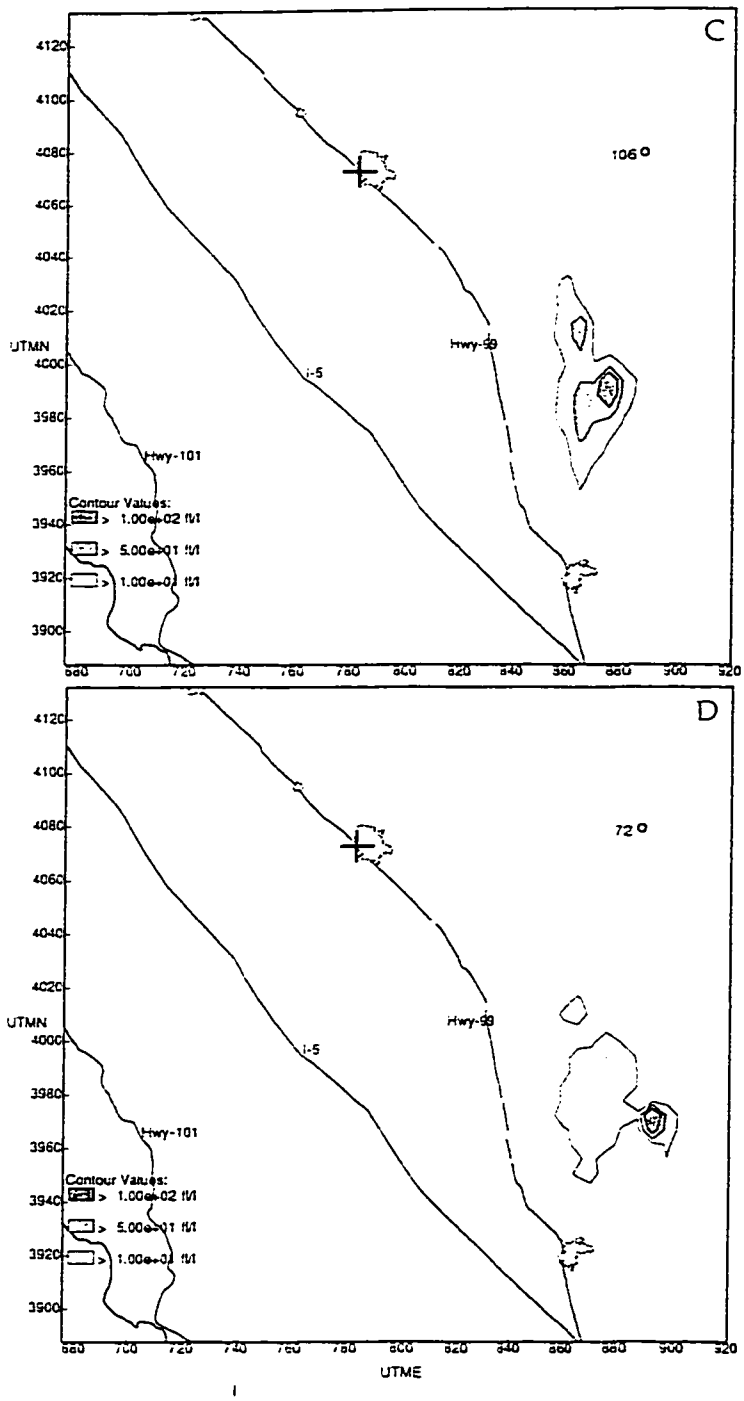

Fig. 65 (continued)

IMAGE EVALUATION
TEST TARGET (QA-3)

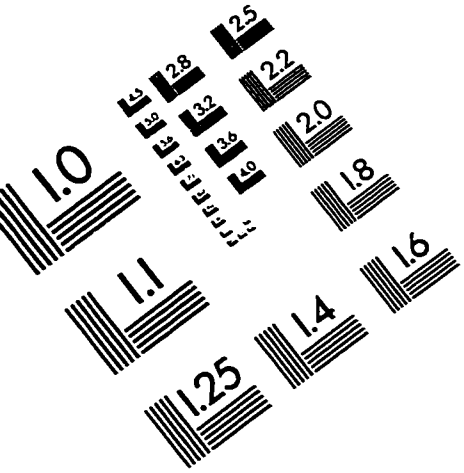

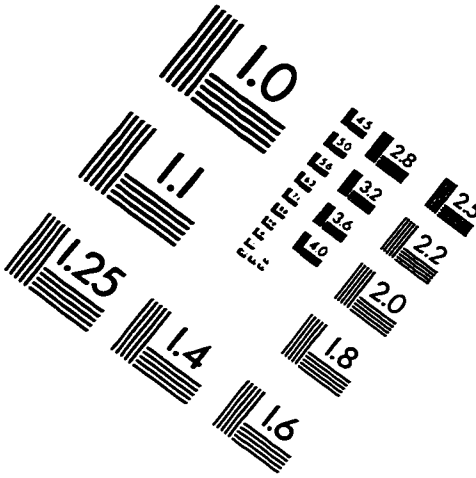

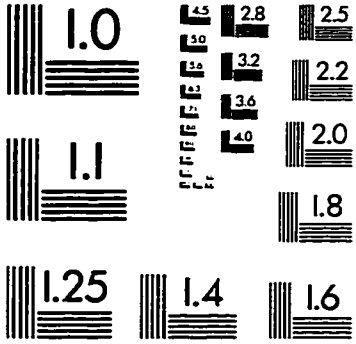

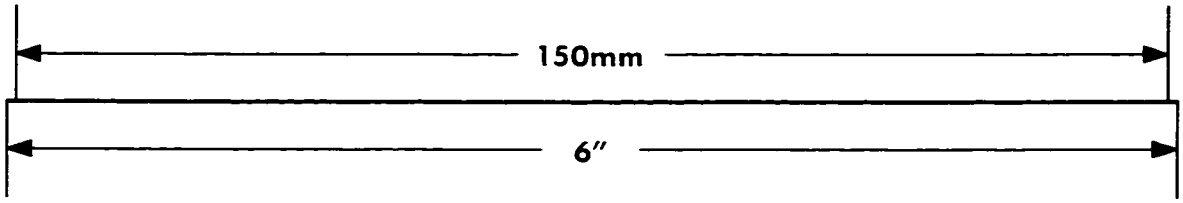

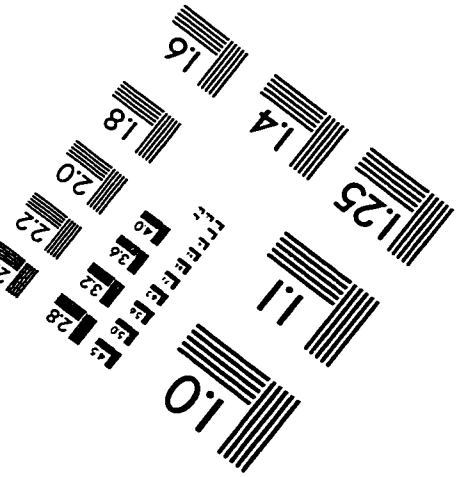

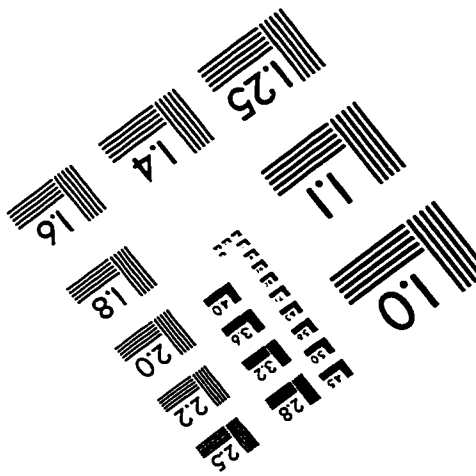

APPLIED IMAGE, Inc
1653 East Main Street
Rochester, NY 14609 USA
Phone: 716/482-0300
Fax: 716/288-5989